

## **Impact of metal oxide nanoparticles on the photosynthetic apparatus monitored by chlorophyll *a* fluorescence and optical spectroscopy**

Acadêmico: Montcharles da Silva Pontes  
Orientador: Prof. Dr. Etenaldo Felipe Santiago  
Co-orientador: Prof. Dr. Anderson Rodrigues Lima Caires  
Co-orientador: Prof. Dr. Luís Humberto da Cunha Andrade

“Dissertação apresentada ao programa de pós-graduação em Recursos Naturais, área de concentração em Recursos Naturais, da Universidade Estadual de Mato Grosso do Sul, como parte das exigências para a obtenção do título de Mestre em Recursos Naturais”.

Dourados – MS  
Fevereiro - 2019

## **Impact of metal oxide nanoparticles on the photosynthetic apparatus monitored by chlorophyll *a* fluorescence and optical spectroscopy**

Acadêmico: Montcharles da Silva Pontes  
Orientador: Prof. Dr. Etenaldo Felipe Santiago  
Co-orientador: Prof. Dr. Anderson Rodrigues Lima Caires  
Co-orientador: Prof. Dr. Luís Humberto da Cunha Andrade

“Dissertação apresentada ao programa de pós-graduação em Recursos Naturais, área de concentração em Recursos Naturais, da Universidade Estadual de Mato Grosso do Sul, como parte das exigências para a obtenção do título de Mestre em Recursos Naturais”.

Dourados – MS  
Fevereiro - 2019

S\_\_ Pontes, Montcharles da Silva

Impact of nanomaterials on the photosynthetic organisms monitored by chlorophyll *a* fluorescence and optical spectroscopy/Montcharles da Silva Pontes. Dourados, MS:

UEMS, 2019

Número de páginas 144 p.; 30 cm

Dissertação (Mestrado) – Recursos Naturais –  
Univesidade Estadual de Mato Grosso do Sul, Unidade  
Universitária de Dourados, 2019.

Orientador: Prof. Dr. Etenaldo Felipe Santiago

1. Palavra-chave. 2. Palavra-chave. 3. Palavra-chave

Título

**MONTCHARLES DA SILVA PONTES**

**IMPACT OF METAL OXIDE NANOPARTICLES ON  
THE PHOTOSYNTHETIC APPARATUS MONITORED  
BY CHLOROPHYLL *a* FLUORESCENCE AND  
OPTICAL SPECTROSCOPY**

Este exemplar compreende a redação final da dissertação de mestrado defendida por Montcharles da Silva Pontes.

Dourados/MS, 15 de fevereiro de 2019.

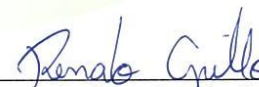
Banca Examinadora:



Prof. Dr. Etenaldo Felipe Santiago – Presidente



Prof. Dr. Eriton Rodrigo Botero



Prof. Dr. Renato Grillo

---

Dourados/MS, fevereiro de 2019.

*In 1794, the French chemist Antoine Lavoisier, who discovered the concept of oxidation in plants, recognized and named oxygen (1778) and hydrogen (1783), helped to establish the metric system, established the mass conservation law in chemistry, and so many other important scientific contributions, was executed by beheading during the "French Revolution". The "judge" who pronounced sentence said: "-The Republic has no need for scientists".*

*El futuro es hoy*  
-Café Tacvba

*"A História é escrita pelas grandes transgressões, de quem mudou o mundo com suas inquietações."*

-Tonho Gerbara

*"Nunca seremos felizes, nunca!"*  
-Simón Bolívar.



Dedicated to each deep breath my mom “Dona” Beth and my father “Seu” Tanio had to bear me these last three decades, and to my beautiful flower Geysel Santos.

## ACKNOWLEDGMENTS

First and foremost, I would like to express my most sincere thanks to my advisor, Prof. Dr. Etenaldo Felipe Santiago, who supported motivated and guided me through my undergraduate and M.Sc degree (during the many technical, analytical, and intellectual challenges). My heartfelt thanks to my co-advisors Prof. Dr. Luís Humberto and Prof. Dr. Anderson Caires, who were valuable guide throughout this process. Thank you all the doctors and lecturers of our program (PGRN) and to our coordinators, Prof. Dra. Claudia Cardoso and Prof. Dr. Yzel Suárez. I express my sincere thanks to Dr. Renato Grillo (Laboratório de Nanoquímica Ambiental, UNESP, Ilha Solteira, SP) for critical reading of this dissertation. I also thank Ronald Maldonado Rodriguez (The Fluoromatics Lab., Geneve, Switzerland) for his collaboration in another project.

At last but not the least, I thank all the staff of UEMS, CERNA, and PGRN. Thank you to the amazing classmates of this research group (Santiago's Lab) Plant Resources Study Group (GeRV). I am thankful to Daniela Graciano and William Falco for his comments and suggestions during the development of this research.

My heartfelt grateful to Conselho Nacional de Desenvolvimento Científico e Tecnológico (CNPq) for my scholarship, and Univesidade Estadual de Mato Grosso do Sul (UEMS).

## SUMMARY

RESUMO GERAL.....	1
GENERAL ABSTRACT .....	2
<b>CHAPTER I – GENERAL BACKGROUND.....</b>	<b>3</b>
1.1. Photosynthesis: the basis .....	4
1.1.1. Photosynthetic pigments.....	5
1.1.2. Photosynthetic electron flow around thylakoid membranes.....	8
1.2. Chlorophyll <i>a</i> fluorescence: a fingerprinting of photosynthesis .....	10
1.2.1. Begin at the beginning: the Kautsky effect.....	10
1.2.2. Pulse-Amplitude Modulated (PAM) chlorophyll fluorescence.....	12
1.2.3. Polyphasic kinetics of chlorophyll <i>a</i> fluorescence transient: the JIP-test.....	14
1.2.3.1 The O-J phase of OJIP fluorescence induction transient.....	14
1.2.3.2. The L and K bands of OJIP fluorescence induction transient .....	15
1.2.3.3. The J-I phase of OJIP fluorescence induction transient .....	15
1.2.3.4. The I-P phase of OJIP fluorescence induction transient .....	16
1.2.3.3. The calculated parameters stored in OJIP fluorescence induction transient .....	16
1.3. Optical spectroscopy.....	19
1.3.1. UV-Vis absorption and fluorescence spectroscopy .....	20
1.3.2. Vibrational spectroscopy .....	22
1.4. Engineered nanomaterials.....	24
1.4.1. What is and why study nanoscience and nanotechnology? .....	24
1.4.2. Classification of nanoparticles: natural and anthropogenic.....	24
1.4.3. Potential problems of nanoparticles on the photosynthetic organisms.....	25
1.5. Aim .....	26
1.6. References.....	26



<b>CHAPTER II – ENVIRONMENTALLY FRIENDLY SYNTHESIS OF COLLOIDAL COPPER OXIDE NANOPARTICLES: ANTIOXIDANT, ANTIMICROBIAL AND IN VITRO TOXICITY</b> .....	34
1. Introduction.....	37
2. Experimental.....	39
2.1. Materials and synthesis of copper oxide nanoparticles .....	39
2.2. Nanoparticles characterization.....	40
2.2.1. Scanning electron microscopy and energy dispersive spectroscopy, and atomic force microscopy (AFM) .....	40
2.2.2. Ultraviolet-visible absorption spectroscopy .....	40
2.2.3. Fourier transform infrared photoacoustic spectroscopy (FTIR-PAS) .....	41
2.3. Determination of antioxidant activity.....	41
2.4. Antimicrobial activity.....	42
2.5. <i>In vitro</i> toxicity of CuO nanoparticles on C-Phycocyanin .....	43
2.6. Statistical analysis.....	44
3. Results and discussion .....	44
4. Conclusion .....	58
5. References.....	59
<b>CHAPTER III – USING NETWORK CONNECTANCE FOR ESTIMATING BULK AND NANOSIZED COPPER EFFECTS ON THE PHOTOSYSTEM II ACTIVITY IN A FLOATING MACROPHYTE <i>Lemna valdiviana</i> Phil. (LEMNACEAE)</b> .....	65
1. Introduction.....	68
2. Materials and methods .....	70
2.1. Plant materials .....	70
2.2. Toxicity assay .....	70
2.3. Copper uptake.....	71
2.4. Determination of photosynthetic pigment .....	71
2.5. Chlorophyll <i>a</i> fluorescence assessment .....	71
2.5.1. Performance indexes parameters (PI <sub>ABS</sub> and PI <sub>Total</sub> ).....	72
2.5.2. Driving forces of photosynthesis .....	73
2.6. Statistical analysis.....	73

3. Results and discussion .....	73
3.1. Copper uptake .....	73
3.2. Photosynthetic pigments and steady state absorption.....	75
3.3. JIP-test fluorescence transient .....	78
3.4. Biophysical parameters derived.....	80
3.5. Photoenergetic system network .....	81
4. Conclusion .....	83
5. References.....	83
<b>CHAPTER IV - SYNERGISM AND INTERFERENCE OF BICARBONATE IONS ON NANOCERIA EFFECTS IN <i>Salvinia auriculata</i> Aubl LEAF TISSUE: A CHLOROPHYLL A FLUORESCENCE AND FOURIER TRANSFORM INFRARED PHOTOACOUSTIC SPECTROSCOPY STUDY .....</b>	<b>94</b>
1. Introduction.....	98
2. Materials and methods.....	100
2.1. Cerium oxide nanoparticles .....	100
2.2. Plant materials and treatment.....	101
2.3. Leaf uptake cerium oxide nanoparticles .....	101
2.4. Fourier transform infrared photoacoustic spectroscopy (FTIR).....	101
2.5. Chlorophyll <i>a</i> fluorescence imaging.....	102
2.6. Statistical analysis.....	103
3. Results and discussion .....	103
4. Conclusion .....	117
5. References.....	118
• List of publication.....	129
General conclusion and future works .....	130
Cadastro SISGEN .....	131

## RESUMO GERAL

Obter informações acerca dos potenciais efeitos nocivos de nanomateriais projetados sobre as respostas fotossintéticas em organismos aquáticos pode ser relevante para o monitoramento ambiental destes ecossistemas. Alguns estudos têm evidenciado danos ao aparato fotossintético em vegetais expostos à diversos nanomateriais, especialmente, às nanopartículas metálicas. Neste sentido, torna-se importante o conhecimento relacionando à habilidade de ajustes fotoquímicos rápidos do aparelho fotossintético quando submetidos a estes nanomateriais. Dentro desta perspectiva, o uso de técnicas não-invasivas, como a análise de fluorescência da clorofila *a* e métodos baseados em espectroscopia óptica tornam-se cada vez mais relevantes, uma vez que podem detectar e diagnosticar alterações metabólicas e fisiológicas induzidas pelos nanomateriais. Diante disso, de forma a complementar o conhecimento existente, o objetivo deste trabalho foi avaliar *in vitro* e *in vivo* as respostas fotossintéticas de organismos aquáticos (cianobactéria e macrófitas) sob exposição de nanopartículas de óxido de cobre (CuONPs) e cério (CeO<sub>2</sub>NPs). O trabalho foi dividido em duas etapas, a primeira constituiu-se da síntese, caracterização, avaliação da atividade biológica (antioxidante e antifúngica) e toxicidade (*in vitro* e *in vivo*) ao metabolismo fotossintético de nanopartículas de cobre, como descrito nos capítulos II e III. As nanopartículas sintetizadas apresentaram um tamanho médio entorno de 130 nm, com atividade antioxidante e antimicrobiano. No entanto, potenciais respostas nocivas foram observadas nos ensaios *in vitro* com pigmento-proteína ficocianina do complexo coletor de luz da cianobactéria *Arthrospira platensis*, e análise *in vivo* com a macrófita aquática *Lemna valdiviana*. A segunda etapa constituiu em avaliar as respostas metabólicas e fotossintéticas foliares de *Salvinia auriculata* a nanopartículas de óxido de cério associadas a co-exposição com íons de bicarbonato, por meio de técnicas de fluorescência da clorofila *a* e espectroscopia fotoacústica no infravermelho por transformada de Fourier (FTIR-PAS). As nanopartículas afetaram metabolicamente o tecido foliar de *Salvinia auriculata*, porém a co-exposição de íons bicarbonato foi responsável por uma maior alteração, sugerindo efeito sinérgico entre nanopartícula-bicarbonato.

**PALAVRAS-CHAVE:** Nanopartículas; Fotossíntese; Toxicidade, Nanotecnologia

## GENERAL ABSTRACT

Obtain information about the harmful effects of engineered nanomaterials on photosynthetic responses in aquatic organisms must be relevant for monitoring marine ecosystems. Some studies have shown damages to photosynthetic apparatus in plants exposed to nanomaterials, especially metallic nanoparticles. In this context, it becomes important the knowledge related to the ability of photosynthetic apparatus adjust their components upon nanomaterials exposure. In this perspective, the use of non-invasive techniques, such as chlorophyll *a* fluorescence analysis and methods based on optical spectroscopy, are becoming increasingly relevant as they can detect and diagnose metabolic and physiological changes induced by nanomaterials. In order to complement the existing knowledge, the objective of this work was to evaluate *in vitro* and *in vivo* the photosynthetic responses of aquatic organisms (cyanobacteria and macrophytes) under exposure of copper oxide (CuONPs) and cerium (CeO<sub>2</sub>NPs) nanoparticles. The work was divided in two stages, the first part consisted by synthesis, characterization, evaluation of the biological activity (antioxidant and antifungal) and toxicity (*in vitro* and *in vivo*) of copper nanoparticles to photosynthetic metabolism, chapters II and III. The nanoparticles synthesized presented an average size around 130 nm, with antioxidant and antimicrobial activity. However, potent harmful responses were observed on the pigment-protein phycocyanin from cyanobacteria *Arthrospira platensis*, and in the aquatic macrophyte *Lemna valdiviana*. The second step was to evaluate the metabolic and photosynthetic responses of *Salvinia auriculata* leaves to cerium oxide nanoparticles associated with bicarbonate ions co-exposure, using chlorophyll *a* fluorescence technique and Fourier transform infrared photoacoustic spectroscopy (FTIR-PAS). The nanoparticles metabolically affected leaf tissues of *Salvinia auriculata*, despite the effects of the nanoparticle, co-exposure with bicarbonate ions was responsible for a major change, suggesting a synergistic effect between nanoparticle and bicarbonate.

**KEYWORDS:** Nanoparticles; Photosynthesis; Toxicity, Nanotechnology.

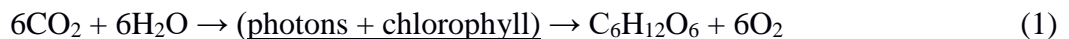


## **CHAPTER I – GENERAL BACKGROUND**

## CHAPTER I – GENERAL BACKGROUND

### 1.1. Photosynthesis: the basis

Photosynthesis (from Greek *Photo* → light, and *Synthesis* → putting together) is of the most important process on Earth, and a research field intrinsically interdisciplinary. In photosynthesis performed by eukaryotes, electrons are extracted from water by solar energy (photons) absorption, following by their incorporation into  $\text{CO}_2$  to synthesize organic compounds such as sugars as storable chemical energy ( $\text{NADPH}^+$  and ATP). Equation (1) shows a basic view of photosynthetic process in the water and  $\text{CO}_2$  utilizing to produce glucose and oxygen.



Chloroplasts (Figure 1) are bioenergetic organelles responsible for photosynthesis, with a range of 5-10  $\mu\text{m}$  diameter, and each plant cell can contain about 10-100 chloroplasts (COOPER, 2013). Chloroplasts comprise an external membrane with contains an internal membrane system (thylakoid) and a soluble matrix (stroma) (COOPER, 2013).

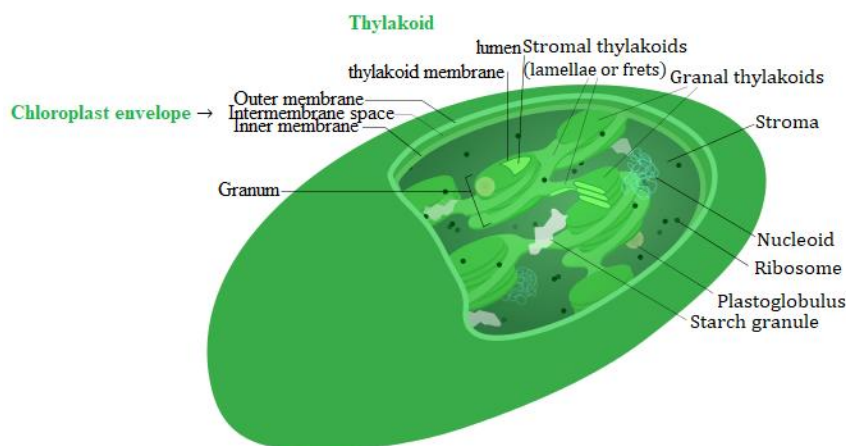


**Figure 1.** Basic structure of chloroplast organelle divided into membrane envelope, thylakoid membranes and stroma matrix. Author.

### 1.1.1. Photosynthetic pigments

Pigments are the part of the macromolecular structures which absorb light in the visible region of the spectrum (WALSBY, 1974). A large range of pigments can be found in different photosynthetic organisms such as chlorophylls (Chl) *a-f*, carotenoids (Car), bacteriochlorophylls (B-Chl) *a-g* and bilins (phycocerythrin, phycocyanin and allophycocyanin). In summary, Chl-*a* molecules are the major responsible for photochemical reactions. The spectral properties of pigments are linked to their chemical structure. In case of Chl depend on the functional groups (methyl, ethyl, formyl, vinyl). For Car two groups can be divided the cyclic hydrocarbons (carotenes) and hydrocarbons containing oxygen (xanthophylls) (KUCZYNSKA et al., 2015).

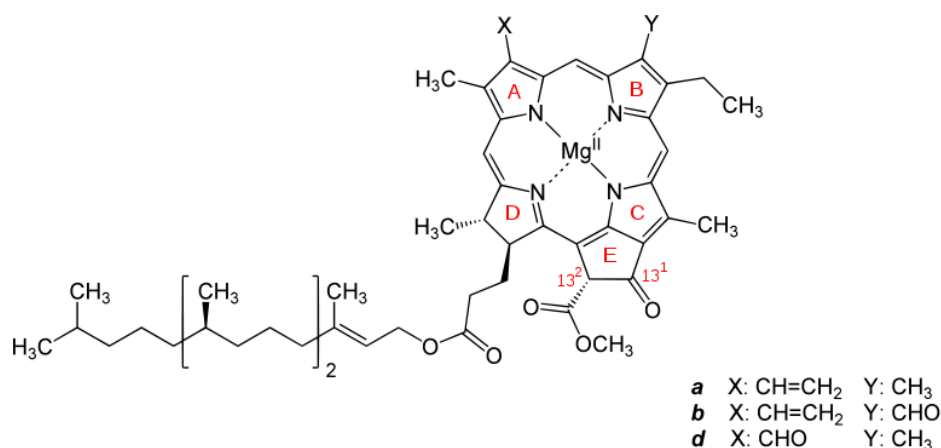


**Figure 2.** Basic structure of chlorophyll *a*, *b* and *d* molecules.

Chlorophylls molecules mainly absorb photons in the blue (Soret band) and red (Qy band) range of the spectrum (BLANKENSHIP, 2014) with some differences in the absorption spectra between Chl *a* and Chl *b*. The spectral absorption profile of Chl *a* and *b* can be found in Figure 3. Chl *a* has absorption maxima at 430 and 662 nm, while the chl *b* molecules around 455 and 644 nm (HANSON, 1991; HOFF AND AMESZ, 1991; BLANKENSHIP, 2014). This limited absorption around the green region of visible spectra, give the characteristic green color of plants.

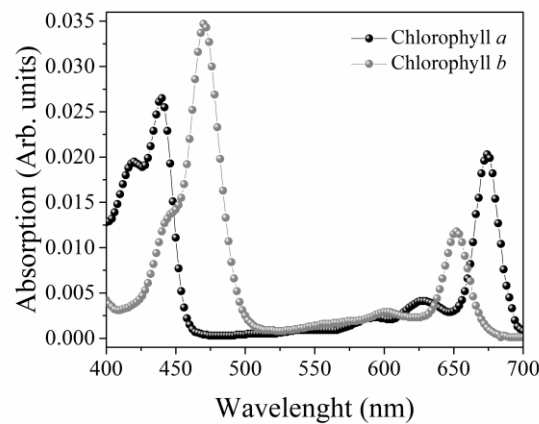


**Figure 3.** Absorption spectra of chlorophyll *a* and *b* molecules. Adapted from Misra et al. 2012.

Carotenoids and bilins are accessory pigments helping light absorption by transferring harvested energy to Chl molecules. In higher plants spectral absorption range are enriched by Car molecules. The Car has absorption maxima at 400 and 500 nm, giving them their characteristic orange colour (Figure 4). Photosynthetic organisms that live underwater use special Car and phycobilins (that absorb between 550 to 650 nm) to fill the spectral gap (CROCE AND AMERONGEN, 2014). In cyanobacteria and red algae, phycobilins are chromophores of light-harvesting (LHC) phycobilisomes (LARKUM AND BARRET, 1983; CROCE AND AMERONGEN, 2014).

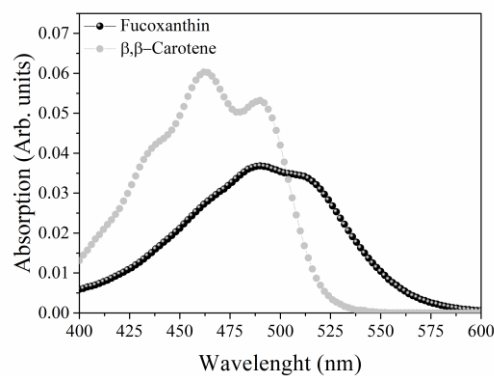


**Figure 4.** Absorption spectra of carotenoids fucoxanthin (photosynthetically active) and  $\beta,\beta$ -Carotene (Photoprotectant). Adapted from Misra et al. 2012.



Accessory pigments in cyanobacteria and red algae from phycobiliprotein LHC can be subdivided into three major categories: Allophycocyanin (APC) are violet with a far-red fluorescence, Phycoerythrins (PE) are red with a golden fluorescence and Phycocyanin (PC) are blue with a red fluorescence emission (LARKUM; BARRET, 1983; CROCE; AMERONGEN, 2014).

In general, steady-state and time-resolved fluorescence studies have been used to detecting excitation energy transfer from these accessory pigments (from a donor pigment to a acceptor pigment). These accessory pigments to Chl *a* molecules exhibit a high quantum yields. Figure 5 show the structure three accessory pigments from phycobiliprotein LHC with the presence of Phycoerythrin.

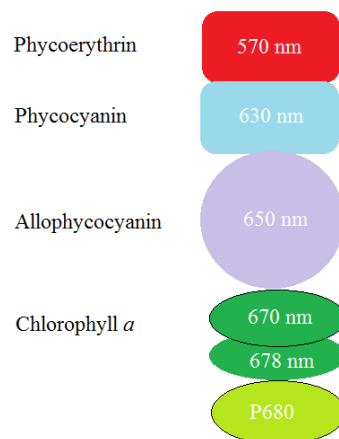


**Figure 5.** Basic structure three accessory pigments from phycobiliprotein LHC.

The general pathway of excitation energy transfer in some algae and cyanobacteria is: Phycoerythrin → Phycocyanin → Allophycocyanin → Chlorophyll *a* molecule at the reaction center. It is important to note that the phycocyanin exhibits an absorbance at ~ 630 nm (Figure 6), and the efficiency of energy transfer process among phycobiliproteins into a phycobilisome LHC is close to 100% (GLAZER, 1984).

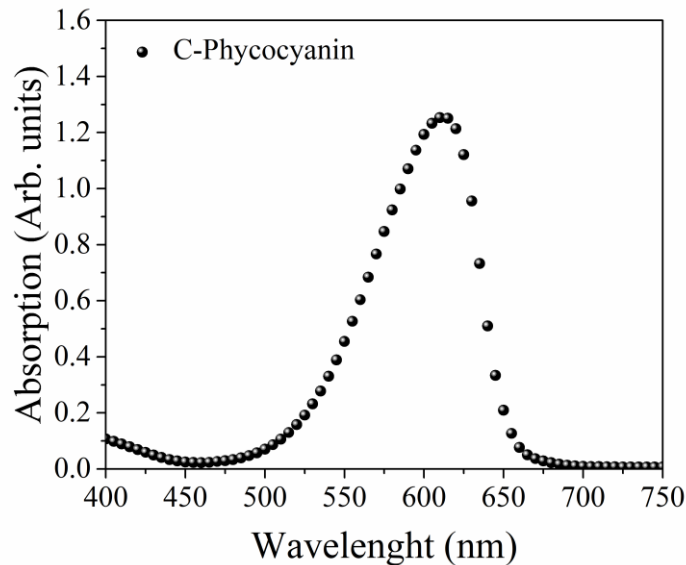


**Figure 6.** Absorption spectra of cyanobacterial phycocyanin.

### 1.1.2. Photosynthetic electron flow around thylakoid membranes

During photosynthetic electron transport, light (photons) energy supplies the driving force for oxygen evolution, nicotinamide adenine dinucleotide phosphate (NADP) reduction and adenosine triphosphate (ATP) formation (TREBST, 1994). The protein-pigment complexes involved in electron transport chain (ETC) into thylakoid membranes are two photosystems (PSI and PSII), and a range of peripheral polypeptides attached to pigments and redox systems from ETC, responsible to connection between PSII and cytochrome  $b_6/f$  complex (Cyt  $b_6/f$ ) at the ETC (WITT, 1996; TREBST, 1994; DEKKER AND VAN GRONDELLE, 2000; NELSON AND YOCUM, 2006).

The conversion of photons to chemical energy at PSII complex is associated with charge separation across the thylakoid membrane (WITT, 1996; NELSON AND YOCUM, 2006). Visible light (400-700 nm wavelengths) drive the photosynthesis. This biological phenomenon is initiated by the absorption of photons by the light-harvesting complex (LHC), common know as antenna system. Photon absorption is an ultrafast process, occurs at approximated 1 femtosecond (fs) and induced a transition from the electronic ground state ( $S_0$ ) to an excited state ( $S_1, S_2, S_3, S_4 \dots S_n$ ). After absorption, molecules exposed to photons go to the  $S_1$  state from the higher excitation states, the excess of energy is losing as heat, and part of

the excitation energy are also lost during the transition to lower sub-level as heat via non-radiative transition (phonons). In general, excited molecules can return from the lowest  $S_1$  sub-level to any  $S_0$  sublevel by heat or fluorescence emission (PAINTER et al., 1992).

For the basis of photosynthesis, the process involves the high probability of Chl molecules transfer their excitation energy via random resonance to their neighbor Chl molecule. The LHC drive the excitation energy to RC of PSI or PSII. In PSII, following by catalyzing the oxidation of water to molecular oxygen and provides electrons and protons (BRICKER et al., 2012; GOVINDJEE et al., 2012; GOVINDJEE et al., 2017), it is driven by oxygen-evolving complex (OEC), and consequently the energy is conserved in reducing equivalents and protons are released to thylakoid inner lumen to driving force for ATP synthesis (GOVINDJEE et al., 2012; GOVINDJEE et al., 2017). The electrons are transported across thylakoid membrane after the light-modulated charge separation from the excited primary donor  $P_{680}$  via pheophytin molecule to the first bound plastoquinone ( $Q_A$ ), tightly bound at the stromal side of polypeptide sub-unit D2. When the cationic radical  $P_{680}^{*+}$  is formed, the pheophytin moves the electron to the electron stabilizing acceptor  $Q_A$ , then the electron of  $Q_A^*$  is passed to a second plastoquinone  $Q_B$ . Following the reduction events, with two electrons  $Q_B$  (now as  $Q_B^{2-}$ ) is fully reduced and, transfer electrons to plastoquinone-pool (PQ-pool), reducing it to  $PQH_2$ . Part of the electrons is transferred to a carrier, plastocyanin (PC), and another fraction enters along the Q cycle. The structure of the photosynthetic electron transport chain on a simplified model is described briefly in Figure 7.

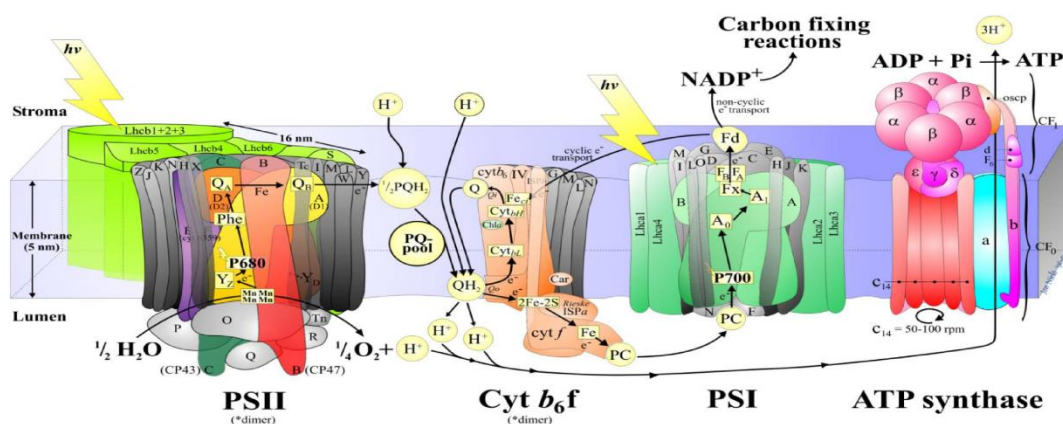


**Figure 7.** Structure of thylakoid membranes showing the four major protein complexes, which are used for the production of ATP and NADPH. From left to right: Photosystem II (PSII; water-plastoquinone oxidoreductase), cytochrome (Cyt)*b<sub>6</sub>f* (plastoquinol-plastocyanin-oxidoreductase), Photosystem I (PSI; plastocyanin-ferredoxin-oxidoreductase), and ATP synthase. The ATP and NADPH produced during the light phase of photosynthesis are used in the Calvin–Benson cycle to fix CO<sub>2</sub> to produce sugars. (Adapted from Stirbet et al., 2014).

## 1.2. Chlorophyll *a* fluorescence: a fingerprinting of light reactions of photosynthesis

### 1.2.1. Begin at the beginning: the Kautsky effect

Most part of the photons absorbed by photosynthetic oxygenic tissues are utilized by photosynthesis via photochemical process or converted into heat (non-radiative decay, infrared emission, non-photochemical quenching) (RABINOWITCH AND GOVINDJEE, 1969; BARBER AND ANDERSON, 1994; BARBER et al., 1997). However, a few part of the absorbed light at most, is re-emitted as fluorescence, most of these by Chl-*a* molecules (Fig. 8). The photochemical reactions in plants, cyanobacteria and algae and fluorescence emission are compete by the same absorbed quanta, due to this complementary chlorophyll *a* fluorescence (ChlF) is a reliable and popular tool to probe photosynthesis in plant physiology studies.

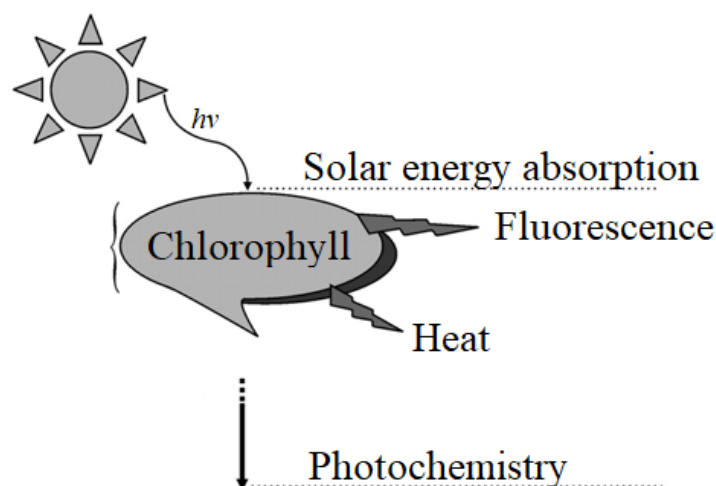


**Figure 8.** Energy dissipation pathways in chlorophyll molecules.

The first report of fluorescence emission by plant leaves after a dark-adapted period followed by switched light pulse shows a yield and rapidly rises and then, curve slowly decreases. This phenomenon has been called the Kautsky effect or Kautsky kinetics (KAUTSKY AND HIRSCH, 1931). Figure 9 shows ChlF kinetics spectra, when a photosynthetic tissue has been kept dark-adapted is transferred to the light condition, a decrease of the ChlF is observed from the initial maximum reached in the first second to a steady state value after a few minutes of illumination (“Kautsky effect”).

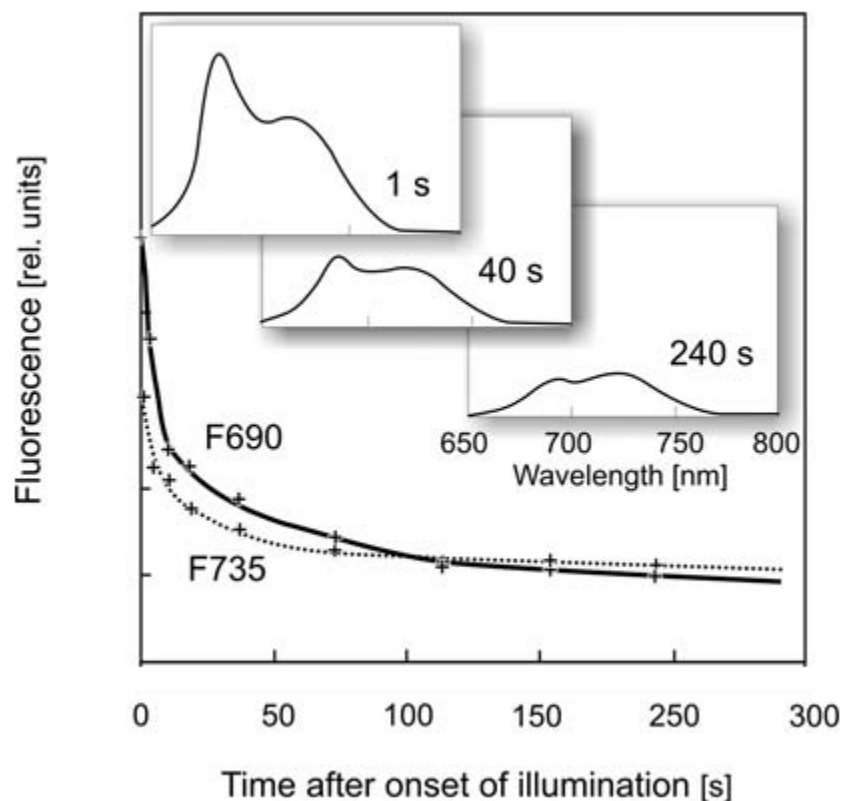


**Figure 9.** Changes of the shape of the ChlF emission spectrum of an intact dark-adapted green leaves during the chlorophyll fluorescence induction kinetics (“Kautsky effect”) within 5 min of illumination. Illustrate the results observed by Kautsky and co-workers for fluorescence intensity at 690 and 735 nm.

Depending on the type of study, the aims and the suitability of the photosynthetic apparatus, distinct chlorophyll fluorescence techniques can be used to evaluate alterations in photosynthetic system (MISRA et al., 2012). A close analysis of the fluorescence curves,

imaging or spectra give us an overview to the photosynthetic light reactions transducing proteins orientation into photosynthetic machinery (MISRA, et al., 2012). The processes that can be studied analyzing the OJIP transients, the analysis of fluorescence decay following a single turnover flash, or the quenching analysis.

Different types of chlorophyll fluorescence measurements can be used for wide array events and alterations in photosynthetic process, most commonly chlorophyll fluorescence methods are summarized in Table 1.

**Table 1.** Some commonly used methods in chlorophyll fluorescence studies. Note that this is included to identify only the most common methods.

Fluorescence technique	Principle	References
77K fluorescence	Low temperature	Rabinowitch and Govindjee, 1969
Advanced laser fluorometry (ALF)		Chekalyuk and Hafez, 2008
Fast repetition rate (FRR)		Kolber et al. 1998
Fluorescence temperature curve		Ilik et al., 2003
Imaging chlorophyll fluorescence		
Laser induced fluorescence (LIF)		Chekalyuk and Hafez, 2008
Prompt Chl fluorescence (OJIP)	$\mu$ -second polyphasic curve	Strasser and Govindjee, 1991
Pulse amplitude modulation (PAM)		Schreiber et al. 1986
Pump and probe (P & P) fluorometry		Mauzeralla, 1972; Falkowski et al., 1986
Pump during probe (PDP)		Olson et al., 1996
Room temperature fluorescence	Fluorescence spectroscopy	Rabinowitch and Govindjee, 1969

\*Adapted from Misra et al., 2012

### 1.2.2. Pulse-Amplitude Modulated (PAM) chlorophyll fluorescence

Since its introduction (~32 years ago; see SCHREIBER et al., 1986), the Pulse-Amplitude Modulated (PAM) method has become a very popular technique for studying photosynthetic electron transport in photosynthetic organisms (KALAJI et al., 2017). The parameters extracted from ChlF based on PAM method provide non-invasive information about the energy fluxes originating from the de-excitation of Chl-*a* molecules in PSII.

In the dark-adapted state the  $F_0$  level represent the minimum fluorescence in which the light-harvesting complex of PSII (LHCII), the pheophytin ( $Phe_{D1}$ ) and their primary acceptor the quinone ( $Q_A$ ) present their oxidized state, at this point all reaction centers (RC) are opened (APOSTOL et al., 2011; KALAJI et al., 2017). Then, the short saturation pulse (with intensity  $\sim 10.000 \mu\text{mol m}^{-2} \text{s}^{-1}$  during 1s) was applied, and fluorescence intensity increase to maximum level ( $F_m$ ), followed by a decrease almost to  $F_0$  level. The  $F_m$  level

represent the maximum fluorescence, all active PSII are closed, the PSII acceptor side is fully reduced. In the light-adapted state, two photochemical processes influence the fluorescence intensity ( $F^v$ ): 1<sup>st</sup> the presence of the closed PSII RC fraction, the reduced form of PSII electron acceptor ( $Q_A^-$ ) leading to an increase in fluorescence intensity; and 2<sup>nd</sup> non-photochemical dissipation energy of absorbed photons and the decrease in the efficiency in light capture by LHC.

Generally, the values of  $F_o'$  is lower than  $F_o$ , and  $F_m'$  is lower than  $F_m$ , the decrease in  $F_m'$  relative to  $F_m$  and the decrease in  $F_o'$  relative to  $F_o$  can be used to estimate the extent of non-photochemical quenching (NPQ) (KALAJI, et al., 2017).

Changes in the  $F_o$  values can be used as an indicator of alterations in PSII photochemistry. The increase in  $F_o$  values, with an increase in  $F_m$  and minor changes in  $F_v/F_m$  can be associated with an increase in PSI fluorescence contribution, particularly due to the reorganization of photosynthetic apparatus and adjustment of PSI/PSII stoichiometry. The separation of LHCII from the PSII core complex can increase the  $F_o$  values (SCHREIBER AND ARMOND, 1978), and  $F_o$  could increase due the inhibition of electron flow from  $Q_A$  to  $Q_B$  (BILGER et al., 1984; BUKHOV et al., 1990). The decrease in  $F_m$  values in response to exogenous stimuli could be used to estimate the fraction of inactive PSII RCs in a given state.

Variable ChlF ( $F_v$ ) intensity represent the amplitude of fluorescence increase from  $F_o$  to  $F_m$  ( $F_v = F_m - F_o$ ). The value of  $F_v/2$  can be used to estimate the PQ pool in special conditions (BOLHÀR-NORDENKAMPF AND ÖQUIST, 1993).

The photochemical quenching  $q_P$  or  $q_L$ , represent a fraction of PSII RCs, which are in oxidized state and are open, in summary quantifies the fraction of PSII RC in the open state with oxidized  $Q_A$ , and the values of  $1-q_P$  or  $1-q_L$  quantifies the fraction of PSII RC which are reduced with  $Q_A^-$  (DUYSENS AND SWEERS, 1963). Also,  $1-q_P$  or  $1-q_L$  represents the redox state of  $Q_A$ , expressed as  $Q_A^-/Q_A^{\text{Total}}$  (WEIS AND BERRY, 1987). However, according to Kalaji et al., (2017) the correct estimation of  $Q_A$  reduction state by means of ChlF is still an open question.

The  $q_N$  (non-photochemical quenching of variable ChlF) reflects the activation of non-photochemical light energy conversion in light-exposed leaves, are linked to non-



radiative thermal dissipation of excitation energy (SCHEREIBER, 1986). In summary, reflects the decrease in Fv due to the activation of non-photochemical processes.

The NPQ (non-photochemical quenching of maximum ChlF) reflects the activation of non-photochemical light energy conversion in the light-exposed leaves (KALAJI et al., 2017). The values of NPQ represent the dissipation of excessive light energy in PSII antennae, and are linearly linked with xanthophyll oxidation in the xanthophylls cycle, and also reflect the decrease in the size of PSII LHC (BILGER AND BJÖRKMAN, 1990).

Derivate fractions of qN and NPQ could be also estimated: qE represents the energy-dependent non-photochemical quenching, qT is referred to the fraction of non-photochemical quenching assigned to state transitions, and qI represents the fraction of non-photochemical with the longest relaxation time also referred to as photoinhibitory quenching (KRAUSE AND JAHNS, 2004).

### 1.2.3 Polyphasic kinetics of chlorophyll *a* fluorescence transient: the *JIP-test*

The central dogma of the chlorophyll *a* fluorescence transient analysis; and adopted by the majority of researchers; are that the energetic state of the PSII RC is determined by the redox state of the Q<sub>A</sub> (primary quinone acceptor), this theoretical approach is based on the quencher theory of Duysens and Sweers (1963). A close analysis of fluorescence transient O-J-I-P by the *JIP-test* can be applied at any experimental and environmental conditions to quantifying the PSII behavior (STRASSER et al., 1995; STRASSER et al., 2000; STRASSER et al., 2004; STRASSER et al., 2010; RODRIGUEZ et al. 2013; SANTIAGO et al. 2015).

The polyphasic fluorescence O-J-I-P transient is based on a saturating light pulse; its signal provides information on the photosynthetic electron transport chain (ETC) related to reduction kinetics of the ETC, PSII antenna size, relative content of ETC components like the PSI. In general, the analysis of the OJIP transients can be used to obtain information on the redox state of the photosynthetic ETC.

#### 1.2.3.1. The O-J phase of OJIP fluorescence induction transient

During the polyphasic fluorescence induction curves (OJIP test), the O-level (at ~20 to 50  $\mu$ s) represent the minimum fluorescence in which the light-harvesting complex of PSII



(LHCII), the pheophytin ( $\text{Phe}_{\text{D1}}$ ) and their primary acceptor the quinone ( $\text{Q}_A$ ) present their oxidized state, at this point all reaction centers (RC) are opened (STRASSER et al., 1995; STRASSER et al., 2000; STRASSER et al., 2004). The O-J phase represents the reduction of PSII acceptor side ( $\text{Q}_A$  is reduced to  $\text{Q}_A^-$  if the site is occupied by a quinone/semiquinone). The J-level ( $\pm 3$  ms) represents the moment when the reduction of PQ-pool starts (STRASSER et al., 2004). The O-J phase is controlled by the redox activity of at least 3 species:  $\text{P680}^+$ , Pheophytin $^-$  and  $\text{Q}_A$ .

#### 1.2.3.2. The L and K band of OJIP fluorescence induction transient

Under certain environmental conditions; *i.e.* high temperatures, nitrogen deficiency, oxygen deprivation; the process of water diffusion is inhibited, and the photosynthetic electron transport between OEC and tyrosine (Tyr) is blocked (STRASSER et al., 2004). During this scenario, appears on the OJIP transient a new inflection point (at  $\sim 0.3$  ms) called K-band, K-point or K-step, characterized by a fluorescence decrease after the K band appearance (the inflections at J and I levels disappear). K-band reflects damages on the PSII donor side by inactivation of the OEC; to obtain the information about the K-band the difference between normalized kinetics of O-J phase reveals the presence of K-band (STIRBET et al., 2014). The K-band is also associated  $\text{RC}_{\text{SII}}$  dissociated from the OEC (SCHANSKER et al., 2005).

The L-band is used to estimation of the energetic connectivity of PSII RC. Different degrees of PSII excitonic connectivity reveals the presence of L-band (around 100-150  $\mu\text{s}$  (YUSUF et al., 2010). According to Strasser et al. (2004), the connectivity between PSII units increases the use of excitation energy and is a significant factor for the stability of the photosynthetic apparatus.

#### 1.2.3.3. The J-I phase of OJIP fluorescence induction transient

The J-I step (rise time  $\sim 200\text{ms}$ ) is intermediate interval of OJIP curve, corresponds to the phase of electron transfer from  $\text{Q}_A$  to  $\text{Q}_B$ , controlled by the donor side of PSII during water photolysis in the OEC (STRASSER et al., 2004; STIRBET et al., 2014). J-I step is

generally correlated with the reduction of the PQ-pool (~6-12 PQ molecules per PSII) by the PSII-driven electron transport (STIRBET et al., 2014).

#### 1.2.3.4. The IP step of OJIP fluorescence induction transient

During I to P steps, the maximum fluorescence dissipation through plastoquinone pool (PQ-pool) are observed. The level P ( $F_m$ ) maximum fluorescence intensity emitted, occurs when the reaction centers and all molecules of  $Q_A$  are in the reduced state (STRASSER et al., 1995; STRASSER et al., 2000; STRASSER et al., 2004).

#### 1.2.3.5. The calculated parameters stored in O-J-I-P transient

The commonly used calculated parameters from *JIP-test* are: the specific (per RC) and phenomenological (per cross section) energy fluxes for absorption, trapping and electron transport; the density of RCs, performance indexes and driving forces; the quantum yields of PSII (for primary photochemistry and electron transport), as well the efficiency by which a trapped exciton (a bound state of an electron) moves an electron into the PSII electron transport chain further than reduced quinone ( $Q_A^-$ ), and the rate of  $Q_A$  reduction can be evaluated by the Area above fluorescence transient. Also, with the double hit method, the fraction of non- $Q_B$  reducing RC may be estimated (STRASSER et al., 2000; STRASSER et al., 2004). The technical and calculated parameters are summarized in Table 2.

**Table 2.** Summary of fluorescence parameters, formulae and their description using data extracted from chlorophyll *a* fluorescence transient (OJIP-test)

<b>Fluorescence parameters Description</b>	
<b>Technical fluorescence parameters</b>	
$F_t$	Fluorescence intensity at time 't' after onset of actinic illumination
$F_o$	Minimum reliable recorded fluorescence at 50 $\mu$ s
$F_m$	Maximum recorded (= maximum possible) fluorescence at P-step
$F_v$	Maximum variable fluorescence ( $F_m - F_o$ )
Area	Total complementary area between fluorescence induction curve and $F = F_m$
$S_M = \text{Area}/F_v$	Normalized total complementary area above the OJIP transient (reflecting multiple turnover $Q_A$ reduction events)
$S_S = V_j/M_o$	Normalized total complementary area corresponding only to the O-J phase (reflecting single-turnover $Q_A$ reduction events)

$N = S_M/S_S = S_M M_0(1/V_j)$	Turnover number: number of QA reduction events between time 0 and $t_{Fm}$
$V_j = (F_{2\text{ ms}} - F_0)/(F_m - F_0)$	Relative variable fluorescence at the J-step (2 ms)
$V_i = (F_{30\text{ ms}} - F_0)/(F_m - F_0)$	Relative variable fluorescence at the I-step (30 ms)
$M_0 = 4 (F_{300\text{ }\mu\text{s}} - F_0)/(F_m - F_0)$	Approximated initial increment (in $\text{ms}^{-1}$ ) of the relative variable fluorescence
<b>Quantum efficiencies or flux ratios</b>	
$\phi_{P_0} = \text{TR}_0/\text{ABS} = 1 - (F_0/F_m) = F_v/F_m$	Maximum quantum yield of primary photochemistry at $t = 0$
$\phi_{E_0} = \text{ET}_0/\text{ABS} = (F_v/F_m) \times (1 - V_j)$	Quantum yield for electron transport at $t = 0$
$\psi_{E_0} = \text{ET}_0/\text{TR}_0 = 1 - V_j$	Probability (at time 0) that a trapped exciton moves an electron into the electron transport chain beyond $Q_A^-$
<b>Specific energy fluxes (per <math>Q_A</math>-reducing PSII reaction center-RC)</b>	
$\text{ABS}/\text{RC} = M_0 (1/V_j)(1/\phi_{P_0})$	Absorption flux (of antenna Chls) per RC (reflecting measure for an average antenna size)
$\text{TR}_0/\text{RC} = M_0 (1/V_j)$	Trapped energy flux per RC (at $t = 0$ )
$\text{ET}_0/\text{RC} = M_0 (1/V_j) \psi_{E_0}$	Electron transport flux per RC (at $t = 0$ )
$\text{DI}_0/\text{RC} = \text{ABS}/\text{RC} - \text{TR}_0/\text{RC}$	Dissipated energy flux per RC (at $t = 0$ )
$\text{PI}_{\text{ABS}} = (\text{RC}/\text{ABS})(\phi_{P_0}/(1-\phi_{P_0})) \times (\psi_{E_0}/(1-\psi_{E_0}))$	Performance index on absorption basis

\* For review see Strasser et al. (2004).

In 2018, the energy flux theory (EFT) of biomembranes developed by Professor Dr. Reto Jörg Strasser (one of the most influential leaders in the deep understanding in application of chlorophyll *a* fluorescence) celebrates its 40<sup>th</sup> anniversary (STRASSER, 1978). We are aware of the significant contributions and influences that Professor Warren Butler and Professor Cyril Sironval had on the development of the Strasser's EFT (STRASSER AND SIRONVAL, 1972; BUTLER, 1977; BUTLER AND STRASSER, 1977; STRASSER AND BUTLER, 1978; SIRONVAL et al., 1984). An illustration of the theory basis is shown in Figure 10. The EFT has enabled Prof. Strasser to establish the theoretical background and experimental framework for developing sophisticated fluorescence analysis methods like the *JIP-test*, an interpretation of fast fluorescence transient (fast Kautsky's curves) (TSIMILLI-MICHAEL AND STRASSER, 2013).

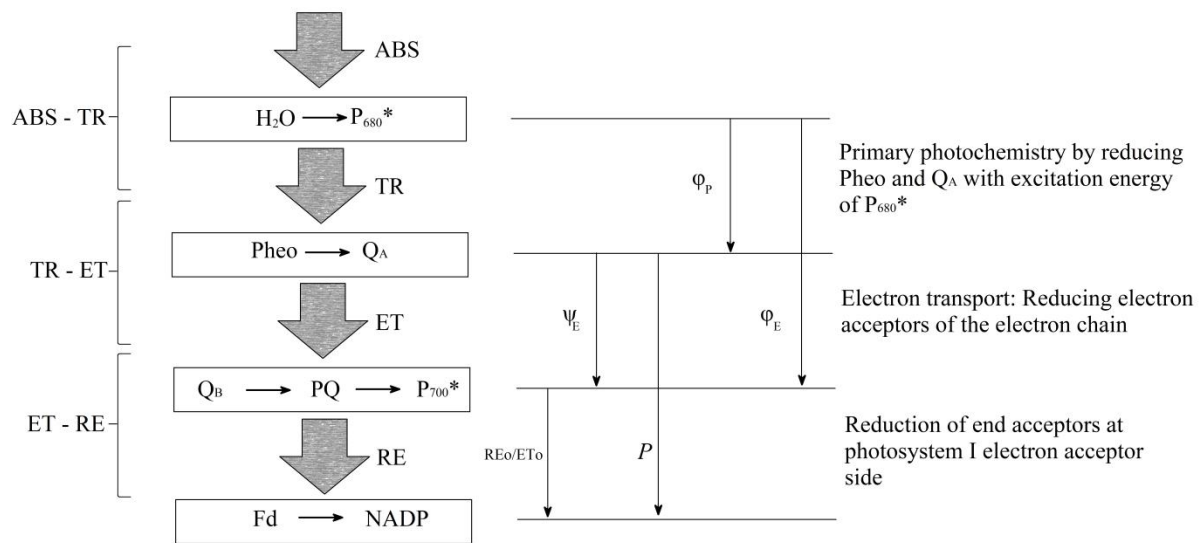


**Figure 10.** Schematic representation of the OJIP extracted information expressed in terms of sequential energy fluxes from absorbance (ABS) of photons by PSII antenna, intermediate trapping flux (TR), electron transport (ET) and the reduction of the end-electron acceptors at the PS I electron acceptor side (RE) driven by PS I.

Chlorophyll *a* fluorescence signals are exploited by an increasingly community of users. It has evolved a growing interest in the last years (e.g., > 6000 articles per year during the last 17 years; a simple research made on *Google scholar* using “chlorophyll + *a* + fluorescence + induction” as keywords shows more than 145,000 connected results), a remarkable interest already reported in details by Ripoll et al. (2016). However, biological systems showing emergent properties (non-linear interactions among the network of their components) (*see* MAZZOCCHI, 2008; LÜTTGE, 2013; SHETH AND THAKER, 2014; SOUZA AND LÜTTGE, 2015), suggest that living organisms should not be considered as a simply conglomeration of elements, but as a complex system that has integration and organization of its parts (AMZALLAG, 2001; SOUZA et al. 2016). We look forward to further developments of the EFT toward its integration into a general systems biology theory, by assuming dynamic models and connectance/complexity among their parts in a network, so that it could be applied to deepen into the study of photosynthetic energy fluxes (per cross section or per reaction center).

### 1.3. Optical spectroscopy

The electromagnetic radiation is usually divided into:  $\gamma$ -rays, x-rays (Roentgen waves), ultraviolet light, visible light, infrared, microwaves and radio waves. All of these, propagate as transverse electromagnetic waves with a same speed (speed of light,  $c = 2.99792458 \times 10^8$  ms<sup>-1</sup>) around the space in a vacuum (SOLE<sup>È</sup> et al., 2005). Table 3 show the most common spectroscopic methods based on electromagnetic radiation.

**Table 3.** Most common spectroscopy techniques based on electromagnetic radiation used in basic research.

Type spectroscopy	Wavelength range	Wavenumber (cm <sup>-1</sup> )	Quantum transition
$\gamma$ -ray emission	0.005 - 1.4 Å	---	Nuclear
X-ray absorption, emission, fluorescence and diffraction	0.1 - 100 Å	---	Inner electron
Vacuum ultraviolet (UV) absorption	10 - 180 nm	$1 \times 10^{-6}$ to $5 \times 10^{-4}$	Bonding electrons
UV-Vis absorption, emission, and fluorescence	180 - 780 nm	$5 \times 10^{-4}$ to $1.3 \times 10^4$	Bonding electrons
Infrared absorption and Raman scattering	0.78 - 300 $\mu$ m	$1.3 \times 10^4$ to $3.3 \times 10^1$	Rotation/vibration of molecules
Microwaves absorption	0.75 - 3.75 mm	13 - 27	Rotation of molecules
Electron spin resonance	3 cm	0.33	Spin of electrons in a magnetic field
Nuclear magnetic resonance	0.6 - 10 m	$1.7 \times 10^{-2}$ to $1 \times 10^3$	Spin of nuclei

\*Where: 1 Å =  $10^{-10}$  m; 1 nm =  $10^{-9}$  m; and 1  $\mu$ m =  $10^{-6}$  m. Adapted from Skoog et al., 1996.

Differences observed in electromagnetic spectrum are related to their wavelength and frequency. Monochromatic electromagnetic radiation is commonly labeled by interrelated magnitudes: frequency ( $\nu$ ), wavelength ( $\lambda$ ), wavenumber ( $\bar{\nu}$ ), or energy of photon ( $E$ ). Its correlation is given by:

$$E = h\nu$$

In terms of wavelength and wavenumber.

$$E = \frac{hc}{\lambda}$$

where  $h$  is the Planck's constant ( $6.62 \times 10^{-34}$  J.s).

The wavenumber as well as frequency, is directly proportional to energy. Electromagnetic radiation is made up of packets of energy called *photons* or *quanta*. During interactions between radiation and matter, molecules in the lowest energy state (ground state), can commonly absorbing, transmitted, reflected absorbed radiation.

### 1.3.1. UV-Vis absorption and fluorescence spectroscopy

Ultraviolet-visible (UV-Vis) molecular absorption spectroscopy (spectral range from 200-800 nm) is based on the Beer-Lambert law. According to Beer-Lambert law, the absorbed energy fraction by a sample ( $I(\lambda)$ ), depends of the incident intensity ( $I_o(\lambda)$ ), absorption coefficient of the material ( $\alpha$ ) and sample thickness (L) (HOLLER et al., 2009), and its can be correlated by following equation:

$$\frac{I(\lambda)}{I_o(\lambda)} = e^{-\alpha L}$$

For absorption process, can be assumed two simple energy level quantum system which  $N$  and  $N'$  are the ground and excited population density state, respectively (SOLE` et al., 2005). The absorption coefficient of this system is given by:

$$\alpha(\nu) = \sigma(\nu) (N - N')$$

where  $\sigma(\nu)$  is the so-called transition cross section (normally given in  $\text{cm}^2$ ) represents the ability of our system to absorb the incoming radiation of frequency  $\nu$  (SOLE` et al., 2005).

In the context of absorbance (A) we have:

$$A = \log\left(\frac{I_o(\lambda)}{I(\lambda)}\right)$$

Table 4 summarizes the regions of the spectrum. UV-Vis molecular absorption spectroscopy also provides an excellent tool with which to obtain quantitative information and characterization of some materials (organic, inorganic and biological samples), also, quantify

samples concentration in solutions, that absorbing/emitting radiation at these regions of the spectrum (SKOOG et al., 1996; HOLLER et al., 2009).

**Table 4.** The ultraviolet-visible spectrum.

Region	Wavelength range (nm)
Ultraviolet	180-400
Violet	400-435
Blue	435-480
Blue-green	480-490
Green-blue	490-500
Green	500-560
Yellow-green	560-580
Yellow	580-595
Orange	595-650
Red	650-750

Adapted from Skoog et al., 1996.

The fluorescence phenomenon is based on the principle of excitation and emission of characteristic radiation by determined materials. Excluding non-radiative mechanisms, all other forms of light emission are known as luminescence. Fluorescence spectroscopy is a method of analysis where the molecules of samples are excited by irradiation at a certain wavelength and emits radiation at a distinct wavelength. A fluorescence emission spectrum of a sample is recorded by scanning the emission monochromator for a constant excitation wavelength ( $\lambda_{ex}$ ). On the other hand, the excitation spectrum is recorded by scanning the excitation monochromator at a fixed emission wavelength ( $\lambda_{em}$ ). Absorbed light for fluorophores, which may then release their excess energy by radiative decay, producing fluorescence (light emission). This phenomenon of light emission called fluorescence and the molecules or compounds that emits fluorescence are called fluorophores. The phenomenological processes involved in fluorescence and phosphorescence emission are represented by an energy diagram referred to as Jablonski Diagram in Figure 11 (LAKOWICZ, 1999).

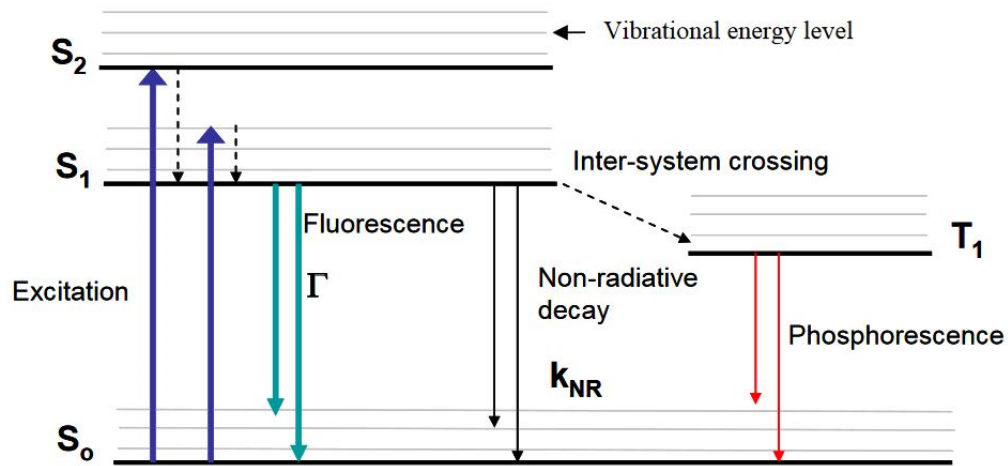


**Figure 11.** Jablonski diagram showing the energy level transitions when excitation light is absorbed and emitted by a fluorophore. Adapted from Lakowicz, 1999.

### 1.3.2. Vibrational spectroscopy

Mid-infrared spectroscopy utilizes the interaction of matter with electromagnetic radiation approximately in the spectral region of  $4000 - 400 \text{ cm}^{-1}$  (2500 - 25000 nm), which enables excitation of vibrational or vibrational/rotational transitions of molecules involving transitions from rotational and/or vibrational levels in the same ground electronic state (AVRAM AND MATEESCU, 1972; STUART et al., 1996), can be used to study the fundamental vibrations of some materials including organic, inorganic and biological substances. Examples of some basic infrared active modes are shown in Figure 12, and these modes are dependent on the type of atoms present and their structural arrangements (STUART et al., 1996; BARBOSA, 2013).



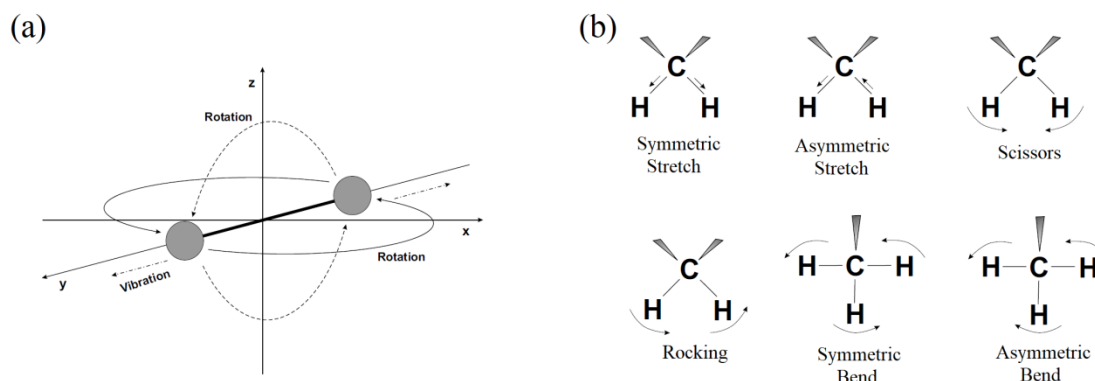


**Figure 12.** Schematic representation of vibrational modes. Adapted from Barbosa, 2013.

In general, mid-infrared spectra are measured in absorption or transmission mode with gas, liquid or solid samples, coupled with the Fourier transform algorithm (BARBOSA, 2013). Thus, is commonly called Fourier transform mid-infrared spectroscopy (FTIR). FTIR is based on the specific vibrations of sample chemical bonds corresponding to the energy levels of the molecules (vibrational levels), the photon energy is not enough to excite electrons. However, can induce vibrational movements of atoms and connected groups by means of covalent bonds (BARBOSA, 2013).

The role of FTIR spectroscopy associated with chemometric analysis in the metabolomic study has increased in the recent years, particularly applied to understanding the stress tolerance mechanisms in plant (SHARMA AND UTTAM, 2016; SHARMA et al., 2018).

Metabolite FTIR signature could lead identification of clusters of similarities and/or differences providing classification of individual plant samples upon environmental fluctuations and experimental induced factors. FTIR spectroscopy provides a snapshot of metabolic and biochemical composition of biological samples, it can be compared with conventional techniques without the necessity of extraction procedures or sample preparation.

## 1.4. Engineered nanomaterials

### 1.4.1. What is and why study nanoscience and nanotechnology?

Nanoscience refers to the study, engineering and manipulation of matter, particles and several structures on the nanometer scale (materials in the order of  $10^{-9}$  m). In nanoscale size, specific properties of diverse materials, such as the electrical, optical, thermal and mechanical properties are often different from on macro scale, due to quantum mechanical effects (QME) become important at this scale. Engineered nanomaterials (NMs) shows a large range of benefit than bulk materials because of their unique physical-chemical properties and characteristics; *i.e.* high surface area in relationship to volume ratio, small size, shape, optical properties and functional groups (SCHRAND et al., 2010).

Nanotechnology are the design and application of nanoscience to the use of new NMs nanoparticles (NPs) and nanosized components in useful products and process. However, the fast-growing economy in this modern research field requires a multidisciplinary scientific background to provide new products, methods and technologies. Recently, nanotechnology and nanoscience have received a great attention due to their applications in a wide range of technological fields, including agriculture, health, industry, electronics, energy, and commerce. Its results in a significantly increase in the development and applications of NMs (HANSEN et al., 2016; MEDINA-VELO et al., 2017; GIESE et al., 2018). Consequently, an increase in engineered waste in nanometric scale can be expected.

### 1.4.2. Classification of nanoparticles: natural and anthropogenic

According to their source and composition NPs can be classified in three main classes: natural, incidental and engineered (Figure 12). Natural NPs have been presented in the natural environment as results of natural sources such as vulcanoes, aerosols or soil minerals (HANDY et al., 2008). Incidentals indirectly result from human activities such as burning coal and diesel exhaust (MONICA AND CREMONINI, 2009). On the other hand, engineered NPs show different characteristics compared to their bulk form, and this NPs may be chemical, thermo/electrical or biogenic synthesized for a range of proposes.

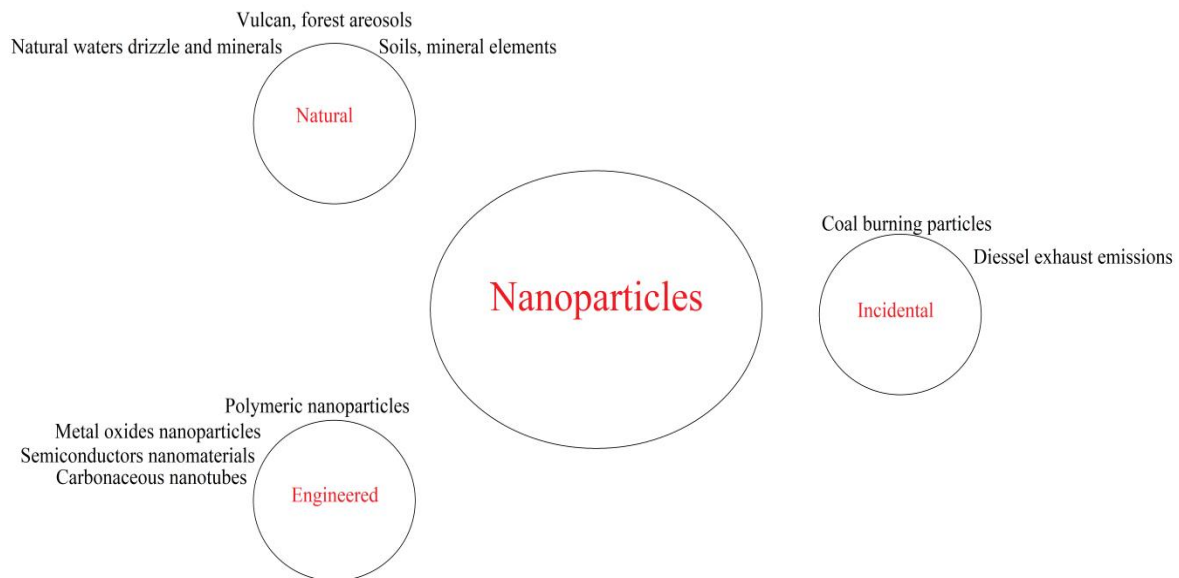


**Figure 13.** Types of natural, incident, and engineered nanoparticles.

#### 1.4.3. Potential risks of nanoparticles on the photosynthetic organisms

Possible risk assessment must be evaluated to elucidate all relevant aspects of NMs impact on ecosystems. Nanotechnology and its application have become a key point of discussion related to their environmental impact. Nanoparticles release into the environment may occur over short or long time periods, once released can be in their original form (as a single or large particle forms) or may undergo changes in their physic-chemical characteristics, with possible toxic effects to natural ecosystems (WHATMORE, 2006; BOUR et al., 2015).

Photosynthetic organisms are highly sensitive to metallic and metal oxide nanoparticles. At present, several works reports increment likely to negative impact on plant germination, growth, development, photosynthetic metabolism and productivity in oxygenic photosynthetic organisms. However, little information is available its impacts induced by their uptake at the photosynthetic bioenergetic metabolism, particularly, associated with photochemical electron transport reactions. Therefore, it becomes relevant to evaluate and monitoring the potential impact of these nanostructured materials on the photosynthetic apparatus.

### 1.5. Aim

It is hypothesized that engineered nanomaterials may be internalized by leaves and intervene at photosynthetic level in aquatic organisms. Due to low information available related to the impacts induced by NPs at the photosynthetic energy transfer, the main aim of this dissertation is understanding the impact of metal oxide nanoparticles on photosynthetic apparatus. Two NPs are used in our study, cerium oxide nanoparticles and copper oxide nanoparticles. Due to the increased demand for these two nanomaterials in modern technologies.

### 1.6. References

AMZALLAG, G.N. Data analysis in plant physiology: are we missing the reality? **Plant Cell and Environment**. v.24, p.881-890, 2001.

APOSTOL, S.; BRIANTAIS, J.M.; MOISE, N.; CEROVIC, Z.G.; MOYA, I. Photoinactivation of the photosynthetic electron transport chain by accumulation of over-saturating light pulses given dark adapted pea leaves. **Photosynthesis Research**. v.67, n.3, p.215-227, 2001.

AVRAN, M.; MATEESCU, G.D. **Infrared spectroscopy: applications in organic chemistry**. 1<sup>st</sup> ed. Wiley-Interscience, 1972. P.527.

BARBER, J.; ANDERSON, B. Revealing the blueprint of photosynthesis. **Nature**. v.370, p.31-34, 1994.

BARBER, J.; NIELD, J.; MORRIS, E.P.; ZHELEVA, D.; HANKAMER, B. The structure, function and dynamics of photosystem II. **Physiologia Plantarum**. v.100, p.817-827, 1997.

BILGER, H.W.; SCHEREIBER, U.; LANGE, O.L. Determination of leaf heat resistance: comparative investigation of chlorophyll fluorescence changes and tissue necrosis methods. **Oecologia**. v. 63, p. 256-262, 1984.

BILGER, W.; BJÖRKMAN, Q. Role of the xanthophyll cycle in photoprotection elucidated by measurements of light-induced absorbance changes, fluorescence and photosynthesis in leaves of *Hedera canariensis*. **Photosynthesis Research**. p.25, n.3, p.173– 185, 1990.

BLANKENSHIP, R.E. **Molecular mechanisms of photosynthesis**. 2nd Ed. Wiley-

Blackwell, Oxford, UK. 2014. 312p.

BOLHÀR-NORDENKAMPF, H.R.; ÖQUIST, G. Chlorophyll fluorescence as a tool in photosynthesis research. In. HALL, D.O.; SCURLOCK, J.M.O.; BOLHÀR-NORDENKAMPF, H.R.; LEEGOOD, R.C.; LONG, S.P. (Ed.) **Photosynthesis and production in a changing environment: a field and laboratory manual**. Springer, Dordrecht, Germany. 1993. p193-206p.

BOUR, A.; MOUCHET, F.; SILVESTRE, J.; GAUTHIER, L.; PINELLI, E. Environmentally relevant approaches to assess nanoparticles ecotoxicity: a review. **Journal of Hazardous Materials**. v.283, p. 764-777, 2015.

BRARBOSA, L.C.A. Espectroscopia no infravermelho na caracterização de compostos orgânicos. 1<sup>st</sup> ed. Viçosa-MG. Editora UFV. 2013. p.189.

BRICKER, T.M.; ROOSE, J.L.; FAGERLUND, R.D.; FRANKEL, L.K.; EATON-RYE, J.J. The extrinsic proteins of photosystem II. **Biochimica et Biophysica Acta: Bioenergetics**. v.1817, p.121-142, 2012.

BUKJOV, N.G.; SABAT, S.C.; MOHANTY, N. Analysis of chlorophyll *a* fluorescence changes in weak light in heat treated *Amaranthus* chloroplasts. **Photosynthesis Research**. v.23, p.81-87, 1990.

BUTLER, W.L. Energy distribution in the photochemical apparatus of photosynthesis. Annual Review in Plant Physiology. v.29, n. 6, p.345-378, 1977.

BUTLER, W.L.; STRASSER, R.J. Tripartite model for the photochemical apparatus of green plant photosynthesis. **Proceedings of the National Academy of Sciences PNAS**. v.74, n.8, p.3382-3385, 1977.

COPPER, G.M. **The Cell: a molecular approach**. 6th Edition. Sinauer Associates: Sunderland, MA. 2013. 864p.

CROCE, R.; AMERONGEN, H.V. Natural strategies for photosynthetic light harvesting. **Nature Chemical Biology**. v.10, n.7, p.492-501, 2014

DEKKER, J.P.; VAN-GRONDELLE, R. Primary charge separation in photosystem II. **Photosynthesis Research**. v.63, p.195-208, 2000.

- DUYSENS, L.N.M; SWEERS, H.E. mechanisms of two photochemical reactions in algae as studied by means of fluorescence. In. ASHIDA, J. (Ed) **Studies on microalgae and photosynthetic bacteria**. Tokyo: Tokyo University Press. 1963. p.353-372.
- GIESE, B.; KLAESSIG, F.; PARK, B.; KAEGI, R.; STEINFELDT, M.; WIGGER, H.; et al. Risks, release and concentrations of engineered nanomaterials in the environment. **Scientific Reports**. v.8, 1565.
- GLAZER, A.N. Phycobilisome a macromolecular complex optimized for light energy transfer. **Biochimica et Biophysica Acta: Reviews on Bioenergetics**. v.768, p.29–51, 1984.
- GOVINDJEE, BJORN, L.O.; NICKELSON, K. Evolution of the Z-scheme of electron transport in oxygenic photosynthesis. In: (LU, C. ed) **Photosynthesis research for food, fuel and future**. 15<sup>th</sup> International Conference on Photosynthesis, Symposium: Education Session: University Press, Springer-Verlag GmbH, Zhejiang, 2012. pp. 835-841.
- GOVINDJEE, SHEVELA, D.; BJORN, L.O. Evolution of the Z-scheme of photosynthesis: a perspective. **Photosynthesis Research**. v.133, p.5-15, 2017.
- HANDY, R.D.; OWEN, R.; VALSAMI-JONES, E. The ecotoxicology of nanoparticles and nanomaterials: current status, knowledge gaps, challenges, and future needs. **Ecotoxicology**. v.17, p.315-325, 2008.
- HANSEN, S.F.; HEGGELUND, L.R.; BESORA, P.R; MACKEVICA, A.; BOLDRIN, A.; BAUN, A. Nanoproducts – what is actually available to European consumers? **Environmental Science: Nano**. v.3, p.139-180, 2016.
- HANSON, L.K. Chlorophylls. In: (SCHEER, H. Ed.) **Chlorophylls**. CRC Press, FL, 1991, p. 994
- HOFF, A.J.; AMESZ, J. Chlorophylls, In: (SCHEER, H. Ed.) **Chlorophylls**. CRC Press, FL, 1991, p. 724.
- HOLLER, F. J.; SKOOG, D. A.; CROUCH, S. R. **Princípios de análise instrumental**. 6. ed. Porto Alegre: Bookman, 2009. 1055 p
- KALAJI, M.H.; GOLTSEV, V.N.; ŽUK-GOŁASZEWSKA, K.; ZIVCAK, M.; BRESTIC, M. **Chlorophyll fluorescence: understanding crop performance - basics and applications**; 1<sup>st</sup> Ed. CRC Press, T&F Group: Abingdon, UK, 2017; p. 222.
- Kautsky, H. and Hirsch, A. 1931.

- KAUTSKY, H.; HIRSCH, A. Neue Versuche zur Kohlensäureassimilation. **Naturwissenschaften**. v.19, n. 48, p.964–964, 1931.
- KRAUSE, G.H.; JAHNS, P. Non-photochemical energy dissipation determined by chlorophyll fluorescence quenching: Characterization and function. In: PAPAGEORGIOU, G.C.; GOVINDJEE **Chlorophyll a Fluorescence: A Signature of Photosynthesis**, Dordrecht: Springer. 2004 p.463–495.
- KUCZYNSKA, P.; JEMIOŁA-RZEMINSKA, M.; STRZALKA, K. Photosynthetic pigments in diatoms. **Marine Drugs**. v.3, p.5847–5881, 2015.
- LAKOWICZ, J.R. **Principles of fluorescence spectroscopy**. 2<sup>nd</sup> ed. (Kluwer Academic Plenum, New York, 1999).
- LARKUM, A.W.D.; BARRETT, J. Light-harvesting Processes in Algae. **Advances in Botanical Research**, v.10, p.1-219, 1983.
- LÜTTGE U. Whole-plant physiology: synergistic emergence rather than modularity. - In: LÜTTGE. U.; BEYSCHLAG, W.; FRANCIS, D.; CUSHMAN, J. (eds) **Progress in Botany (Genetics - Physiology - Systematics - Ecology)**, vol 74, Springer, Berlin, Heidelberg 2013. p.165-190.
- MALDONADO-RODRIGUEZ, R.; PAVLOV, S.; GONZALEZ, A.; OUKARROUM, A. STRASSER, R.J. Can machines recognize stress in plants? **Environmental Chemistry Letters**. v.1, n3, p.201-205, 2003.
- MAZZOCCHI, F. Complexity in biology. Exceeding the limits of reductionism and determinism using complexity theory. **EMBO Reports**. v.9, p.10–14, 2008.
- MEDINA-VELO, I.A.; PERALTA-VIDEA, J.R.; GARDEA-TORRESDEY, J.L. Assessing plant uptake and transport mechanisms of engineered nanomaterials from soil. **MRS Bulletin**. v.42, p.379-383, 2017.
- MISRA, A.N.; MISRA, N.; SINGH, R. Chlorophyll fluorescence in plant biology. In: Misra, A.N. (Ed) **Biophysics**. InTech, 2012. 171-192 p.
- MONICA, R.C.; CREMONINI, R. Nanoparticles and higher plants. **Caryologia**. v.62, p.161-165, 2009.
- NELSON, N.; YOCUM, C.F. Structure and function of photosystem I and II. **Annual Review in Plant Biology**. v.57, p.521-565, 2006.



- PAINTER, P.C.; COLEMAN, M.M.; KOENING, J.L. **Theory of vibrational spectroscopy and its application to polymeric materials.** John Wiley and Sons, Inc., New York. 1982.
- RABINOWITCH, E.; GOVINDJEE. **Photosynthesis.** John Wiley and Sons Inc. New York, 1969. 273p.
- RIPOLL, J.; BERTIN, N.; BIDEI, L.P.R.; URBAN, L. A user's view of the parameters derived from the induction curves of maximal chlorophyll *a* fluorescence: perspectives for analyzing stress. **Frontiers in Plant Science.** v.7, p.1679-1684, 2016.
- SANTIAGO, E.F.; LARENTIS, T.C.; BARBOSA, V.M.; CAIRES, A.R.L.; MORAIS, G.A.; SÚAREZ, Y.R. Can the chlorophyll-a fluorescence be useful in identifying acclimated young plants from two populations of *Cecropia pachystachya* Trec. (Urticaceae), under elevated CO<sub>2</sub> concentrations? **Journal of Fluorescence.** v.25, p.49-57, 2015.
- SCHANSKER, G.; TÓTH, S.Z.; STRASSER, R.J. Methylviologen and dibromothylmoquinone treatments of pea leaves reveal the role of photosystem I in Chl *a* fluorescence rise OJIP. **Biochimica et Biophysica Acta A. Bioenergetics.** v.1706, p.250-261, 2005.
- SCHRAND, A.M.; RAHMAN, M.F.; HUSSAIN, S.M.; SCHLAGER, J.J.; SMITH, D.A.; SYED, A.F. Metal-based nanoparticles and their toxicity assessment. **Wiley Interdisciplinary Reviews in Nanomedicine and Nanobiotechnology.** v.2, n.5, p.544-568, 2010.
- SCHREIBER, U. Detection of rapid induction kinetics with a new type of high-frequency modulated chlorophyll fluorometer. **Photosynthesis Research.** v.9, p.261-272, 1986.
- SCHREIBER, U.; ARMOND, P.A. Heat-induced changes of chlorophyll fluorescence in isolated chloroplasts and related heat-damage at the pigment level. **Biochimica et Biophysica Acta.** v. 502, p. 138-151, 1978.
- SHARMA S, UTTAM KN. Investigation of the manganese stress on wheat plant by attenuated total reflectance Fourier transform infrared spectroscopy. **Spectroscopy Letters.** v.49, p.520-28, 2016.
- SHARMA, S.; UTTAM, R.; SINGH, P.; UTTAM, K.N. Detection of vibrational spectroscopy biomarkers of the effect of gold nanoparticles on wheat seedlings using attenuated total



reflectance Fourier transform infrared spectroscopy. **Analytical Letters**. v.51, n.14, p.2271-2294, 2018

SHETH, B.P.; THAKER, V.S. Plant systems biology: insights, advances and challenges. **Planta**. v.240, p.33–54, 2014.

SIRONVAL, C.; STRASSER R.J.; BROUERS, M. The bioenergetic description of light energy migration in photoactive membranes; equivalence between the theory of the energy fluxes and the theory of the proportion of pigments forms to total pigments. In: SIRONVAL, C.; BROUERS M. (eds) **Protochlorophyllide Reduction and Greening. Advances in Agricultural Biotechnology**, Springer, Dordrecht, Martinus Nijhoff, The Hague 1984. p.307-316.

SKOOG, D.A.; WEST, D.M.; HOLLER, F. J. **Fundamentals of analytical chemistry**. 7<sup>a</sup>ed. Fort Worth: Saunders College, 1996.

SOLÉ, J.G.; BAUSÁ, L.E.; JAQUE, D. **An introduction to optical spectroscopy of inorganic solids**. John Wiley and Sons, Ltd. West Sussex, England, 2005. p.306.

SOUZA, G.M.; LÜTTGE, U. Stability as a phenomenon emergent from plasticity–complexity–diversity in eco-physiology. - In: LÜTTGE, U.; BEYSCHLAG W. (eds) **Progress in Botany (Genetics - Physiology - Systematics - Ecology)**, vol 76. Springer, Cham 2015. Pp 211–239.

SOUZA, G.M.; PRADO, C.H.B.A., RIBEIRO, R.V. et al. Toward a systemic plant physiology. **Theoretical and Experimental Plant Physiology**. v.28, n.4, p.341-346, 2016.

STIRBET, A.; RIZNICHENKO, G.Y.; RUBIN, A.B.; GOVINDJEE. Modeling chlorophyll a fluorescence transient: relation to photosynthesis. **Biochemistry**. v.79, p.291–323, 2014.

STRASSER, R.J. The grouping model of plant photosynthesis. In: AKOYUNOGLU, G.; ARGYROUDI-AKOYUNOGLU, J.H. (eds) **Chloroplasts development**. Elsevier/North Holland Biomedical Press, Amsterdam, 1978. p.513-524.

STRASSER, R.J.; BUTLER, W.L. Energy transfer and distribution of excitation energy in the photosynthetic apparatus of spinach chloroplasts. **Biochimica et Biophysica Acta A. Bioenergetics**. v.460, p.230-238, 1977.

STRASSER, R.J.; SIRONVAL, C. Induction of photosystem II activity in flashed leaves. **FEBS letters**. v.28, p.55-60, 1972.

STRASSER, R.J.; SRIVASTAVA, A.; GOVINDJEE. Polyphasic chlorophyll *a* fluorescence transient in plants and cyanobacteria. **Photochemistry and Photobiology**. v.61, p.32-42, 1995.

STRASSER, R.J.; SRIVASTAVA, A.; TSIMILLI-MICHAEL, M. Analysis of the chlorophyll *a* fluorescence transient. In: PAPAGEORGIO, G.C.; GOVINDJEE (Eds.). **Chlorophyll *a* Fluorescence: A Signature of Photosynthesis. Advances in Photosynthesis and Respiration**. Springer, Dordrecht, 2004. pp. 321–362.

STRASSER, R.J.; SRIVASTAVA, A.; TSIMILLI-MICHAEL, M. The fluorescence transient as a tool to characterize and screen photosynthetic samples. In (YUNUS, M.; PATHRE, U.; MOHANTY, P. (ed)): **Probing Photosynthesis: Mechanism, Regulation and Adaptation**. Taylor and Francis, UK, 2000. pp. 445–483.

STRASSER, R.J.; TSIMILLI-MICHAEL, M. QIANG, S.; GOLSTEV, V. Simultaneous in vivo recording of prompt and delayed fluorescence and 820-nm reflection changes during drying and after re-hydration of the resurrection plant *Haberlea rhodopensis*. **Biochimica et Biophysica Acta: Bioenergetics**.v.1797, n.(6-7), p.1313-1326, 2010.

Stribet A, Riznichenko YG, Rubin AB, Govindjee. (2014) Modeling chlorophyll *a* fluorescence transient: relation to photosynthesis. *Biochemistry* 79(4): 291-323.

STRIBET, A.; RIZNICHENKO, Y.G.; RUBIN, A.B.; GOVINDJEE. Modeling chlorophyll *a* fluorescence transient: relation to photosynthesis. **Biochemistry**. v.79, n.4, p.291-322, 2014

STUART, B.; GEORGE, W.O.; McINTYRE, P.S. **Modern infrared spectroscopy**. 1<sup>st</sup> ed. New York, John Wiley and Sons Ltd. 1996. p.180.

TREBST, A. Dynamics in photosystem II structure and function. In: SCHULZE, E.D.; CALDWELL, M.M (Eds). **Ecophysiology of photosynthesis**. Springer: Germany. 1994. 579p.

TSIMILLI-MICHAEL, M.; STRASSER R.J. The energy fluxes theory 35 years later: formulations and applications. **Photosynthesis Research**. v.117, p.289-320, 2013.

WALSBY, A.E. The extracellular products of *Anabaena cylindrica* Lemn. I. Isolation of macromolecular pigment-peptide complex and other components. **British Phycology**

**Journal.** v.9, n.4, p.371-381, 1974.

WEIS, E.; BERRY, J.A. Quantum efficiency of photosystem II in relation to energy-dependent quenching of chlorophyll fluorescence. **Biochimica et Biophysica Acta.** v.894, n.2, p.198-208, 1987.

WHATMORE, R.W. Nanotechnology – what is it? Should we be worried? **Occupational Medicine.** v.56, p.295-299, 2006.

WITT, H.T. Primary reactions of oxygenic photosynthesis. **Berichte der Bunsengesellschaft für physikalische Chemie.** v.100, p.1923±1942, 1996.

YUSUF, M.A.; KUMAR, D.; RAJWANSHI, R.; STRASSER, R.J.; TSIMILLI-MICHAEL, M.; GOVINDJEE.; SARIN, N.B. Overexpression of  $\gamma$ -tocopherol methyl transferase gene in transgenic *Brassica juncea* plants alleviates abiotic stress: Physiological and chlorophyll a fluorescence measurements. **Biochimica et Biophysica Acta A. Bioenergetics,** v.1797, p.1428-1438, 2010.



**CHAPTER II – ENVIRONMENTALLY FRIENDLY SYNTHESIS OF  
COLLOIDAL COPPER OXIDE NANOPARTICLES: ANTIOXIDANT,  
ANTIMICROBIAL ACTIVITY AND *IN VITRO* TOXICITY**

## Environmentally friendly synthesis of nanocolloidal copper oxide: antioxidant, antimicrobial activity and phototoxicity

Montcharles da Silva Pontes<sup>1</sup>, Renato Grillo<sup>2</sup>, Anderson Rodrigues Lima Caires<sup>3</sup>, Luís Humberto da Cunha Andrade<sup>1</sup>, Etenaldo Felipe Santiago<sup>1\*</sup>

<sup>1</sup> Natural Resources Program, Center for Natural Resources Studies (CERNA), Mato Grosso do Sul State University (UEMS), Dourados, Mato Grosso do Sul, 79804-970, Brazil.

<sup>2</sup> Department of Physics and Chemistry, School of Engineering, São Paulo State University (UNESP), Ilha Solteira, São Paulo, 15385-000, Brazil.

<sup>3</sup> Optics and Photonics Group, Institute of Physics, Federal University of Mato Grosso do Sul (UFMS), Campo Grande, 79070-900, Brazil.

\*Correspondence author: Prof. Dr. Etenaldo Felipe Santiago

felipe@uems.br

### ABSTRACT

The development of ecofriendly green synthesis of nano-colloids has been growing in the last years, offering not only a reliable way to fabricate nanomaterials, but also reducing the use, and generation of hazardous substances to human health and environment. This paper reports the synthesis of copper oxide nanoparticles (CuONPs) synthesized by green synthetic process at room temperature using *Ilex paraguariensis*'s leaves extract as an efficient reduction/oxidizing agent. The structural and morphological properties of CuONPs were investigated using ultraviolet-visible absorption spectral studies (UV-Vis), Fourier transform-Infrared spectroscopy (FTIR-PAS), scanning electron microscopy (SEM) and energy dispersive spectroscopy (EDS). An intense surface Plasmon resonance between 250-300 nm in the UV-vis spectrum clearly reveals the formation of CuONPs. The FTIR-PAS spectroscopy results reveal the occurrence of functional groups required for the reduction of copper ions. The results of SEM exhibited that the green synthesized copper oxide nanoparticles are spherical with an average particle size of ca. 130 nm. In addition, EDS shows that the nanoparticles consist of Cu. Furthermore, these green synthesized CuONPs effectively act as a potent antimicrobial agent for *Candida albicans*. Also, biogenic CuONPs showed a high antioxidant activity, despite *in vitro* toxicity was observed to light-harvesting protein phycocyanin. In this way, this ecofriendly synthesis method may reduce harmful side effects of the CuONPs in the environment and human health as well as applied as a new tool for antibacterial and antioxidant application.

**Keywords:** Green synthesis; Copper oxide; nanostructures; *Ilex paraguariensis*

## RESUMO

O desenvolvimento sustentável de nanopartículas coloidais, obtidas por meio da química verde tem crescido nos últimos anos, oferecendo não só uma metodologia confiável para síntese de novos nanomateriais, mas também atuando na redução de resíduos e geração de substâncias nocivas para a saúde humana e ambientes naturais. Neste trabalho, relata-se a síntese de nanopartículas de óxido de cobre (CuONPs) sintetizadas pelo processo de síntese verde em temperatura ambiente utilizando extrato foliar de *Ilex paraguariensis* (erva mate) como agente redutor/oxidante. As propriedades estruturais e morfológicas das CuONPs foram avaliadas por meio da espectroscopia de absorção ultravioleta-visível (UV-Vis), espectroscopia de transformada de Fourier-Infravermelho (FTIR-PAS), microscopia eletrônica de varredura (MEV) acoplada a espectroscopia de energia dispersiva (EDS) e microscopia de força atômica (MFA). A banda espectral entre 250-300 nm no espectro UV-Vis evidencia claramente a formação das CuONPs. Os resultados da espectroscopia FTIR-PAS revelam a ocorrência de grupos funcionais relacionados a redução de íons cobre. Os resultados do MEV mostraram que as nanopartículas de óxido de cobre sintetizadas apresentam uma tendência a serem esféricas com um tamanho médio na gama de ca. 130 nm, os dados do EDS revelam que as nanopartículas apresentam Cu em sua constituição. Além disso, foram observados a capacidade destas nanopartículas atuarem como um potente agente antimicrobiano para cepa *Candida albicans*, assim como, uma alta atividade antioxidante foi observada, embora tenha sido relatada possível toxicidade *in vitro* para a proteína ficocianina.

**PALAVRAS-CHAVE:** Síntese verde; Óxido de cobre; nanoestruturas; *Ilex paraguariensis*

## 1. Introduction

Metal oxide nanoparticles (MONPs) are promising materials for biological applications due to their physicochemical properties (KATWAL et al., 2015; KHASHAN et al., 2016). MOPs may present a useful and advantageous range of applications, including targeted drug delivery, diagnosis, imaging, cosmetics, and nanosensors (BHATTACHARYA & GUPTA, 2005). Among the MONPs, copper oxide nanoparticles (CuONPs) are highlighted due to their antibacterial, antioxidant, photocatalytic, and photovoltaic properties (BHATTACHARYA & GUPTA, 2005; KHASHAN et al., 2016).

Several different techniques can be used to obtain CuONPs, such as metal vapor synthesis (GIOVANNI et al., 2002), laser irradiation (YEH et al., 1999), thermal reduction (DHAS et al., 1998), and chemical reduction (SONG et al., 2011), obtaining different dimensions, morphologies, and structures; the most widely used are the chemical techniques because their easy preparation procedures. However, a large amount of hazardous chemicals residues is generated during their synthesis procedures (GUILGER et al., 2017). Additionally, it is important to stress that despite the beneficial application of CuONPs, their extensive industrial, technological, and commercial applications have raised concerns about their environmental safety and human health effects.

Recently, with increasing development of sustainable and green technologies, nano-scientists have been focused on development of ecofriendly and biocompatible nanomaterial synthesis in green chemistry (GUILGER et al., 2017; RHEDER et al. 2018). The green synthesis of CuONPs offers not only a reliable way to fabricate engineered nanomaterials, but also reducing the use, and possible generation of hazardous substances to human health and environment (JADHAV et al., 2018). The increased use of CuONPs, by incorporating into several commercial products (for instance, personal care and household products), have instigated a large production and use of these NPS day by day. In 2010, at around 200 metric tons of nanoparticles containing Cu and CuO were produced (KELLER & LAZAREVA, 2014), while over 300 tons of CuONPs were manufactured only in the United States of America in 2014 (MASHOCK et al., 2016).

The use of plant systems to synthesize CuONPs has heightened attention as an alternative ecofriendly and cost-effective method when compared with physical and chemical

methods. The presence of phytochemical compounds in plant extracts can act as a capping and reducing agents to synthesis of nanomaterials (IRAVANI, 2011; JADHAV et al., 2018). Plant can mediate the synthesis of CuONPs due to its metabolite compounds like alkaloids, polyphenols, starch, sugars, phenolic acids, terpenoids, and proteins, which play a major role on the bio-reduction of metal ions and, consequently, forming nanoparticles (IRAVANI, 2011).

*Ilex paraguariensis* St.- Hil (Aquifoliaceae), commonly known as Yerba Mate (YM), is traditionally manufactured and widely consumed as an infusion (cold or hot) in countries such as Argentina, Brazil, Paraguay, and Uruguay (BRACESCO et al., 2011). Studies on biological synthesis of CuONPs using plant extracts have been increasing. However, to the best of our knowledge, there is no study about the use of YM leaf extract as stabilizing and reducing agent for green mediated copper nanoparticles synthesis. Thus, a better understanding of biocompatible nanomaterial synthesis methodologies may contribute to the industry sector, as well as to minimize the hazardous residues generated during nanoparticles production. High concentrations of bioactive phytochemical compounds in YM, such as phenolic compounds (gallic acid, gallocatechin and chlorogenic acid), methylxanthines (theobromine and caffeine), flavonoids (rutin and quercetin) and saponin (BRAVO et al., 2007; HECK & MEJIA, 2007), are the responsible for their properties as stabilizing and reducing agent for nanoparticles synthesis. The YM leaf extract has been used as an interesting coating natural material to expand magnetic nanoparticles application (MERCADO et al., 2018). Silver nanoparticles (AgNPs) were also obtained using YM extract, the YM acted simultaneously as a reducing and stabilizing agent to the effective formation of AgNPs (SILVEIRA et al., 2018).

Ecofriendly synthesized nanoparticles have been applied in a large field, particularly due to their biological activity, such as antibacterial and antifungal properties (GUILGER et al., 2017; RHEDER et al. 2018), also some nanomaterials are widely applied in the field of catalysis (ELANGO & ROOPAN, 2015). However, the increasing production and utilization of nanoparticles may result in the release into the environment. The potential hazardous effects of engineered metal nanoparticles should be monitored due to their toxic action by using *in vivo* and *in vitro* assays (FALCO et al., 2011; CAIRES et al., 2013; QUEIROZ et al.,



2016; MADHAV et al., 2017; ZSIROS et al., 2018). Based on *in vitro* methods, several authors study the interaction between nanomaterials and proteins or photosynthetic pigments by means of spectroscopic studies (QUEIROZ et al., 2016; TAHARA et al., 2016), aiming to determine the alterations on the optical behavior of the pigments or proteins induced by nanomaterials, and, consequently, their potential impact on photosynthetic activity of plants. Some studies of algae and cyanobacteria have also reported the toxicity of CuONPs (MELEGARI et al., 2013; ZHAO et al., 2016; CHE et al., 2018). Yet no specific research has been conducted to evaluate the toxicity of CuONPs to phycocyanin.

In this context, the present study aimed to perform a close investigation about the use of YM as a reducing and stabilizing agent for nanostructured copper synthesis, as well as to evaluate its biological activity, and the potential impact of these nanoparticles on the optical and structural properties of the phycocyanin; an important pigment-protein complex from the light-harvesting phycobiliprotein family. Thus, the present investigation contributes to elucidate the potential impacts that CuONPs may cause on environment.

## 2. Experimental

### 2.1. Material and synthesis of copper oxide nanoparticles

The leaves of the wild YM were collected from their local region (Dourados, Mato Grosso do Sul, Brazil). Their phytochemical activity is basically due to presence of phenolic compounds (gallic acid, galocatechin and chlorogenic acid), methylxanthines (theobromine and caffeine), flavonoids (rutin and quercetin) and saponin (BRACESCO et al., 2011).

The YM leaves were thoroughly washed using normal water, followed by distilled water. Intended for the synthesis of CuO nanoparticles, YM leaves were washed systematically with deionized water and shadow dried for 16 days. The dried leaves were powdered using a mixer grinder. Formerly, 10 g of powder dispersed in 100 mL of deionized water in an Erlenmeyer flask followed by boiling at 60 °C for 10 min. After bringing back to room temperature, the extract filtered using Whatman No. 1 filter paper and the filtrate was stored at 4°C until further use. Meant for copper oxide nanoparticles synthesis 90 mL of 5 mM cupric sulphate ( $\text{CuSO}_4 \cdot 5\text{H}_2\text{O}$  from Sigma–Aldrich) solution was mixed with 10 mL of

leaves extract and allow to stand at room temperature until further color change occurs (ca. 20 minutes).

An indicator for synthesis of nanoparticles the color change was compared with (leaf extract and 5 mM Copper sulphate) control solution using UV-Vis spectrophotometer analysis. The obtained precipitation was purified by repeated centrifugation at 12000 rpm for 20 min, dried in oven at 80°C and stored in properly containers. For optical characterization and biological assays, CuONPs was diluted in aqueous buffer. In all analysis performed, the CuONPs were suspended in a dilute aqueous citrate buffer ( $10^{-1}$ M) for stabilizing nanoparticles and to prevent aggregation.

## 2.2. Nanoparticle Characterization

### 2.2.1. Scanning electron microscopy (SEM), energy dispersive spectroscopy (EDS) and Atomic Force Microscopy (AFM)

Scanning electron microscopy (SEM) was performed in order to investigate the morphology and size distribution of the CuO nanoparticles. Nanoparticles suspensions were diluted (1:100), dried in a silicon grids and analyzed by scanning electron microscopy (EVO-LS-15, Carls Zeiss). SEM was operated at 15 kV of high voltage with a spot size between 3.0-4.0 and working distance (WD) of 8.5 mm. The energy dispersive X-ray spectroscopy (EDS) analysis was performed using an Apollo X Silicon Drift Detector (EDXA, USA). Size distribution histogram of the CuONPs was calculated using ImageJ and GraphPad Prism 7.0 software, and approximately 100 nanoparticles were counted in each study. The shape factors size and perimeter were estimated, after SEM measurement, using ImageJ software (100 nanoparticles were counted) by analogy with a sphere of same geometric mean diameter (MOHSENIN, 1986; IGATHINATHANE et al., 2008).

The atomic force microscopy (AFM) analysis was performed using a Nano-R Atomic Force Microscope (Pacific Nano Technology Inc., USA). Images were obtained in tapping mode, in ambient conditions, and nanoparticles suspensions diluted (1:200, v/v) were deposited on a silicon surface for AFM measurements that had been previously cleaned and dried. Typical scan rates were in the range of 0.5 – 1.0 kHz at  $500 \times 500$  pixels and  $1.000 \times 1.000$  pixels, with a scan speed between 1 and  $5\mu\text{m/s}$ . The raw data obtained from the

microscope were processed by using the modular multiplatform Gwyddion (v. 2.49) open source software and plane leveling algorithm, following by a post-processing with ImageJ software with Open\_MI plugin and WSxM software (v5.0).

### 2.2.2 X-ray diffraction (XRD) pattern

The XRD pattern was obtained using an X-ray diffractometer XRD-6000 (Shimadzu Corp.), Bragg-Brentano geometry, with Cu K $\alpha$  radiation (1.54056 Å) was used to study of size and crystalline structure of the particles. The average crystalline size of the CuONPs was estimated from the Debye-Scherrer's equation ( $D = 0.9\lambda/\beta \cos \theta$ ), where  $\lambda$  is wavelength of X-rays (1.5409 Å),  $\beta$  is the full width at half maximum of the diffraction peak (in radians) and  $\theta$  is the Bragg angle, respectively.

### 2.2.3. Ultraviolet-visible absorption spectroscopy

For the study optical properties of CuONPs photosynthesized, ultraviolet-visible (UV-Vis) spectra were obtained by a UV-Vis spectrophotometer Cary 50, Varian. The UV-Vis absorption spectrophotometer had a pulsed xenon lamp, a 0.25 m Czerny-Turner monochromator and a Si diode detector, measurements were performed using a quartz sample holder with two polished faces and a 10 mm optical path. All measurements were performed at room temperature in triplicate.

The optical band gap of the sample was estimated by using the energy-wavelength relation;  $E_g = hc/\lambda$ , where  $h$  is the Plank's constant,  $c$  is the velocity of light and  $\lambda$  is the wavelength determined from the absorption tail.

The Tauc's equation was used to determine the relationship between the absorption coefficient ( $\alpha$ ) and the incident photon energy ( $h\nu$ ):  $(\alpha h\nu)^{1/n} = A[h\nu - E_g]$ , where  $A$  is a constant and  $E_g$  is the energy band gap of the material and the exponent 'n' depends on the type of transition, for directly allowed transitions  $n=1/2$ , for indirectly allowed transitions  $n=2$ , and for directly forbidden transitions  $n=3/2$ . In order to determine the possible transitions,  $(\alpha h\nu)^{1/n}$  versus  $h\nu$  were plotted and by the extrapolation of the linear portion of the graph on "h $\nu$ " axis at  $\alpha = 0$ , and the corresponding band gap were obtained.

#### 2.2.4. Fourier transform-infrared spectroscopy (FTIR-PAS)

Fourier transform infrared spectroscopy was performed using a spectrophotometer Nexus 670 Thermo Nicolet with photoacoustic detection (FTIR-PAS) in the spectral range from 4000 to 400  $\text{cm}^{-1}$ . Throughout the experiment, the spectrophotometer was purged with dry air to remove any water vapor.

The photoacoustic cell was purged with helium gas. A carbon black spectrum was collected for reference, and the all spectra were obtained with 8  $\text{cm}^{-1}$  resolution and 128 scans. All measurements were performed at room temperature in triplicate.

#### 2.3. Determination of antioxidant activity

The antioxidant activity of the synthesized CuO nanoparticles was measured by the free radical scavenging potential by the DPPH (1, 1-diphenyl 2-picrylhydrazyl) method (SERPEN et al., 2007; DAS et al., 2013). DPPH scavenging activity was determined in relation to that of the standard antioxidant BHT (butylated-hydroxy-toluene). Three milliliters of a solution of DPPH (0.1 mM) in methanol was mixed with different concentrations (25, 50, 75, and 100  $\mu\text{g}/\text{ml}$ ) of the phytosynthesized CuONPs and BHT.

Each solution was continuously stirred for ten minutes at room temperature to attain homogeneity, and then allowed to stand for 1 h. Then absorbance was measured in a spectrophotometer at 517 nm against methanol as blank. DPPH scavenging activity is calculated using the following equation:

$$\text{DPPH scavenging activity (\%)} = \left[1 - \frac{A_s}{A_c}\right] \times 100 \quad (1)$$

where  $A_s$  and  $A_c$  are the absorbance intensity of peak at 5117 nm for sample and control (DPPH), respectively.

#### 2.4. Antimicrobial activity

*Candida albicans* (WDCM 00054) was obtained from Sigma Aldrich. The yeasts were maintained in PetriFilm (3M<sup>®</sup>) on agar Sabouraud. To monitor the effect of CuO nanoparticles on the growth of yeasts, cells ( $10^4$  in 1 mL Sabouraud broth) were incubated the

presence of the CuONPs (0, 25, 50, 75 and 100  $\mu\text{g/mL}$ ) at 28°C in 100 $\mu\text{L}$  PetriFilm. The spectrophotometer was blanked with culture medium alone then optical readings at 670 nm at the zero time point and then every 6 h for the following 36 h. Subsequently, the optical densities were plotted as a function of nanoparticles concentration (BROEKAERT et al., 1990; ZOTTICH et al., 2011).

The culture was pelleted by centrifugation at 3000 $\times g$  (5 min, 4°C), followed by three washes with water. The impact of CuO NPs on the membrane integrity was determined by the incubation of yeast cells ( $1 \times 10^4$  mL) with 0.8 mL of 5mM Tris-HCL, pH 6.0. CuO nanoparticles were added to final concentrations of 25, 50, 75, and 100  $\mu\text{g/mL}$ . Controls, without the addition of CuONPs were run to evaluate the influence of NPs on the  $\text{H}^+$  ion extrusion by yeast cells. The pH was measured during 30 min (taken regarding each minute). After 1 h incubation, a 0.5 M glucose solution was added to a final concentration of 0.1 M. The  $\text{H}^+$  ion extrusion was calculated using the  $\Delta\text{pH}$  (as the difference between the initial and final pH), and the resultant values were input into the equation  $\text{pH} = -\log[\text{H}^+]$ . Data were analyzed with respect to the negative control (100% acidification) (ZOTTICH et al., 2011).

For measure the zones of inhibition, 100  $\mu\text{L}$  of the tested organism was swab incubated onto the sterile Nutrient agar petri plates for 4 wells were then bored for 6 mm. A total of four concentrations of the synthesized nanoparticles were added to the respectively labeled wells. These plates were incubated at 37 °C for 24 hours followed by observing and measuring the antimicrobial activity of CuONPs.

### 2.5. *In vitro* toxicity of CuO nanoparticles on C-Phycocyanin

*Arthrospira platensis* (NCBI accession no. JN088471), was obtained from microalgal culture repository (MCR), Viçosa, MG, Brazil; and stock culture were maintained in a climate-controlled chamber at  $25 \pm 2$  °C into a glass becker with culture medium, and subjected to light intensity of c.a. 50  $\mu\text{mol quanta m}^{-2}\text{s}^{-1}$  at 12:12 light-dark cycle. A homogenized culture (500 mL) was centrifuged at 4000 rpm to obtain pellet. The pellet was suspended in 150 mL of 20 mM acetate buffer containing 50 mM sodium chloride and 0.002 M sodium azide (pH 5.1).

The extraction of cyanobacterial phycocyanin (C-PC) was carried out by repeated freezing under liquid nitrogen ( $-20\text{ }^{\circ}\text{C}$ ) and thawing at room temperature until the blue color becomes in acetate buffer. To remove cell debris, the extract was centrifuged at 5000 rpm for 10 min and the extract thus obtained was termed as crude extract. The crude extract was purified by means of ammonium sulphate precipitation followed by size exclusion chromatography. The purity of C-PC was determined by using the purity ratio (PR):  $\text{PR} = A_{620}/A_{280}$  ( $\sim 4.2$ ), measured in the range of 200–800 nm, were pooled, lyophilized and stored in the dark at ( $\pm 4\text{ }^{\circ}\text{C}$ ) for experimental purpose.

To study the interaction between CuO NPs and C-PC, 0.5 mL of the C-PC solution at  $5\text{ }\mu\text{M}$  with the pH solution of 7.0, was added to 2.5 mL of the CuONPs-containing solution at concentrations of 0, 10.4, 20.8, 30.2, 41, 50.3, 75.6, 100.7  $\mu\text{M}$ . The absorption spectra of CuONPs-C-PC interaction were obtained using an UV-Vis spectrophotometer Cary 50, Varian. The molecular absorption measurements were performed in the 400-800 nm range, using a sample holder with two polished faces and a 10 mm optical path. Fluorescence measurements of the C-PC extract were performed on a Cary Eclipse spectrophotometer (Varian). The excitation wavelength was set at 278 nm with emission wavelength range set at 500-800 nm. The FTIR data of C-PC in the absence and presence of CuONPs was recorded using a spectrophotometer Nexus 670 Thermo Nicolet in the spectral range from 4000 to  $400\text{ cm}^{-1}$ . Throughout the experiment, the spectrophotometer was purged with dry air to remove any water vapor. A second order derivative analysis was performed on the spectra to search changes at amide vibration modes. All measurements were performed at room temperature in triplicate for each sample.

### *2.6 Statistical analysis*

In order to identify differences among treatments, the statistical analysis was performed by Student t test and LSD test ( $p < 0.05$ ) using R-Studio software to evaluate whether the values were significantly different. Data were expressed on figure as means followed by standard error bars (S.E.).

## **3. Results and discussion**

### 3.1. Characterization of biogenic copper oxide nanoparticles

#### 3.1.1. SEM/EDS, AFM, and XRD analysis

The study of environmentally synthesis of nanomaterials as alternative to physical and chemical synthesis offers a valuable contribution to nanotechnology. Distinct parts of plants and a varied metallic salt may be used to synthesize nanoparticles with different sizes and morphological shapes (IRAVANI, 2011; ZHOU et al., 2014; ELANGO AND ROOPAN, 2015). In the present, report we have biosynthesized CuONPs using leaves extract of YM, with a regular size and biological properties. The morphology and size of green synthesized CuONPs analyzed with AFM is shown in Figure 1 (a-b). In general, the majority of nanoparticles exhibited nearly spherical to spheroid shape (with some agglomeration) (Fig. S1), and size range varying from 30 to 240 nm with average size nearly  $123.54 \pm 2.73$  nm (Fig. 1c). Perimeter showed an average nearly to  $302.38 \pm 10.96$  nm (the length of the resulting active contour around the studied particle). The EDS study (Fig. S1c) show the presence of carbon, oxygen, copper, phosphorus and sulphur elements present in green synthesized CuONPs, which help us to understand and confirm elemental composition of the sample. Similar results can be found in Sharma and colleagues (2015) using leaf extract of *Calotropis gigantean* to synthesize CuONPs.



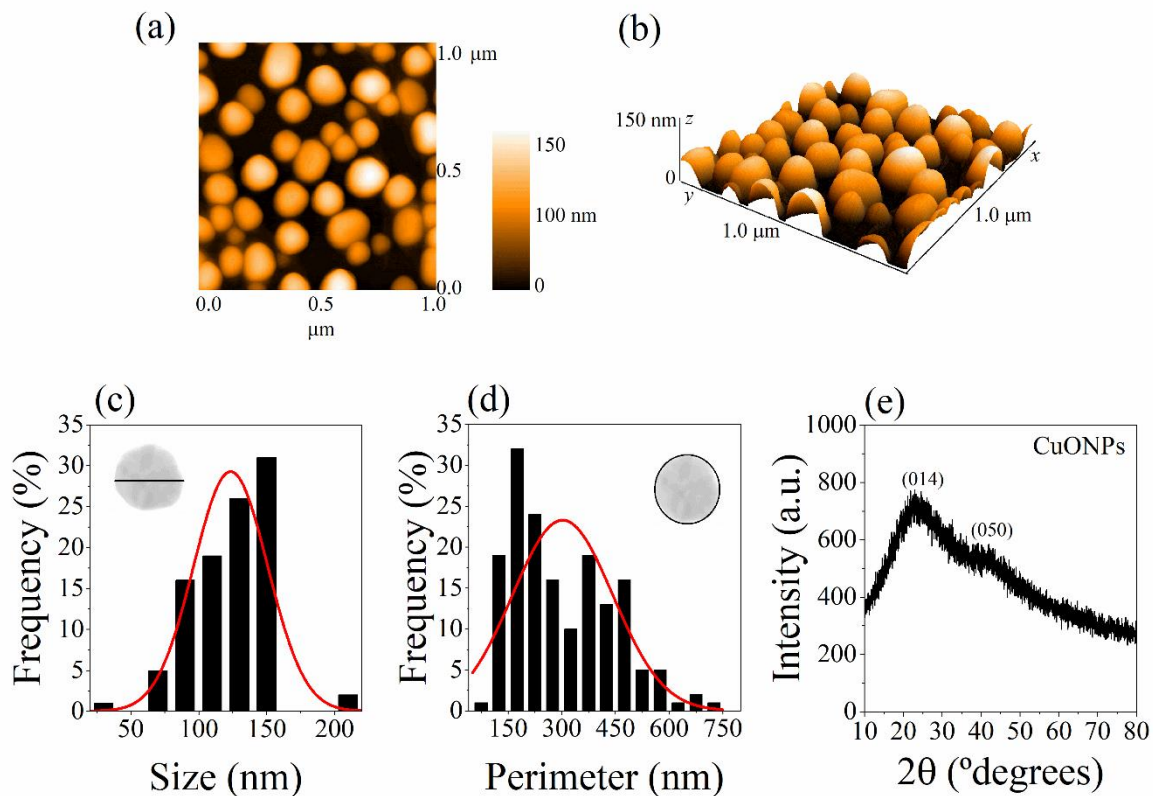


**Figure 1.** (a-b) Atomic Force Microscopy (AFM) images (1000 nm square scan) of biogenic colloidal copper oxide nanoparticles (CuONPs) at room temperature. (c) Size distribution histogram of colloidal copper oxide nanoparticles estimated using scanning electron microscopy (SEM) images; inset – nanoparticle size. (d) Perimeter distribution histogram of colloidal copper oxide nanoparticles estimated using scanning electron microscopy (SEM) images; inset – nanoparticle perimeter. (e) X-ray diffraction spectrum (XRD) of colloidal copper oxide nanoparticles.

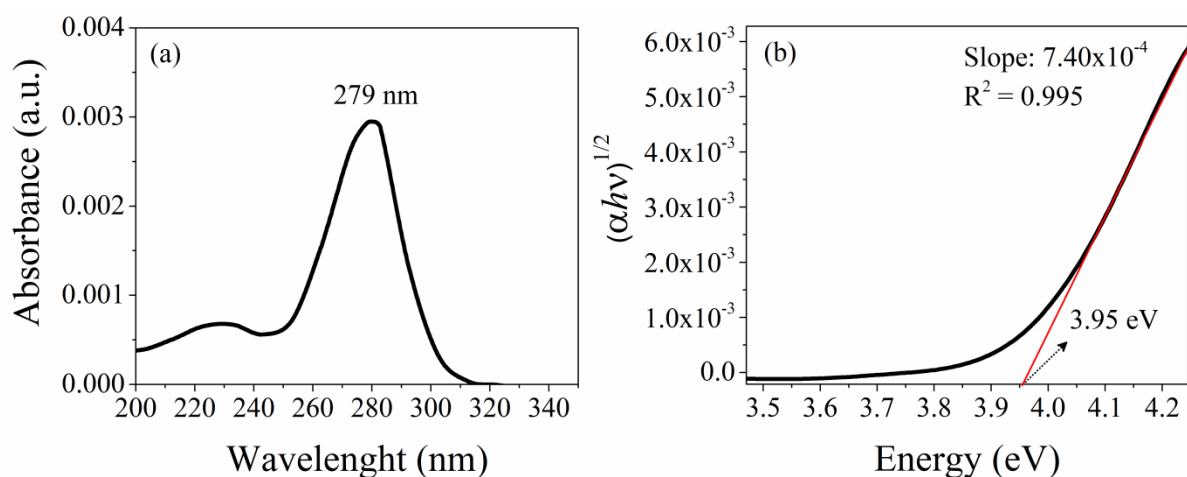
The XRD pattern of CuONPs synthesized by YM leaf extract has been shown in Fig. 1e. Two main diffraction peaks for CuONPs were observed at 2-theta values of 23.055° and 42.684°. The diffraction pattern is identical to that of CuO with an orthorhombic structure. Lattice cell parameters are  $a=5.476$ ,  $b=6.025$ ,  $c=9.351$  for end centered and sharp peaks observed correspond to 014 and 050 crystallographic planes of copper. According to the Debye-Scherrer equation, the average size of the products was found to be 108.33 nm for the most intensive planes, which is in agreement with the particle size range measured from SEM and AFM.



The dominant absorption band of CuONPs is found at 278 nm (Fig. 2a). The absorption band was obtained from optical edge of absorption spectra, to find the energy band gap of CuONPs we using the Tauc's Plot equation, the absorption coefficient nearer to absorption edge is expressed as:

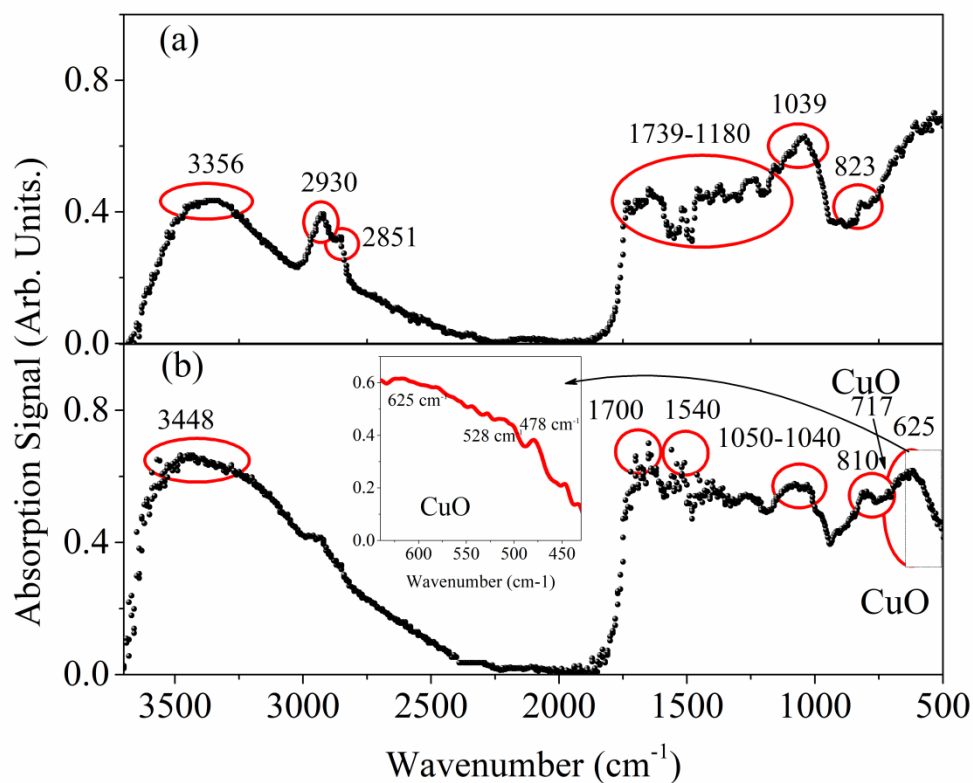
$$\alpha h\nu = A(h\nu - E_g)^n \quad (9)$$

Where,  $h\nu$  is the photon energy,  $\alpha$ - the absorption coefficient, A- is a constant which is different for different transitions,  $n$ -  $\frac{1}{2}$  or 2 (for direct or indirect transitions). Fig. 2b shows estimated band gap energy of CuONPs and it is found to be 3.95 eV. The general shape of the absorption edge of an allowed indirect-gap material [ $\alpha(\omega) \propto (\omega - \omega_g \pm Q)^2$ ] has been observed in Fig. 2b. The band gap energy is a characteristic feature of the materials; it also extends to traits like their crystallinity and stoichiometry (JADHAV et al., 2018). The observed band gap is larger than reported value from bulk material (CuO around 1.2 eV), suggesting a proximity with the band gap energy of Cu<sub>2</sub>O, and which may be attributed to the well-known quantum confinement effect (QCE), usually, the decrease in particle size results in the band gap increase (WU et al., 2015; MOHAMMADIKISH AND AHMADVAND-AKRADI, 2019).



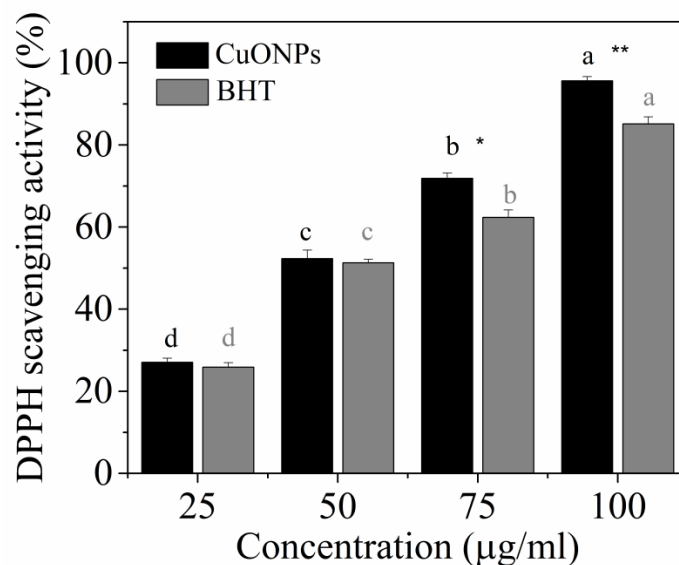
**Figure 2.** (a) The room temperature ultraviolet-visible absorption spectra (UV-Vis) and (b) the square of the absorption coefficient plotted versus the photon energy using Tauc's plot to estimate the allowed-indirect band gap of colloidal copper oxide nanoparticles (CuO NPs).

The bioactive molecules present in the *I. paraguariensis* leaf extract reduce precursor and formation of CuO nanoparticles were confirmed by Fourier transform infrared (FTIR) photoacoustic spectroscopy (PAS) are shown in Figure 6. Band  $1739\text{ cm}^{-1}$  shows aldehyde (carbonyl group) attributed to (C=O), and  $1050\text{ cm}^{-1}$  attributed to (C-O), functional groups of carboxylic acids. The peaks  $1650$  and  $1606\text{ cm}^{-1}$  reveal the presence of N-H bend of amide groups, related to proteins/enzymes present in the *I. paraguariensis* leaf extract. The presence of C-H functional group of alkanes was observed in peaks  $2930$  and  $2851\text{ cm}^{-1}$ . The out-of-phase C–C–O stretching mode observed at  $1260\text{--}1180\text{ cm}^{-1}$  can be associated with phenolic compounds, peak  $823\text{ cm}^{-1}$  is probably from CH wagging of  $\alpha$ -terpenes. The existence of CuO nanoparticles band at  $625\text{ cm}^{-1}$  related to vibration mode of Cu-O, associated with the band at  $1050\text{--}1040\text{ cm}^{-1}$  observed on FTIR spectra corresponding to the coordination of Cu by O-H. Our data confirm that the bioactive compounds present in the leaf extracts are able to synthesis CuO nanoparticles.



**Figure 5.** The room temperature Fourier transform-infrared photoacoustic spectra (FTIR-PAS) of (a) *Ilex paraguariensis* leaf extract; and (b) colloidal copper oxide nanoparticles (CuO NPs).

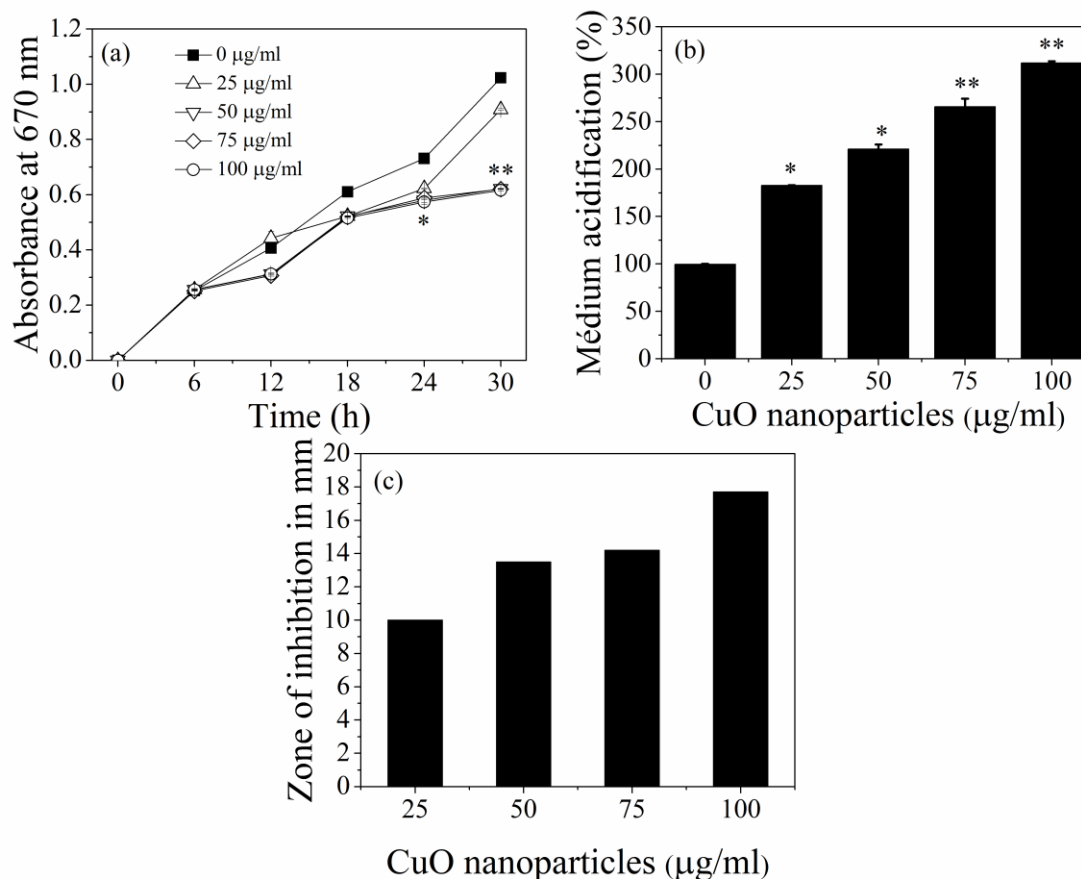
Antioxidant activity of CuONPs was analyzed using DPPH free radical scavenging assay. DPPH has more stability and free radical based on the electron from donor or reduction of accepting hydrogen. Antioxidant activity of CuONPs is shown in terms of concentration in  $\mu\text{g/mL}$  and percentage of free radical scavenging activity in Figure 6. CuONPs may be a potent free radical scavenger comparable to standard BHT. Free radical scavenger activity of CuONPs in higher concentration is superior to standard BHT ( $p < 0.0001$ ). The CuONPs exhibited an effective inhibition activity when compared with the standard.



**Figure 6.** Antioxidant activity of colloidal copper oxide nanoparticles (CuO NPs) phytosynthesized and standard butylated-hydroxy-toluene (BHT) by DPPH free radical scavenging assay.

We tested the effects of green synthesized copper oxide nanoparticles against the yeast *C. albicans*. Fig. 7a shows the patterns of antimicrobial activity against yeast growth and stimulated acidification on the yeast growth medium (Fig 7b) in the presence of CuONPs. An inhibitory effect on the growth was detected in *C. albicans* culture as a function of CuONPs concentration, particularly, at higher levels of nanoparticles. The ability of CuONPs to

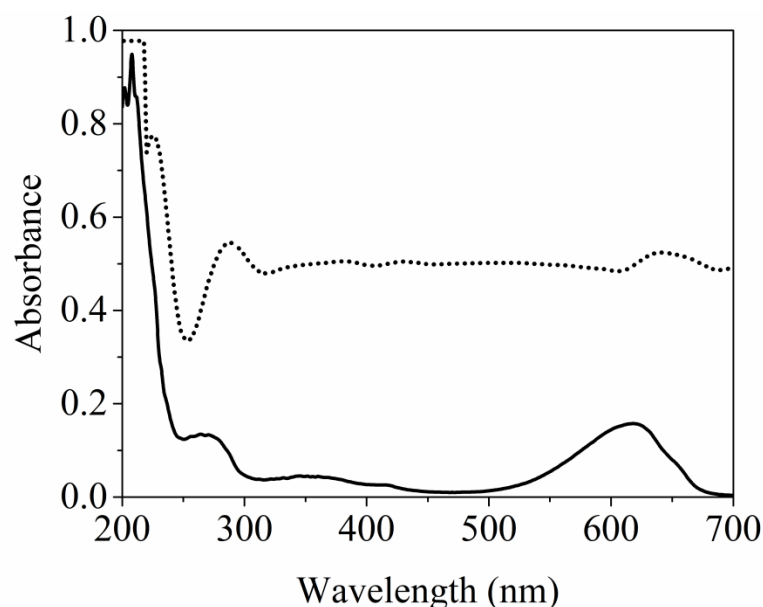
permeabilize the plasma membrane of *C. albicans* cell was examined using the stimulated-acidification of the culture medium. Our results reveal an enhanced acidification of the culture medium by increase in extrusion of H<sup>+</sup> ions by the yeast cell; a dose-dependent behavior was observed (Fig. 7b). Fig. 7c shows the zone of inhibition on *C. albicans* due to the effect of CuONPs for different concentrations. Synthesized nanoparticles exhibit a good antimicrobial activity with zone of inhibition against *C. albicans*, indicating the antibacterial nature of these nanoparticles.



**Figure 7.**(a) Inhibition growth in the presence of phytosynthesized copper oxide nanoparticles (CuONPs) concentrations at 30 h of experiment and, (b) acidification of the culture medium in the presence of CuONPs. The values are means ( $\pm$ SE) of triplicates. Asterisks indicate significant differences (\* $P < 0.05$ ; \*\*  $P < 0.001$ ) between experimental treatment and control samples.

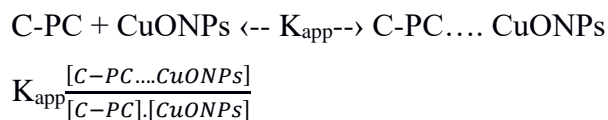
Antimicrobial agents act to inhibit the growth of microorganisms or to cause their death (MUSUMECI AND PUGLISI, 2013). Thus, the investigation and synthesis of biogenic nanoparticles with antimicrobial activity have been reported as a potentially safe therapy for human health (KHASHAN et al., 2016; GUILGER et al., 2017). From the experiment with *C. albicans*, it can be assumed that CuONPs can inhibit the yeast growth. It is observed that higher concentrations of CuONPs are significant in antifungal effect. The possible reason for this behavior may be attributed to the direct interaction of CuONPs and the external membrane surface of *C. albicans*. The similar results related to damages in membrane wall have been reported with zinc oxide nanoparticles (ZnONPs) in *E. coli* (ZHANG et al., 2007).

Figure 8 shows the UV-Vis absorption and corresponding second derivative spectra of the C-PC molecules. The absorption at ~630 nm is attributed to  $\alpha$  and  $\beta$  subunits of C-PC. The band at 200-250 nm is related to protein skeleton, the region around 260-300 nm is attributed to phenylalanine (Phe) residue, band at 300-450 to disulfide bond and the tetrapyrrole band is shown at 550-690 nm. The C-PC contains linear tetrapyrrole molecules with fluorescence properties and cysteine amino acid residues. Their energy transitions of  $\pi-\pi^*$  are related to their fluorescence properties.



**Figure 8.** Ultraviolet-visible absorption spectra of cyanobacterial light-harvesting protein phycocyanin and their second derivative spectra. Dot-lines: second derivative, black-line: absorption spectra.

Figure 9a shows the absorption spectrum of the C-PC at various concentrations of CuONPs. The absorbance maximum of C-PC (~ 630 nm) showed an enhancement in intensity in the presence of CuONPs concentrations. Also, CuONPs had a peak broadening effect, with the peak shift around 12 nm. The equilibrium for the formation of complex between C-PC and CuONPs is given by the following equation, where  $K_{app}$  represents the apparent association constant.



The changes in intensity of the absorption peak at 630 nm as a result of formation of the surface complex were utilized to obtain  $K_{app}$  according to Benesi and Hildebrand equation (BENESI AND HILDEBRAND, 1949):

$$A_{obs} = (1-\alpha)C_0\varepsilon_{C-PC}I + \alpha C_0\varepsilon_c I$$

where  $A_{obs}$  is the observed absorbance of the solution containing different concentrations of the CuONPs at 630 nm;  $\alpha$  is the degree of association between C-PC and CuONPs,  $\varepsilon_{C-PC}$  are the molar extinction coefficients at the defined wavelength ( $\lambda_{max} = 630$  nm) for C-PC and the formed complex in aqueous solution, respectively. However, this equation can be expressed as:

$$A_{obs} = (1-\alpha)A_0 + \alpha A_c$$

where  $A_0$  and  $A_c$  are the absorbances of C-PC and C-PC complex, respectively, with the concentration of  $C_0$ . At relatively high CuONPs concentrations,  $\alpha$  can be equated to  $(K_{app}[CuONPs]) / (1 + K_{app}[CuONPs])$ , thus expressed as:

$$\frac{1}{A_{obs} - A_0} = \frac{1}{A_c - A_0} + \frac{1}{K_{app}(A_c - A_0)[CuONPs]}$$

Based on the enhancement of absorbance at 630 nm due to absorption of surface complex formed, one would expect a linear relationship between  $1/(A_{obs}-A_0)$  and the reciprocal concentration of CuO NPs with a slope equal to  $1/K_{app}(A_c-A_0)$  and an interceptor equal to  $1/(A_c-A_0)$ . The value of apparent association constant ( $K_{app}$ ) determined is  $1.60 \times 10^6 \mu M^{-1}$ , and there is a higher linear dependence ( $R^2 = 0.964$ ). The effects of interaction between CuONPs and C-PC results in the peak shift around 12 nm (Figure 8a). Probably due to adsorption of C-PC on the surface of CuONPs through its anchoring group (-COOH). These changes are been reported to the possibility of ground state complex formation of surface complex between C-PC and CuONPs (BARAZZOUK et al., 2005; KATHIRAVAN et al., 2009; FALCO et al., 2011; CAIRES et al., 2013). Similar patterns have been found earlier work which interaction between silver NPs and chlorophyll molecules has been analyzed by Queiroz et al., (2016).

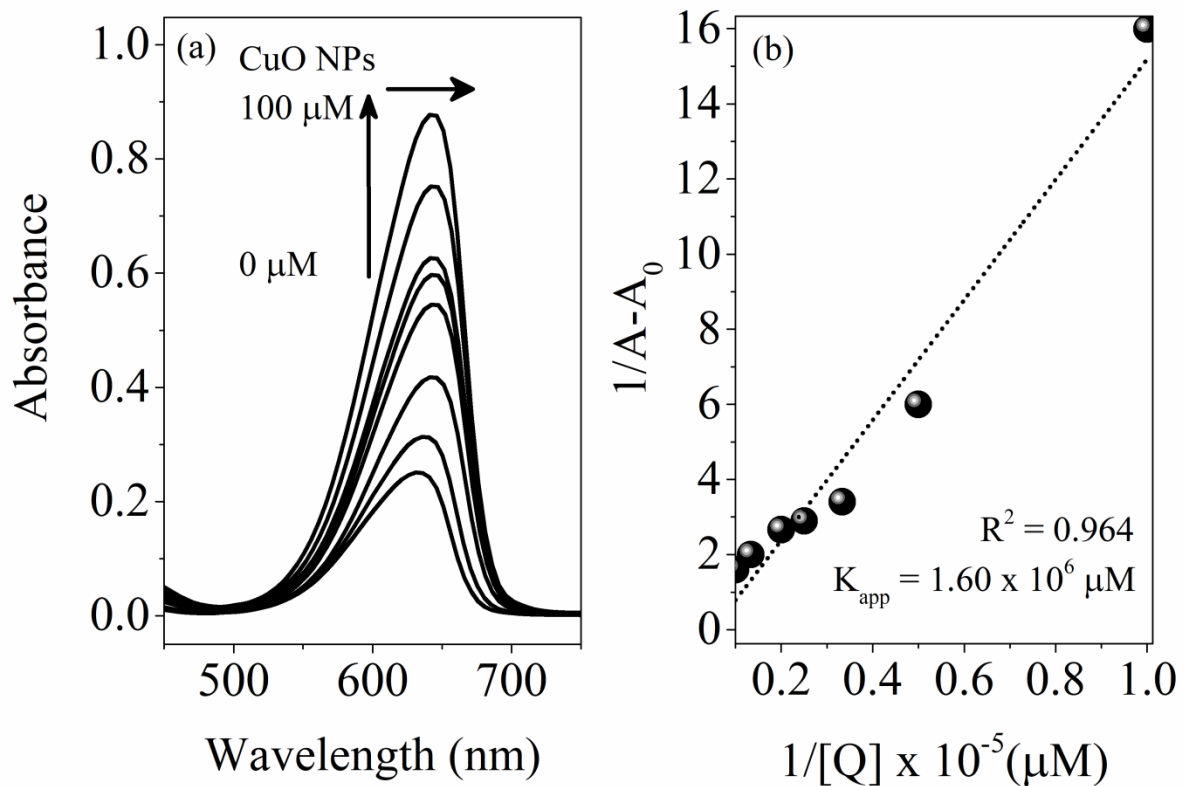


**Figure 9.** (a) Absorption spectrum of phycocyanin (C-PC) in the presence of phyto-synthesized copper oxide nanoparticles (CuONPs) in the concentration range of 0 - 100  $\mu M$ . (b) The dependence of  $1/A_{obs} - A_0$  on the reciprocal concentrations of copper oxide nanoparticles (CuONPs).

In order to analyzing the potential interaction between CuO NPs and light-harvesting protein C-PC, the fluorescence quenching measurement was recorded. Figure 10 show the EEM of the crystal structure of C-PC with a emission band in the region of 650-700 nm. The C-PC suspension was diluted in water, and the major emission spectrum of C-PC water suspension is around 630-650 nm (Fig. 11).



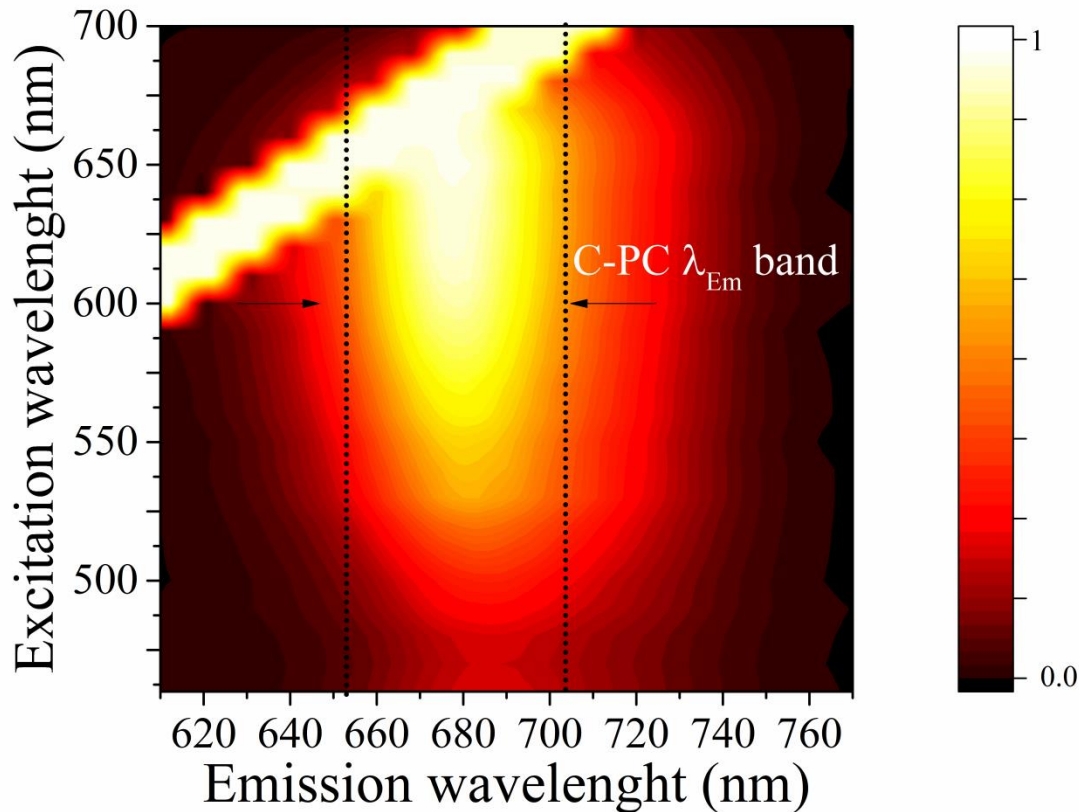


**Figure 10.** Excitation-emission map spectra of cyanobacterial light-harvesting protein phycocyanin during their crystal solid phase.

Figure 11a shows the effects of green synthesized CuONPs on the fluorescence emission spectrum of light-harvesting C-PC. Addition of CuONPs to the solution of C-PC resulted in the quenching of its fluorescence emission. In order to eliminate the inner-filter effects, the fluorescence intensity was corrected by the following equation:

$$F_{\text{obs}} = F_{\text{corr}} \times 10^{\frac{(A_{\text{ex}} + A_{\text{em}})}{2}}$$

where  $F_{\text{obs}}$  and  $F_{\text{corr}}$  were the fluorescence intensities observed and corrected, respectively.  $A_{\text{ex}}$  and  $A_{\text{em}}$  were the absorbance value of C-PC at the excitation and emission wavelength, respectively. The fluorescence intensity used in this paper was corrected.

Stern-Volmer equation was used to investigate the fluorescence quenching data with respect to dose-response.

$$\frac{F_0}{F} = 1 + K_s[Q]$$

where  $F_0$  and  $F$  denote the steady-state fluorescence intensities in the absence and presence of quencher (CuONPs) respectively.  $K_s$  is the Stern-Volmer constant, and  $[Q]$  is the concentration of CuONPs.

According to the slope of the  $F_0/F$  vs  $[Q]$  yields, the data points in the Stern-Volmer constant (Fig 11b) fitted linearly which suggest that the quenching mechanisms in the presence of CuONPs is of the static type. The  $K_s$  value is  $8.5 \times 10^3 \text{ M}^{-1}$ .

From the fluorescence quenching data we can calculate the  $K_{app}$  by using the following equation:

$$\frac{1}{F_0 - F} = \frac{1}{F_0 - F'} + \frac{1}{K_{app}(F_0 - F')[CuONPs]}$$

where  $K_{app}$  is the apparent association constant,  $F_0$  is the initial fluorescence intensity of C-PC, in the absence of CuONPs,  $F'$  is the fluorescence intensity of C-PC in the presence of CuO NPs and  $F$  is the observed fluorescence intensity at its maximum. The plot of  $1/(F_0-F)$  vs  $1/[Q]$  is shown in the Fig. 11c. A good linear relationship was obtained between  $1/(F_0-F)$  and the reciprocal concentration of colloidal CuONPs, with a highest coefficient of determination ( $R^2 = 0.929$ ). The slope ( $K_{app}$ ) has been assessed and the obtained value is  $0.464 \times 10^4 \text{ M}^{-1}$ . Thus, the behavior observed in the  $K_{app}$  of the samples highlighted the validity of assumption proposed for the association between C-PC and CuONPs. It can be noted that,  $K_{app}$  depends on the CuONPs concentration. The fluorescence quenching may be attributed to electron transfer or energy transfer process between C-PC and the CuONPs. The energy transfer efficiency ( $E$ ) was calculated as:  $E = 1-F/F_0$ , where the  $F$  is the fluorescence of donor in the presence of acceptor, and  $F_0$  is the emission intensity of the donor alone. Our

results suggest an increase in energy transfer with increasing concentration of CuONPs (Fig. 11d).

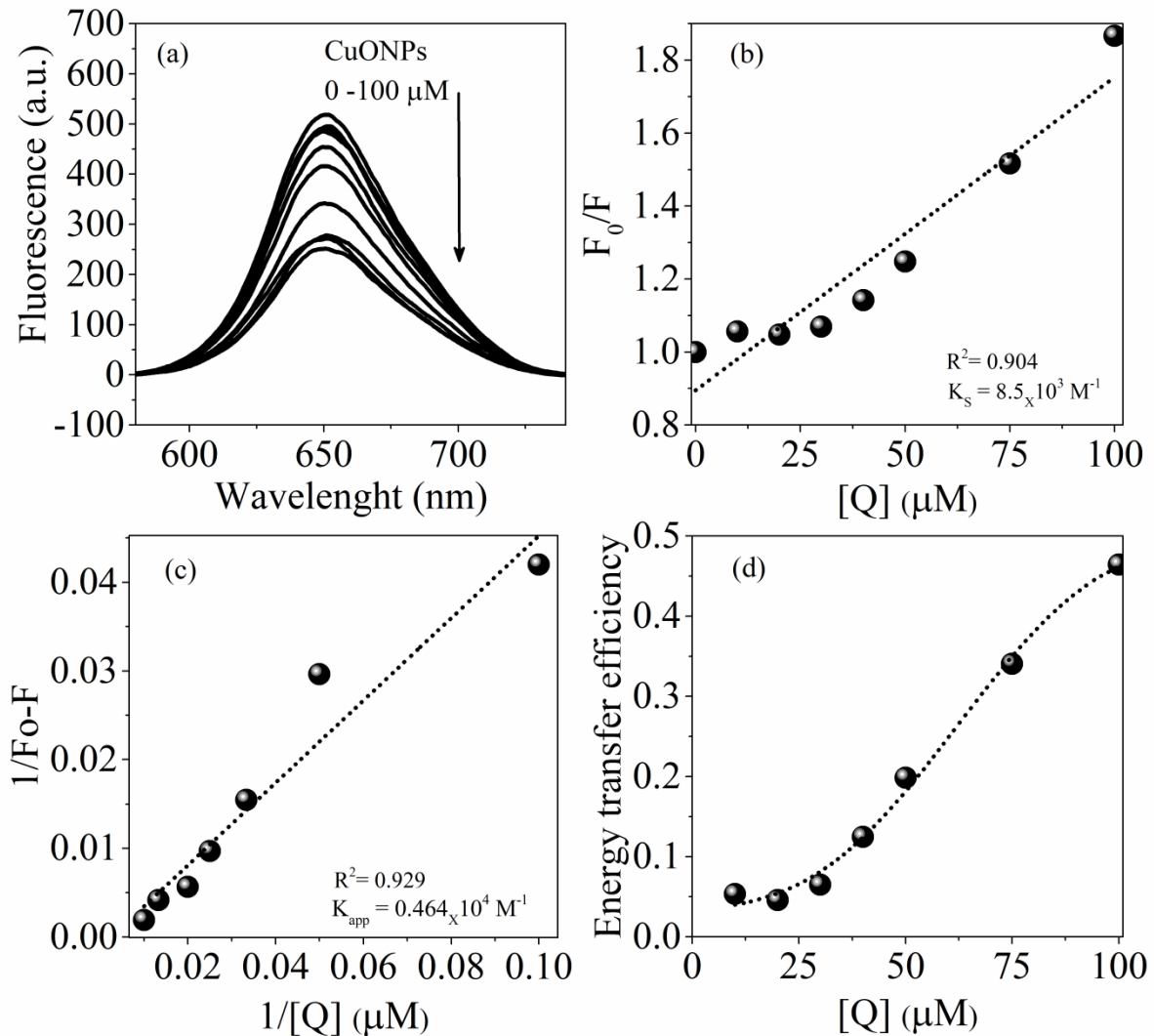


**Figure 11.** (a) Fluorescence quenching of phycocyanin in the presence of phyto-synthesized colloidal copper oxide nanoparticles (CuONPs) in the concentration range of 0, 10, 20, 30, 40, 50, 75, and 100  $\mu\text{M}$ . (b) Stern-Volmer quenching constant ( $K_S$ ). Ratio  $F_0/F$  versus nanoparticles concentration. (c) The dependency of  $1/(F_0 - F)$  on the reciprocal concentrations of CuONPs. (d) Energy transfer efficiency of C-PC to CuONPs.

As the NPs enter into biological tissues interface, they have to encounter immediate and first exposure to many proteins of different concentrations, and the interaction is

influenced by the number and type of proteins. The medium association constants of  $K_{app}$  ( $0.464 \times 10^4 \text{ M}^{-1}$ ) suggest that the affinity of CuONPs for C-PC protein is very high compared with the report binding constants ranging from  $10^2$  for the affinity of C-PC for  $\text{TiO}_2\text{NPs}$  and of phycoerythrin with  $\text{AuTiO}_2\text{NPs}$ ,  $\text{AgTiO}_2\text{NPs}$  and  $\text{TiO}_2\text{NPs}$  (KATHIRAVAN et al., 2009; KATHIRAVAN et al., 2009b; KATHIRAVAN AND RAGANATHAN, 2009), with a good agreement to the affinity of chlorophyll for  $\text{TiO}_2\text{NPs}$  with the report binding constants ranging from  $10^4$  (RAGANATHAN, 2009). The energy transfer efficiency values steadily increase with increasing donor concentration, this occurs probably due to while increasing the concentration, number of C-PC molecules gets adsorbed on the surface of CuONPs is increased. This behavior suggests a quenching associated to the electron injection from the excited state of C-PC molecules to the conduction band of CuONPs (KATHIRAVAN et al., 2009).

The assignments of the Amide modes were monitored by Fourier transform infrared spectroscopy (FTIR) and data shown in Fig. 12 by second derivative and infrared absorption spectra. Our observed results suggest changes related to Amide B ( $2829 \text{ cm}^{-1}$ ), Amide III ( $1325 \text{ cm}^{-1}$ ), Amide V ( $859 \text{ cm}^{-1}$ ) and Amide VI due to the presence of peak shift, as revealed by second derivative spectra. Amide B are related to NH stretching, Amide III to CH stretching or NH bending, Amide V to out-of-plane NH bending, and Amide VI to out-of-plan C=O bending modes (ELLIOTT AND AMBROSE, 1950; MIYAZAWA et al., 1959; KRIMM AND BANDEKAR, 1986; KAUPPINEN et al., 1986), the Amide B in the C-PC-CuONPs is shifted to  $2851 \text{ cm}^{-1}$ , Amide III to  $1299 \text{ cm}^{-1}$ , and amide V to  $849 \text{ cm}^{-1}$ . In the terms of intensity changes Amide III and Amide V were significantly sensitive to CuONPs exposure. Also, the data observed in Fig. 12 provide information on protein structural stability to validity the assumption proposed for the association between C-PC and CuONPs. It is probably due to the structural changes induced by CuONPs and C-PC interaction. The FTIR analysis suggests that the CuONPs preferably interacts with the -NH groups in the protein molecule. Similar results were observed to  $\text{Hg}^{2+}$  metal ion interactions with C-PC (BAHYANI et al., 2016).

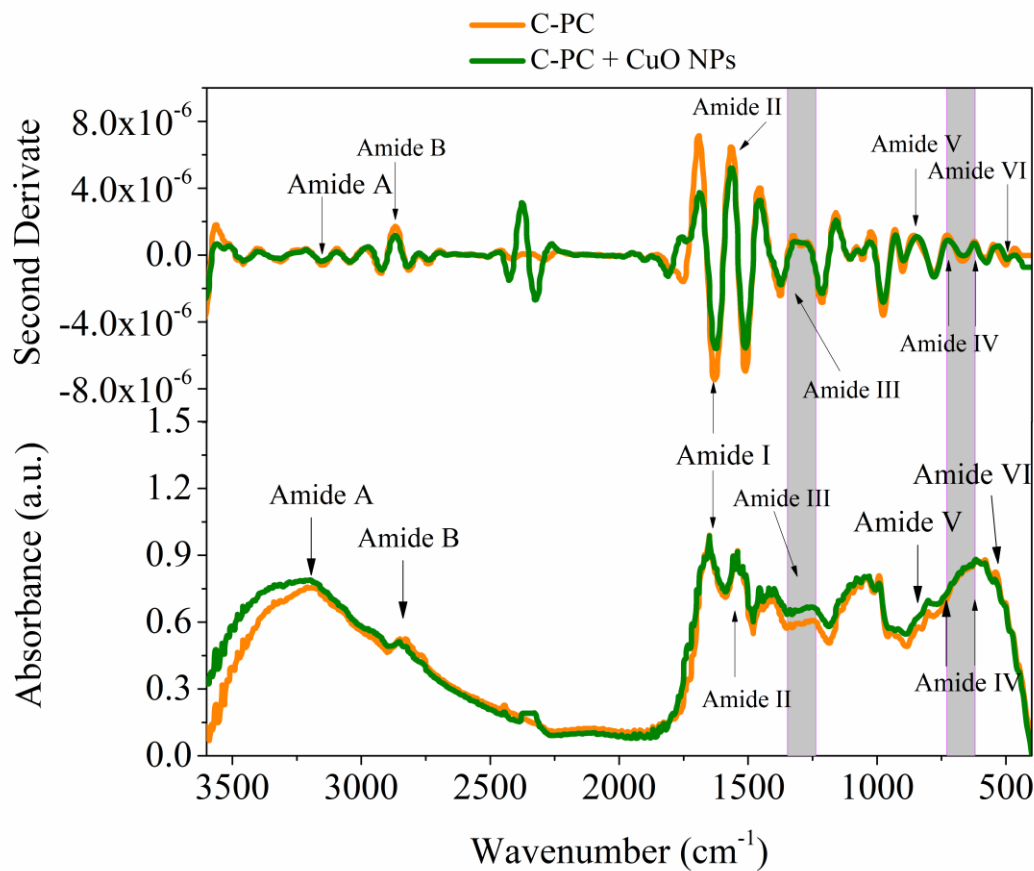


**Figure 12.** Amide modes from Fourier transform infrared spectroscopy (FTIR) data, Second derivative and absorption signal of phycocyanin and copper oxide nanoparticles.

#### 4. Conclusion

The present work, demonstrated that it is possible to perform simple, environmentally and ecofriendly green synthesis of copper oxide nanoparticles using *Ilex paraguariensis* leaf extract as capping and reducing agent, and that the nanoparticles exerted antioxidant activity and inhibitory action on the yeast growth. In the future, the green synthesized copper oxide nanoparticles could be used as an efficient antioxidant agent or antifungal material. In the terms of toxicity, their interaction with cyanobacterial light-harvesting phycocyanin was analyzed, comparison with the controls showed that the green synthesized nanoparticles have potential phototoxic behavior to photosynthetic pigments that varied according to the exposure concentration.

## 5. References

- BARAZZOUK, S.; KAMAT, P.V.; HOTCHANDANI, S. Photoinduced electron transfer between chlorophyll *a* and gold nanoparticles. **Journal of Physical Chemistry B**. v.109, p.716-723, 2005.
- BENESI, H.A.; HILDEBRAND, J.H. A spectrophotometric investigation of the interaction of iodine with aromatic hydrocarbons. **Journal of the American Chemistry Society**. v.71, n.8, 2703-2707, 1949.
- BHATTACHARYA, D.; GUPTA, R.K. Nanotechnology and potential of microorganisms. **Critical Reviews in Biotechnology**. v.25, p.199–204, 2005.
- BHAYANI, K.; MITRA, M.; GHOSH, T.; MISHRA, S. C-phycoyanin as a potential biosensor for heavy metals like Hg<sup>2+</sup> in aquatic systems. **RSC Advances**. v.6, p.111599-111605, 2016.
- BRACESCO, N.; SANCHEZ, A.G., CONTRERAS, V.; MENINI, T.; GUGLIUCCI, A. Recent advances on *Ilex paraguariensis* research: mini review. **Journal of Ethnopharmacology**. v.136, p.378-384, 2011.
- BRAVO, L.; GOYA, L.; LECUMBERRI, E. LC/MS characterization of phenolic constituents of mate (*Ilex paraguariensis* St. Hill) and its antioxidant activity compared to commonly consumed beverages. **Food Research International**. v.40, n.3, p. 393-405, 2007
- BROEKAERT, W.F.; TERRAS, F.R.G.; CAMMUE, B.P.A.; VANDERLEYDEN, J. An automated quantitative assay for fungal growth. **FEMS Microbiology Letters**. v.69, p.55–60, 1990.
- CAIRES, A.R.L.; COSTA, L.R.; FERNANDES, J. A close analysis of metal-enhanced fluorescence of tryptophan induced by silver nanoparticles: wavelength emission dependency. **Central European Journal of Chemistry**. v.11, p. 111-115, 2013.
- CHE, X.; DING, R.; LI, Y.; ZHANG, Z.; GAO, H.; WANG, W. Mechanism of long-term toxicity of CuO NPs to microalgae. **Nanotoxicology**. v.5, p.1-17, 2018.
- DAS, D.; NATH, B.C.; PHUKON, P.; DOLUI, S.K. Synthesis and evaluation of antioxidant and antibacterial behavior of CuO nanoparticles. **Colloids and Surfaces B. Biointerfaces**. v.101, p.430-433, 2013.

- DEWEZ, D.; GOLTSEV, V.; KALAJI, H.M.; OUKARROUM, A. Inhibitory effects of silver nanoparticles on photosystem II performance in *Lemna giba* probed by chlorophyll fluorescence. **Current Plant Biology**. 2018. in Press: DOI: 10.1016/j.cpb.2018.11.006
- DHAS, N.A.; RAJ, C.P.; GERDANKEN, A.A. Synthesis, characterization and properties of metallic copper. **Chemistry of Materials**. v.10, p. 1446-1452, 1998.
- ELANGO, G.; ROOPAN, S.M. Green synthesis, spectroscopic investigation and photocatalytic activity of lead nanoparticles. **Spectrochimica Acta Part A: Molecular and Biomolecular Spectroscopy**. v.139, p.367–373, 2015.
- ELLIOTT, A.; AMBROSE, E.J. Structure of synthetic polypeptides. **Nature**. v.165, p.921–922, 1950.
- FALCO, W.F.; BOTERO, E.R.; FALCÃO, E.A.; SANTIAGO, E.F.; BAGNATO, V.S.; CAIRES, A.R.L. In vivo observation of chlorophyll fluorescence quenching induced by gold nanoparticles. **Journal of Photochemistry and Photobiology A: Chemistry**. v.225, p.65–71, 2011.
- GIOVANNI, V.; MARISTELLA, B.; BERTOZZI, S.; PITZALLS, E.; SALVADOR, P.; COLUCCIA, S.; MARTRA, G. Nanoscale copper particles derived from solvated Cu atoms in the activation of molecular oxygen. **Chemistry of Materials**. v.14, p.1183-1186, 2002.
- GUILGER, M.; PASQUOTO-STIGLIANI, T.; BILESKY-JOSE, N.; GRILLO, R.; ABHILASH, P.C.; FRACETO, L.F.; LIMA, R. Biogenic silver nanoparticles based on *Trichoderma harzianum*: synthesis, characterization, toxicity evaluation and biological activity. **Scientific Reports**. v.7 (44421), 2017. DOI: 10.1038/srep44421
- HECK, C.I.; MEIJA, E.G. Yerba mate tea (*Ilex paraguariensis*): a comprehensive review on chemistry, health implications, and technological considerations. **Journal of Food Science**. v.72, n.9, p.138-151, 2007.
- IGATHINATHANE, C.; PORDESIMO, L.O.; COLUMBUS E.P.; BATCHELOR, W.D.; METHUKU, S.R. Shape identification and particles size distribution from basic shape parameters using ImageJ. **Computers and Electronics in Agriculture**. v.63, n.2, p.168-182, 2008.
- IJAZ, F.; SHAHID, S.; KHAN, S.A.; AHMAD, W.; ZAMAN, S. Green synthesis of copper oxide nanoparticles using *Abutilon indicum* leaf extract: Antimicrobial, antioxidant and



- photocatalytic dye degradation activities. **Tropical Journal of Pharmaceutical Research**. v.16, p.743-753, 2017
- IRAVANI, S. Green synthesis of metal nanoparticles using plants. **Green Chemistry**. v.13, n.10, p.2638-2650, 2011.
- JADHAV, M.S.; KULKARNI, S.; RAIKAR, P.; BARRETO, D.A.; VOOTLA, S.K.; RAIKAR, U.S. Green biosynthesis of CuO & Ag-CuO nanoparticles from *Malus domestica* leaf extract and evaluation of antibacterial, antioxidant and DNA cleavage activities. **New Journal of Chemistry**. v.42, n.1, p.204-213, 2018.
- KATHIRAVAN, A.; CHANDRAMOHAN, M.; RAGANATHAN, R.; SEKAR, S. Cyanobacterial chlorophyll as a sensitizer for colloidal TiO<sub>2</sub>. **Spectrochimica Acta Part A: Molecular and Biomolecular Spectroscopy**. v.71, p.1783-1787, 2009.
- KATHIRAVAN, A.; CHANDRAMOHAN, M.; RAGANATHAN, R.; SEKAR, S. Photoinduced electron transfer from phycoerythrin to colloidal metal semiconductor nanoparticles. **Spectrochimica Acta Part A: Molecular and Biomolecular Spectroscopy**. v.72, p.496-501, 2009b.
- KATHIRAVAN, A.; RAGANATHAN, R. Photosensitization of colloidal TiO<sub>2</sub> nanoparticles with phycocyanin pigment. **Journal of Colloid and Interface Science**. v. 335, p.196-202, 2009.
- KATWAL, R.; KAUR, H.; SHARMA, G.; NAUSHAD, M.; PATHANIA, D. Electrochemical synthesized copper oxide nanoparticles for enhanced photocatalytic and antimicrobial activity. **Journal of Industrial and Engineering Chemistry**. v.31, p.173-184, 2015.
- KAUPPINEN, J.K.; MOFFATT, D.J.; MANTSHC, H.H.; CAMERON, D.G. Fourier self-deconvolution: A method for resolving intrinsically overlapped bands. **Applied Spectroscopy**. v.35, p.271-276, 1985.
- KELLER, A.A.; LAZAREVA, A. Predicted releases of engineered nanomaterials: from global to regional to local. **Environmental Science & Technology Letters**. v.1, p.65-70, 2014.
- KHASHAN, K.S.; SULAIMAN, G.M.; ABDULAMMER, F.A. Synthesis and antibacterial activity of CuO nanoparticles suspension induced by laser ablation in liquid. **Arabian Journal for Science and Engineering**. v.41, p.301-310, 2016.



- KRIMM, S.; BANDEKAR, J. Vibrational spectroscopy and conformation of peptides, polypeptides, and proteins. **Advances in Protein Chemistry**. v.38, p.181–364, 1986.
- MASHOCK, M.J.; ZANON, T.; KAPPELL, A.D.; PETRELLA, L.N.; ANDERSEN, E.C.; HRISTOVA, K.R. Copper oxide nanoparticles impact several toxicological endpoints and cause neurodegeneration in *Caenorhabditis elegans*. **PLoS ONE**. v.11, n.12, (e0167613), 2016. DOI: 10.1371/journal.pone.0167613
- MELEGARI, S.P., PERREAUT, F., COSTA, R.H.R., POPOVIC, R., MATIAS, W.G. Evaluation of toxicity and oxidative stress induced by copper oxide nanoparticles in the green alga *Chlamydomonas reinhardtii*. **Aquatic Toxicology**. v.142, n.143, p. 431-440, 2013.
- MERCADO, D.F.; CAREGNATO, P.; VILLATA, L.S.; GONZALEZ, M.C. *Ilex paraguariensis* extract-coated magnetite nanoparticles: a sustainable nano-adsorbent and antioxidant. **Journal of Inorganic and Organometallic Polymers and Materials**. v.28, n.2, p.519-527, 2018.
- MIYAZAWA, T.; SHIMANOUCI, T.; MIZUSHIMA, S. Characteristic infrared bands of mono-substituted amides. **The Journal of Chemical Physics**. v.24, n.2, p.408-418, 1959.
- MOHSENIN, N.M. **Physical properties of plant and animal materials** (2<sup>th</sup> revised ed.), Gordon and Breach Sci. Publisher, New York. 1986.
- MUSUMECI, T.; PUGLISI, G. Antimicrobial agents. In: PIGNATELLO, R. (Ed.) **Drug Biomembrane Interaction Studies**. 1st Edition: Elsevier. 2013. 305-333 pp.
- QUEIROZ, A.M.; MEZACASA, A.V.; GRACINO, D.E.; FALCO, W.F.; M'PEKO, J.C.; GUIMARÃES, F.E.G.; LAWSON M T.; COLBECK, I.; OLIVEIRA, S.L.; CAIRES, A.R.L. Quenching of chlorophyll fluorescence induced by silver nanoparticles. **Spectrochimica Acta Part A: Molecular and Biomolecular Spectroscopy**. v.168, n.5, p.73-77, 2016.
- R CORE TEAM. **R: A language and environment for statistical computing**. R Foundation for Statistical Computing, Vienna, Austria. 2013.
- RHEDER, D.T.; GUILGER, M.; BILESKY-JOSE, N.; GERMANO-COSTA, T.; PASQUOTO-STIGLIANI, T.; GALLEP, T.B.B.; GRILLO, R.; CARVALHO, C.D.S.; FRACETO, L.F.; LIMA, R. Synthesis of biogenic silver nanoparticles using *Althaea officinalis* as reducing agent: evaluation of toxicity and ecotoxicity. **Scientific Reports**. v.8 (12397), 2018. DOI: 10.1038/s41598-018-30317-9.

- SERPEN, A.; CAPUANO, E.; FOGLIANO, V.; GOKMEN, V. A new procedure to measure the antioxidant activity of insoluble food compounds. **Journal of Agricultural and Food Chemistry**. v.55, n.19, p.7676-7681, 2007.
- SHANKAR, R.; MANIKANDAN, P.; MALARVIZHI, V.; FATHIMA, T.; SHIVASHANGARI, K.S.; RAVIKUMAR, V. Green synthesis of colloidal copper oxide nanoparticles using *Carica papaya* and its application in photocatalytic dye degradation. **Spectrochimica Acta Part A: Molecular and Biomolecular Spectroscopy**. v.121, p.746-750. 2014.
- SHARMA, J.K.; AKHTAR, M.S.; AMEEN, S.; SRIVASTAVA, P.; SINGH, G. Green synthesis of CuO nanoparticles with leaf extract of *Calotropis gigantea* and its dye-sensitized solar cells applications. **Journal of Alloys and Compounds**. v.632, p.321-325, 2015
- SILVEIRA, A.P.; BONATTO, C.C.; LOPES, C.A.P.; RIVERA, L.M.R.; SILVA, L.P. Physicochemical characteristics and antibacterial effects of silver nanoparticles produced using the aqueous extract of *Ilex paraguariensis*. **Materials Chemistry and Physics**. v.216, p.476-484, 2018.
- SONG, Y.; LI, R.; SUN, Q.; JIN, P. Controlled growth of Cu nanoparticles by a tubular microfluidic reactor. **Chemical Engineering Journal**. v.168, p.477-484, 2011.
- SORBIUM, M.; MEHR, E.S.; RAMAZANI, A.; FARDOOD, S.T. Green synthesis of zinc oxide and copper oxide nanoparticles using aqueous extract of oak fruit Hull (Jaft) and comparing their photocatalytic degradation of basic violet. **International Journal of Environmental Research**. v.12, p.29-37, 2018.
- TAHARA, K.; MOHAMED, A.; KAWAHARA, K.; NAGAO, R.; KATO, Y.; FUKUMURA, H.; SHIBATA, Y.; NOGUCHI, T. Fluorescence property of photosystem II protein complexes bound to gold nanoparticles. **Faraday Discussions**. v.198, p. 121-134, 2017.
- YEH, M.S.; YANG, Y.S.; LEE, Y.P.; YEH, H.F.; YEH, C.S. Formation and characterization of Cu colloids from CuO powder by laser irradiation in 2-propanol. **Journal of Physical Chemistry B**. v.103, 6851-6857, 1999.
- ZHANG, L.; JIANG, Y.; DING, Y.; POVEY, M.; YORK, D. Investigation into the antibacterial behaviour of suspensions of ZnO nanoparticles (ZnO nanofluids). **Journal of Nanoparticle Research**. v.9, p.479-489, 2007.

ZHAO, J., CAO, X., LIU, X., ZHANG, C., HITE J.C., XING B. Interactions of CuO nanoparticles with the algae *Chlorella pyrenoidosa*: adhesion, uptake, and toxicity. **Nanotoxicology**. v.10, n.9, p.297-305, 2016.

ZHOU, G.J.; LI, S.H.; ZHANG, Y.C.; FU, Y.Z. Biosynthesis of CdS nanoparticles in banana peel extract. **Journal of Nanoscience and Nanotechnology**. v.14, p.4437–4442, 2014.

ZOTTICH, U.; DA CUNHA, M.; CARVALHO, A.O.; DIAS, G.B.; SILVA, N.C.M.; SANTOS, I.S.; NASCIMENTO, V.V.; MIGUEL, E.C.; MACHADO, O.T.L.; GOMES, V.M. Purification, biochemical characterization and antifungal activity of a new lipid transfer protein (LTP) from *Coffea canephora* seeds with  $\alpha$ -amylase inhibitor properties. **Biochimica et Biophysica Acta (BBA): General Subject**. v.1810, p.375-383, 2011.



**CHAPTER III - USING NETWORK CONNECTANCE FOR  
ESTIMATING BULK AND NANOSIZED COPPER EFFECTS ON THE  
PHOTOSYSTEM II ACTIVITY IN A FLOATING MACROPHYTE  
*Lemna valdiviana* Phil. (LEMNACEAE)**

Using network connectance for estimating bulk and nanosized copper effects on the photosystem II activity in a floating macrophyte *Lemna valdiviana* Phil. (Lemnaceae)

Montcharles da Silva Pontes<sup>1</sup>, Renato Grillo<sup>2</sup>, Luís Humberto da Cunha Andrade<sup>1</sup>, Anderson Rodrigues Lima Caires<sup>3</sup>, Etenaldo Felipe Santiago<sup>1\*</sup>

<sup>1</sup>Natural Resources Program, Research Center for Natural Resources, Mato Grosso do Sul State University (UEMS), Dourados, MS, Brazil.

<sup>2</sup>Department of Physics and Chemistry, School of Engineering, São Paulo State University (UNESP), Ilha Solteira, São Paulo, SP, Brazil

<sup>3</sup>Optics and Photonics Group, Institute of Physics, Federal University of Mato Grosso do Sul (UFMS), Campo Grande, MS, Brazil.

#### ABSTRACT

Despite recently, the applications of nanotechnology continue to expand into diverse areas from medicine and agriculture to cosmetics and pharmacology. However, our knowledge concerning how these nanomaterials interacts with plants and its consequences to environmental resources is relatively limited. Thus, the toxic effects of ionic and nanoparticulate copper (CuSO<sub>4</sub> and CuONPs) on photosystem II (PSII) activity were investigated in aquatic plant *Lemna valdiviana*, and the functioning of PSII in plants exposed to suspensions of CuSO<sub>4</sub> and CuONPs (500 and 1000 µML<sup>-1</sup>) was significantly affected. Also, chlorophyll *a* content was significantly affected by CuONPs, and this result can be related with structural changes in PSII. Upon highest CuONPs exposed condition, the alteration of PSII photochemical reactions was indicated by a significant change compared to control and CuSO<sub>4</sub> for different fluorescence parameters value: V<sub>J</sub>, F<sub>300µs</sub>, F<sub>v</sub>/F<sub>o</sub>, F<sub>o</sub>/F<sub>m</sub>, Area, DI<sub>o</sub>/RC, TR<sub>o</sub>/RC, φ<sub>E<sub>o</sub></sub>, δ<sub>R<sub>o</sub></sub>, RC/ABS, PI<sub>ABS</sub> and DF<sub>ABS</sub>. Therefore, network connectance analysis showed evidences of inhibitory effects induced by CuONPs on the photochemical network of PSII for energy fluxes ratios per reaction centers and driving forces of photosynthesis. Our results providing new insights into aquatic plant-nanoparticles interaction at photosynthetic electron transport level, consequently, we propose that photosynthetic related endpoints are sensitive and valuable biomarkers to assess the toxicity of nanoparticles.

**Keywords:** Copper oxide nanoparticles; JIP-test; Photosynthetic electron transport; Toxicity.

## RESUMO

Apesar de recentemente, as aplicações da nanotecnologia continuam a se expandir em diversas áreas, dentre elas, destacam-se medicina, agricultura, cosmética e farmacologia. Contudo, associado à sua produção, transporte e aplicação, temos riscos relacionados à uma possível dispersão ambiental, sobretudo, em ecossistemas aquáticos. Neste contexto, nosso conhecimento acerca da interação de nanomateriais em organismos fotossintetizantes, e suas consequências para os recursos ambientais é relativamente limitado. Assim, investigaram-se os efeitos tóxicos do cobre iônico e nanoparticulado ( $\text{CuSO}_4$  e  $\text{CuONPs}$ ) sobre a atividade do fotossistema II (PSII) na macrófita aquática *Lemna valdiviana*. Nossos dados sugerem que o funcionamento do PSII foi significativamente afetado em plantas expostas aos tratamentos com  $\text{CuSO}_4$  e  $\text{CuONPs}$  ( $500$  e  $1000 \mu\text{ML}^{-1}$ ). Os resultados obtidos mostraram alterações no conteúdo de clorofila *a*, relacionado às mudanças estruturais do PSII. Alterações parâmetros de fluorescência:  $V_J$ ,  $F_{300\mu\text{s}}$ ,  $F_V/F_0$ ,  $F_0/F_m$ , Área,  $D_{I_0}/RC$ ,  $TR_0/RC$ ,  $\phi_{E_0}$ ,  $\delta_{R_0}$ ,  $RC/ABS$ ,  $PI_{ABS}$  e  $DF_{ABS}$  sugerem alterações fotoquímicas no transporte de elétrons do PSII para  $\text{CuONPs}$  na dose  $1000 \mu\text{ML}^{-1}$ , em relação ao controle e a forma iônica  $\text{CuSO}_4$ . Neste contexto, a análise de conectância de rede mostrou evidências de efeitos inibitórios induzidos por  $\text{CuONPs}$  sobre a rede fotoquímica de PSII, especialmente para as razões de fluxos de energia por centros de reação e forças motrizes da fotossíntese. Em geral, nossos resultados fornecem novos insights sobre a interação planta-nanopartícula ao nível de transporte de elétrons fotossintéticos.

**Palavras-chave:** Nanopartículas de óxido de cobre; Teste-JIP; Transporte de elétrons fotossintéticos; Toxicidade

## 1. Introduction

Despite well-known involvement of copper (Cu) ions on plant development (is an essential microelement for plants). But also, it is considered as the most toxic heavy metal upon environmental contamination. The principal sources of contamination are Cu based fungicides and algicides in agriculture and medicine, and most recently its release from industrial nanotechnological activities, particularly, photocatalysis and electronics (KATWAL et al., 2015; KHASHAN et al., 2016; GIESE et al., 2018).

Copper is an essential element to plants, in low concentrations is associated to a large amount of biochemical functions, including oxygen transport, gene control and active center of enzymes (RANA 2008; KHELLAF AND ZERDAOUI, 2010). However, its excess may induce deleterious effects, when exposed to sublethal or lethal concentrations. Nanostructured copper can lead to complex and unpredictable effects on plants and environment, due to physical-chemical properties of these nanomaterial. The fast growth of nanotechnology has led to the use of nanostructured materials in a wide range of products, the annual production of nanomaterials increased from 10 tons in 2011 to 300 tons in 2015 (ELLIS et al., 2018). Copper oxide nanoparticles (CuONPs) are emerging as a next-generation of Cu-based fungicides (KATWAL et al., 2015). Lastly, CuONPs can be released in the environment via accidental contamination inputs or intentional events. The emerging use of these NPs, particularly in agriculture, raises concerns about environmental impacts and possible health risks to the human population (GRILLO et al., 2018).

Copper toxicity generally results in chlorosis by interfering with chlorophyll and carotenoids biosynthesis (FOY et al., 1978; CASPI et al., 1999) and inhibits photosynthetic electron transport at multiple steps including the donor side via oxygen-evolving complex (OEC) of photosystem II (PSII) (OUZOUNIDOU, 1996) and acceptor side due to inhibition of  $Q_A$  oxidation (MAKSYMIEC AND BASZYNSKI, 1996; SCHRODER et al., 1994; YRUELA et al., 1996). Recently, significant work has been carried out on the impact CuONPs on photosynthetic organisms which include plants and algae (PERREAULT et al., 2012; PERREAULT et al., 2014; ARIF et al., 2018). Some of these studies demonstrated Cu accumulation in plants exposed to CuONPs (XIONG et al., 2017; LIU et al., 2018). However, there are limited reports of CuONPs effects on the effects at electron transport levels in light harnessing photosynthetic events in free floating aquatic macrophyte.

Photosynthesis is a key process to plant development, and also one of the most important bioenergetic processes, sustaining life in Earth. In the last years, the photochemical reactions of photosynthesis (using sunlight to produce chemical energy) have been an important topic of discussion and research, thus is the ultimate goal for researchers in the field of energy generation (BARBER, 2009; BLANKENSHIP et al., 2011; TACHIBANA et al., 2012; ALFAIFI et al., 2018). The first photochemical events of photosynthesis including: light absorption and transfer of excitation energy to reaction centers, electron transport from and its photochemical transfer from a donor to acceptor side; can be monitored by using chlorophyll *a* fluorescence induction curves (*JIP-test*). *JIP-test* has been used as an accurate, precise and non-destructive probe of photosynthetic efficiency that can directly or indirectly reflects the impacts of environmental changes, pollutants contamination, and to gain a more detailed insight into the physiological status of photosynthetic machinery (LAZÁR, 1999; MAXWELL AND JOHNSON, 2000; STRASSER et al., 2004; SANTIAGO et al., 2015; STIRBET et al., 2018).

The chlorophyll *a* fluorescence (ChlF) parameters for ecophysiological studies include the kinetic events in a temporal dimension (*JIP-test*), termed O(L-K)JIP curves, and punctual phenomena (F<sub>o</sub> and F<sub>m</sub>), where the initial chlorophyll *a* fluorescence signal at level O (F<sub>o</sub>) represents the minimum fluorescence yield in which the light-harvesting of PSII (LHCII) molecules, the pheophytin (Phe<sub>D1</sub>) and their primary quinone acceptor (Q<sub>A</sub>) are in the oxidized state. The transition from O to J steps, represents the primary photochemical reactions of PSII, is controlled by the redox activity of at least 3 species: P680<sup>+</sup>, Pheophytin<sup>-</sup> and Q<sub>A</sub>. Thus, the intermediate J to I steps corresponds to the electron transfer from Q<sub>A</sub> to Q<sub>B</sub> and is controlled by the donor side of PSII during water photolysis in the OEC. During I to P steps, the maximum fluorescence dissipation through plastoquinone pool (PQ-pool) are observed. The level P (F<sub>m</sub>) maximum fluorescence intensity emitted, occurs when the reaction centers and all molecules of Q<sub>A</sub> are in the reduced state (STRASSER et al., 1995; STRASSER et al., 2000; STRASSER et al., 2004).

Also, the *JIP-test* enables extraction of several phenomenological and biophysical parameters for quantifying the energy fluxes and yields ratios around PSII (LAZÁR, 1999; STRASSER et al., 2004; LAZÁR AND SCHANSKER, 2009; STRASSER et al., 2000; STRASSER et al., 2010). Photosynthetic apparatus, as a biological systems component, are



hierarchically organized and composed by a network of interactive elements. According to Maldonado-Rodriguez et al., (2003), the *JIP-test* does not exploit the whole information stored on the curve. Thus, the sensitivity of a network in relation to exogenous stimuli or environmental inputs may be quantified by the average connective strength among the network elements (SOUZA et al., 2009); the strength of links between network elements is called network connectance (AMZALLAG, 2001; SOUZA et al., 2009).

Strongly connected elements (high connectivity) may induce a great capacity of network control, since it would make possible a more fast and accurate adjustments to environmental changes and exogenous stimuli. However, the holistic application of systems biology has been neglected in the study of photosynthetic redox process (SOUZA et al., 2018; PONTES et al., 2019).

In this study, a close analysis of *JIP-test* was used as a probe to evaluate the functioning of light-induced photosynthetic reactions in a neotropical free-floating aquatic macrophyte *Lemna valdiviana* Phil. (Duckweed) exposed to copper on its free form and nanoparticles. Here, we answer the following question: How copper on its free form and nanoparticles interfere in the photosynthetic apparatus and the regulation of photosynthetic energy dissipation? Our investigations also found that *JIP-test* can be used as a non-destructive and accurate tool for evaluating the impact of ionic and nanoparticulate states of copper on photosynthetic apparatus, contributing to elucidate the possible impacts that these nanomaterials may have on photosynthetic organisms and, thus, on the environment.

## **2. Materials and methods**

### **2.1. Plant materials**

Fresh matrices of *Lemna valdiviana* Phil. (Lemnaceae) were collected from the Municipal Ecological Station Veredas of Taquarussu, MS, Brazil (22°37'50.4"S and 53°16'50.3"W) and cultivated in polyethylene water tanks (500 liters), inside a greenhouse covered with a polyethylene screen (Sombrite®) with 50% of shading for six months, without additional fertilization considering the absence of evident nutritional deficiency symptoms and the intensive plant growing.

### **2.2. Toxicity assay**

*L. valdiviana* plants at the stage of three fronds (during exponential growth) were used, a total of 20 units in triplicate, were exposed for 24-h to CuO NPs or copper sulfate ( $\text{CuSO}_4 \cdot 5\text{H}_2\text{O}$  from Sigma-Aldrich, USA) in crystallizing cups (7 cm height, 5 cm in diameter) containing 100 mL of ionic and nanoparticulate (0, 500 and 1000  $\mu\text{M}$ ) solution diluted in nutrient medium, while CuO nanoparticles was obtained from green synthesis method as described in chapter II. CuO NPs had an average particle range varying from 30 to 240 nm with average size nearly 130 nm. During experiment, aquatic macrophytes were cultured at  $25 \pm 1$  °C with light ( $100 \mu\text{Em}^{-2} \text{s}^{-1}$ ) phase of 12 h per day.

### 2.3. Copper uptake

After 24 h of treatment, the plants were dried at 70 °C until constant weight and digested with 10 mL nitric acid (69%  $\text{HNO}_3$ ), diluted to 25 mL with distilled water and impurities were removed by filtration (ZARCINAS et al., 1987). The Cu concentration in plant biomass was carried out with a flame atomic absorption spectrophotometer (Shimadzu AA 6601F). Three replicates were made per bioassay.

### 2.4. Determination of photosynthetic pigment

The extraction and determination of chlorophyll *a*, chlorophyll *b*, and carotenoids concentrations were determined spectrophotometrically in buffered aqueous 80% acetone immediately after stress treatment following Lichtenthaler (1987).

$$[\text{Chl}a] = 12.25A_{663.2} - 279A_{646.8}$$

$$[\text{Chl}b] = 21.5A_{646.8} - 5.1A_{663.2}$$

$$[\text{Car}] = (1000A_{470} - 1.82\text{Chl } a - 85.02\text{Chl } b)/198$$

where, Chl *a* is the chlorophyll *a*, Chl *b* is the chlorophyll *b*, and Car is carotenoids.  $A_n$  correspond to the maximum absorption on *n* wavelength in nm.

### 2.5. Chlorophyll *a* fluorescence assessment

All chlorophyll *a* fluorescence (ChlF) measurements were conducted at room temperature with a portable fluorometer (Handy-PEA, built by Hansatech Instruments Ltd.

King's Lynn, UK) coupled with a liquid-phase adapter, a single light pulse  $1.500 \mu\text{mol photon m}^{-2} \text{ s}^{-1}$  during 6-s with a peak in 650 nm provide an excitation intensity to ensure closure of all PSII reaction centers. The samples of isolated chloroplasts were dark-adapted for at least 30 min before the measurements were started, to allow the PSII reaction centers to open state (re-oxidize) and the electron transport chain to be fully oxidized.

Chloroplasts were prepared by gently macerating 1g of leaf in 5 mL of isolation medium (Plant Media, USA) for 90 sec in a mortar maintained on ice. The resulting slurry was filtered successively through  $20\mu\text{m}$  filter and centrifuged at  $500\times g$  for 3 min. Finally, the pellet was suspended in the re-suspension medium. All procedures are made under dim-green light conditions to maintain thylakoid integrity. The fluorescence induction curves are plotted in logarithmic time scale to represent the polyphasic transient.

The data extracted from the recorded fluorescence curves are shown in Table 1. The energy fluxes in the energy cascade for the events Absorption (ABS), Trapping (TRo), Electron Transport (ETo), Dissipation (Dio), and excited Reaction Centers (RC) was extracted as following Strasser et al. (2000, 2004, and 2010).

Each transient was analyzed according to following data:  $F_0$ , fluorescence intensity at  $50 \mu\text{s}$  (all RCs are open);  $F_{300}$ , fluorescence intensity at  $300 \mu\text{s}$ ;  $F_J$ , fluorescence intensity at 2 ms;  $F_I$ , fluorescence intensity at 30 ms; and  $F_m$ , maximum fluorescence intensity (closed RCs), respectively.

### 2.5.1. Performance indexes parameters ( $PI_{\text{ABS}}$ and $PI_{\text{Total}}$ )

The performance index  $PI_{\text{ABS}}$  on an absorption basis (overall photosynthetic activity of PSII) and  $PI_{\text{Total}}$  (overall activity from PSII and PSI) are two fluorescence parameters that indicate quantitative information about the physiological state of photosynthetic organisms. The expression  $PI_{\text{ABS}}$  according to Strasser et al. (2004) is:

$$PI_{\text{ABS}} = [\gamma_o / (1 - \gamma_o)] \cdot [\phi_{\text{P}o} / (1 - \phi_{\text{P}o})] \cdot [\psi_o / (1 - \psi_o)]$$

where,  $\gamma_o$  is the ratio of reaction centers per chlorophyll;  $\phi_{\text{P}o}$  corresponds to the maximum quantum yield of primary photochemistry (the efficiency of an absorbed photon will be trapped by PSII reaction centers) and;  $\psi_o$  is related to the fraction (probability) of electrons

transported beyond  $Q_A^-$  per excitation trapped by the reaction centers of PSII. The  $PI_{Total}$  is defined as:

$$PI_{Total} = PI_{ABS} \cdot \delta_{Ro}/(1 - \delta_{Ro}) = [\gamma_o/(1 - \gamma_o)] \cdot [\phi_{Po}/(1 - \phi_{Po})] \cdot [\psi_o/(1 - \psi_o)] \cdot [\delta_{Ro}/(1 - \delta_{Ro})]$$

where,  $\delta_{Ro}$  (calculated as  $[(1 - V_I)/(1 - V_T)]$ ) is defined as the efficiency with which an electron can move from the reduced intersystem electron acceptors to the PSI end electron acceptors.

### 2.5.2. Driving forces of photosynthesis

The absorption basis partial ( $DF_{ABS}$ ) and total ( $DF_{total}$ ) driving forces for photosynthesis were performed as following equations:

$$DF_{ABS} = \log PI_{ABS}$$

$$DF_{Total} = \log(PI_{ABS})$$

### 2.6. Statistical analysis

The experiment was performed in a completely randomized design, with three replicates. Two Way analysis of variance (ANOVA) was performed, the mean values were compared by LSD test ( $p < 0.05$ ). To assess changes in the photoenergetic system network, we measured the occurrence of photochemical system modulation under ionic or nanoparticulate copper exposure via measurement of global connectance ( $C_g$ ) related to selected photochemical signals.

The network connectance was estimated using correlation network model by assessing the normalized Pearson's correlation coefficient ( $r$ ) among the parameters of driving forces, energy fluxes in the energy cascade and their related yields, followed by  $z$  transformation of  $r$  values:  $z = (1 + |r|)/(1 - |r|)$ . Finally, we determine the global network connectance ( $C_g$ ) of selected paired parameters as the average of absolute  $z$  values (Amzallag, 2001).

## 3. Results and discussion

### 3.1. Copper uptake

Ionic copper ( $\text{CuSO}_4$ ) and copper oxide nanoparticles (CuONPs) caused visible damage to duckweed at concentration  $1000 \mu\text{ML}^{-1}$  (qualitative observation, data shown in Figure S1). Frond disconnection and chlorosis were toxic signals observed after 24 h of exposing *L. valdiviana* to  $\text{CuSO}_4$  and CuONPs, respectively. Necrosis was observed after 48 h of exposure plants to  $1000 \mu\text{ML}^{-1}$  of CuONPs. These results agree with those reported by copper exposure in *Lemna* plants (BABU et al. 2003; KHELLAF AND ZERDAOUI, 2010). The Cu concentrations in plant biomass were analyzed using atomic absorption method. The Cu concentration in *L. valdiviana* increased with increasing concentrations of  $\text{CuSO}_4$  and CuONPs in the growth medium (Figure 1). The concentration and form of exposed copper intervene the inner level detected. When we compared the effects of  $1000 \mu\text{M}$  of nano and bulk sized copper with respect to control plants, the copper uptake in  $\text{CuSO}_4$  and CuONPs treated plants significantly increase by about 37.79% and 53.34%, respectively. These significantly increase were confirmed with the Two-way ANOVA, and to fit the relation between dose x response of plant copper uptake in upon growth medium, we used linear model with  $R^2 = 0.76$  and  $0.99$  for  $\text{CuSO}_4$  and CuONPs, respectively (Fig. 1bc).

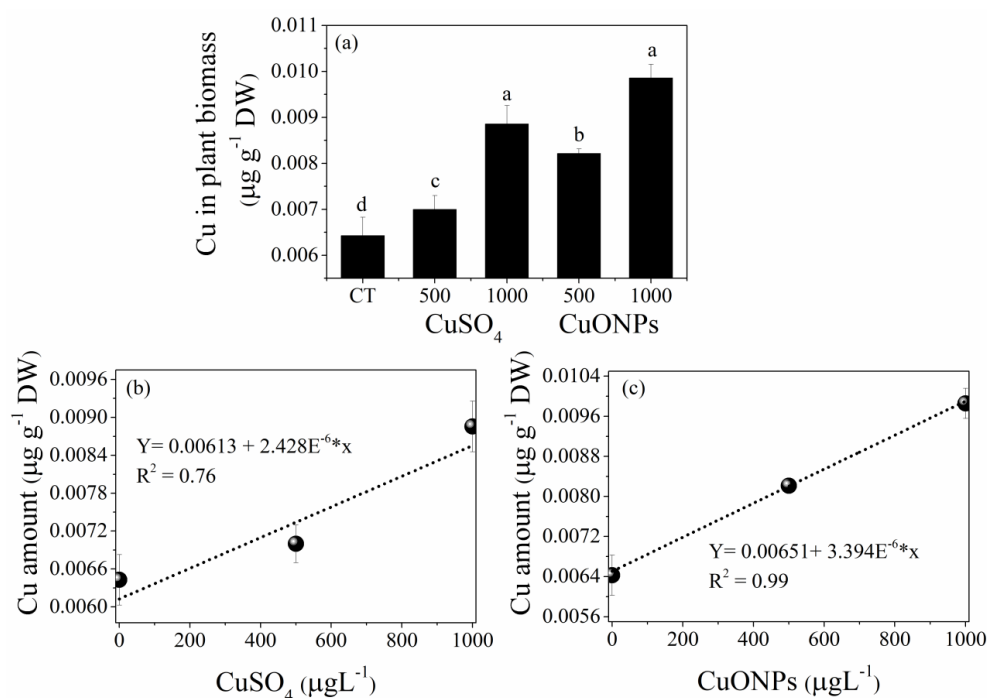


**Figure 1.** (a) Effects of ionic and nanoparticulate copper concentration in solution on the uptake by *Lemna valdiviana* tissues. Linear regression fit (b) for  $\text{CuSO}_4$  and (c) CuONPs treatments. Vertical bars denote standard error.  $n = 3$ .

### 3.2. Photosynthetic pigments and steady state absorption

The damage induced by CuSO<sub>4</sub> and CuONPs was also evaluated by measuring the photosynthetic pigments content. Except for chlorophyll-*b* (Chl-*b*) and carotenoids (Car), the other pigment content ratios differed from control. The chlorophyll *a* (Chl *a*) and total chlorophyll content were both significantly reduced when > 500 μM (CuSO<sub>4</sub> or CuONPs) were added to growth medium (Table 1). A possible response of plants to harmful conditions is the production of reactive oxygen species (ROS). The chloroplasts are an important generator of ROS, and this effect may be manifested by a rapid decrease in chlorophyll biosynthesis (LIOTENBERG et al., 2015). The results of these studies implied that ionic and nanoparticulate copper significantly inhibited the Chl-*a* biosynthesis, and consequently, total amount of chlorophyll, independently of Chl-*b* and Car biosynthesis. It is also possible that localized ROS production may impair chlorophyll biosynthesis. Lastly, the Chl/Car ratio showed a significant decrease at 1000 μM CuSO<sub>4</sub>, and CuONPs at two concentrations, probably associated with the release of dissipation of excess energy in the form of heat (POMPELLI et al., 2010; ARMBRUSTER et al., 2017), when absorbed light cannot be utilized in photochemical reactions and dissipates as heat (non-photochemical energy).

**Table 1.** Photosynthetic pigments concentrations in *Lemna valdiviana* growth in the presence of ionic copper and copper oxide nanoparticles.

Pigments nmol/ml	Copper bulk			Copper oxide nanoparticles	
	Control	500 μM	1000 μM	500 μM	1000 μM
Chl <i>a</i>	1.22 ± 0.06 a	1.01 ± 0.01 b	0.85 ± 0.033 c	0.79 ± 0.004 d	0.77 ± 0.016 d
Chl <i>b</i>	0.45 ± 0.01 a	0.44 ± 0.01 a	0.35 ± 0.01 a	0.36 ± 0.02 a	0.37 ± 0.02 a
Chls <i>a</i> + <i>b</i>	1.67 ± 0.07 a	1.41 ± 0.004 b	1.17 ± 0.05 c	1.12 ± 0.03 d	1.11 ± 0.02 d
Car	0.75 ± 0.03 a	0.69 ± 0.02 a	0.57 ± 0.02 a	0.58 ± 0.03 a	0.63 ± 0.02 a
Chls <i>a</i> + <i>b</i> /Car	2.21 ± 0.02 a	2.04 ± 0.07 a	2.02 ± 0.03 b	1.94 ± 0.07 c	1.77 ± 0.03 c

Chl *a*: chlorophyll *a*; Chl *b*: chlorophyll *b*; Car: carotenoids. <sup>a, b, c, d</sup> Values in lines with different letters indicate significant differences between treatments by Two-way ANOVA (LSD test). The results include mean ± S.E. (n=4).

Chlorophylls have two major steady state absorption bands at room temperature in the visible region; a red (Q<sub>y</sub>) band and blue (Soret) band (Fig. 2) in the spectral range of 600-720 nm and 400-450 nm, respectively (BINNIE et al., 1988; HOFF AND AMESZ, 1991; HANSON, 1991). The Q<sub>y</sub>-band absorption showed a decrease of absorption intensity, compatible with Chl-*a* content reduction. The low absorption intensity in plants treated with

CuSO<sub>4</sub> and CuONPs, can be explained by the replacement of the central Mg-atom of chlorophyll molecules with copper atoms. On the other hand, at CuONPs concentrations, the Soret-band expressed a clear increasing in absorption (not reported for CuSO<sub>4</sub>) in the region of 400 nm. This effect is a result of the resonance plasmon absorption (an enhanced local field near the metal nanoparticles surface) induced by copper oxide nanoparticles surfaces, due to the cooperative oscillation of free electrons is resonant with blue light (BARAZZOUK et al., 2005; Falco et al., 2011; SHEHON AND VERMA, 2011).

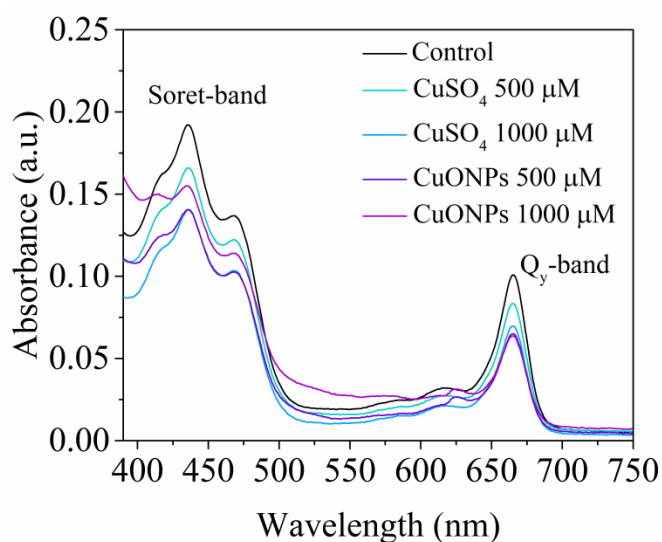


**Figure 2.** Steady state absorption spectra of *Lemna valdiviana* leaf extract after exposure to ionic copper and copper oxide nanoparticles.

In summary, our results demonstrate that the steady state absorption region, specially, Q<sub>y</sub>-band absorption, was dose-dependent, in both cases, with a nearly linear decrease as a function of the concentrations of CuSO<sub>4</sub> or CuONPs (Fig. 3a). The ratios of absorbance intensities for the Soret- and Q<sub>y</sub>-bands ( $A_{\text{Soret}}/A_{\text{Qy}}$ ) at the lowest concentration of CuSO<sub>4</sub> and CuONPs did not differ from control samples (Fig. 3b), and are in accordance with the corresponding literature data reported from chlorophyll fraction from leaves dissolved in acetone solvent (JEFFREY et al., 1996; MILENKOVIĆ et al., 2012). However,  $A_{\text{Soret}}/A_{\text{Qy}}$  is significantly increased at the higher level of bulk and nanosized copper ( $p < 0.05$  and  $0.001$ , respectively). It is worth to point out that the major changes were observed for high level of CuONPs (Fig. 3b). Probably due to the existence of an effective Chl-CuONPs interaction, the findings suggest that the  $A_{\text{Soret}}/A_{\text{Qy}}$  ratio may represent a potential tool for use in future



studies to monitoring the plasmon resonance effect induced by the collective oscillation of the electrons on the metal nanoparticles surface.

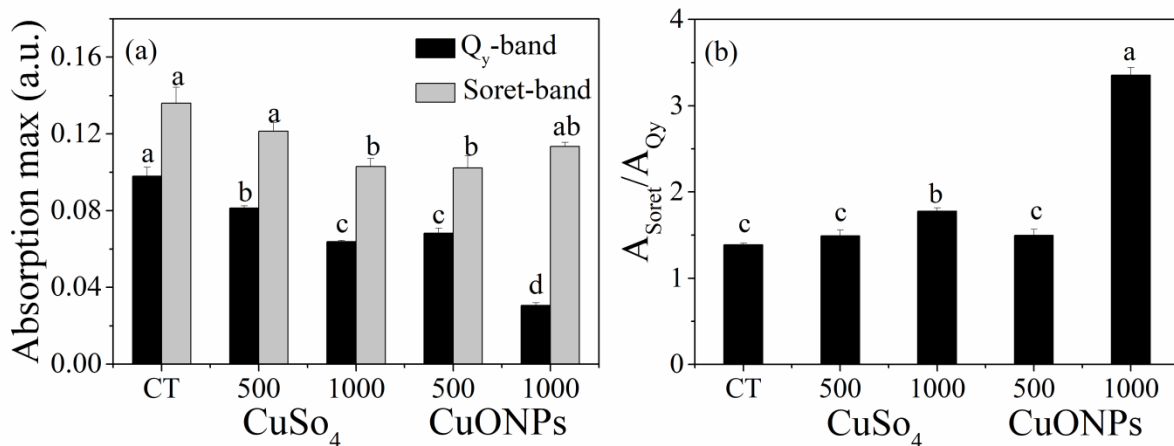


**Figure 3.** (a) Soret and Q<sub>y</sub>-bands of steady state absorption spectra and (b) ratio Soret/Q<sub>y</sub>-band of *Lemna valdiviana* leaf extract after exposure to ionic copper and copper oxide nanoparticles. Letters compare treatments with  $p < 0.05$ .

### 3.3. JIP-test fluorescence transients

To search precision action site of bulk and nanosized copper in PSII, chlorophyll *a* fluorescence transient OJIP (JIP-test) of *L. valdiviana* treated *in vivo* with CuSO<sub>4</sub>, and CuONPs were determined after exposure in isolated chloroplasts. The ChlF data obtained from isolated chloroplasts can differ from intact leaf tissues in terms of emission intensity or sigmoidal shape of transient, however, can reveal adjustments from organism. The fluorescence induction curves showed a typical OJIP shape, and the results are showing in Fig. 4A. To reveal detailed changes in fluorescence transient, the normalized OJIP curves between F<sub>0</sub> and F<sub>m</sub> are presented as  $V_{OP} = (F_t - F_0) / (F_m - F_0)$  in Fig. 4B. A marginal change was observed at J-step, our data showed an elevation in the JI phase, in which  $V_J$  was significant altered at 500  $\mu$ M for CuSO<sub>4</sub> and in both cases for CuONPs (Fig. 4B and Fig. 5c). Further, increased  $V_J$  observed can occur due to a photoprotection strategy (minimization of the electron transport toward PSI), our results suggest a possible accumulation of the reduced Q<sub>A</sub> (Q<sub>A</sub><sup>-</sup>) pool limiting electron transport beyond Q<sub>A</sub><sup>-</sup> (HALDIMAN AND STRASSER, 1999; REDILLAS et al., 2011) due to changes on reduction reactions of P680<sup>-</sup>, Pheo<sup>-</sup>, or Q<sub>A</sub><sup>-</sup>. The normalized fluorescence induction to single turnover region between 50 to 300  $\mu$ s ( $V_{OK} = (F_t -$



$F_o)/(F_{300\mu s}-F_o))$  is compared in Fig. 4C, and there was no effect at intensity on the so-called L-band at 0.15 ms.

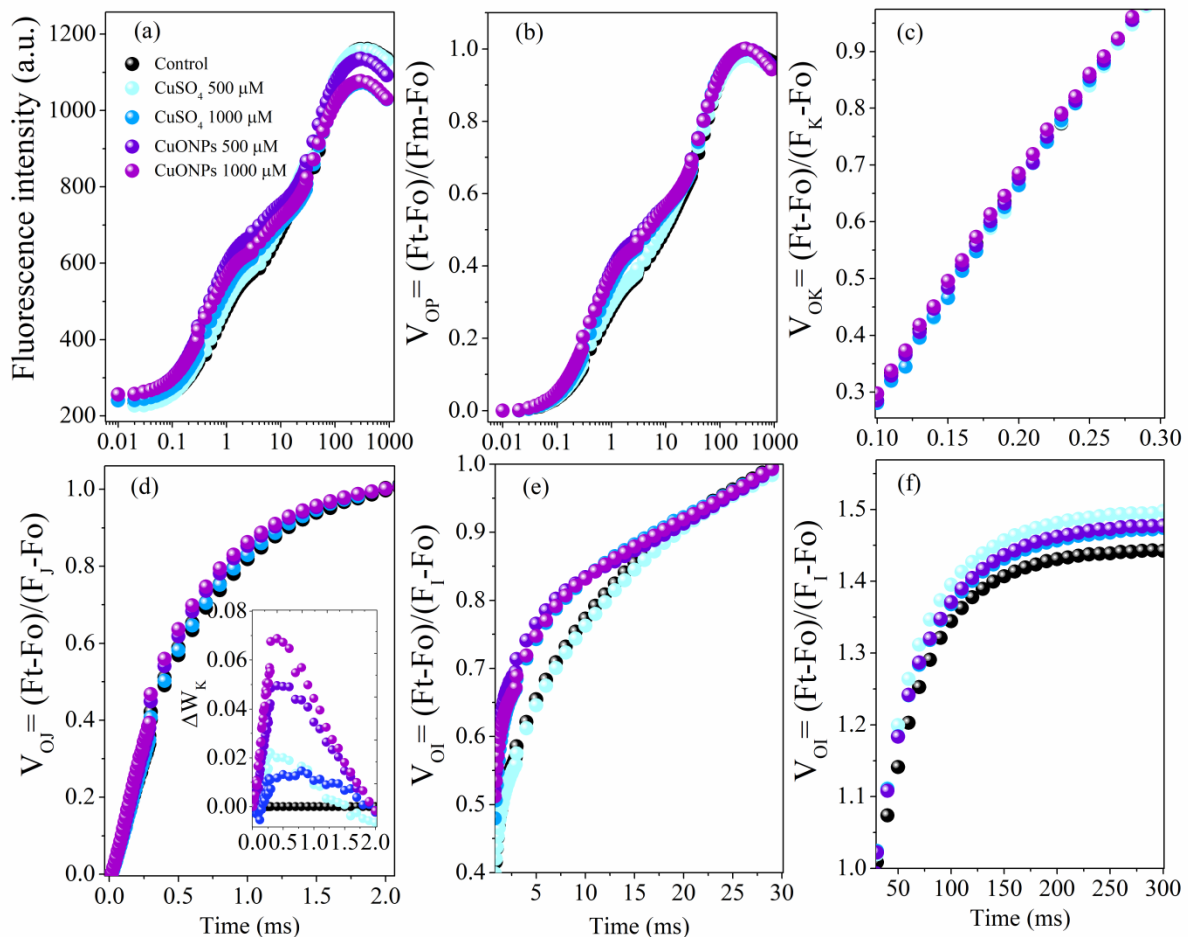


**Figure 4.** The OJIP chlorophyll *a* fluorescence induction kinetics in isolated chloroplasts of *Lemna valdiviana* plants exposed to ionic copper and copper oxide nanoparticles at the indicated concentrations. (a) Raw chlorophyll *a* fluorescence transient curves exhibiting fluorescence intensity ( $F_t$ ) recorded between 0.1 and 1000  $\mu s$  time period (a.u. = arbitrary unit); (b) chlorophyll *a* fluorescence transient double normalized between the two fluorescence extreme O ( $F_o$ ) and P ( $F_m$ ) phases:  $V_{OP} = (F_t - F_o)/(F_m - F_o)$ ; (c) chlorophyll *a* fluorescence transients double normalized between  $F_o$  and  $F_{300\mu s}$  phases:  $V_{OK} = (F_t - F_o)/(F_{300\mu s} - F_o)$ ; (d) chlorophyll *a* fluorescence transient double normalized between  $F_o$  and  $F_J$  phases:  $V_{OJ} = (F_t - F_o)/(F_J - F_o)$ . In inset, kinetic difference of  $V_{OJ}$  [ $\Delta V_{OJ} = (F_t - F_o)/(F_{300\mu s} - F_o)$ ] showing K-band was obtained as treatment dependent; (e-f) chlorophyll *a* fluorescence transients double normalized between  $F_I$  and  $F_m$ :  $V_{IP} = (F_t - F_o)/(F_I - F_o)$ . Each curve is the average of 10 replicates of three independent experiments.

In Fig. 4D, fluorescence rise data were normalized between the steps O and J (2 ms), as  $V_{OJ} = (F_t - F_o)/(F_J - F_o)$ , and plotted as inset graphic with the difference kinetics  $\Delta V_{OJ} = V_{OJ(\text{treatment})} - V_{OJ(\text{control})}$  between the steps O and J in the 50  $\mu\text{s}$  - 2 ms. It was thus possible identify the positive K-band ( $\sim 300 \mu\text{s}$ ). The positive K-band reflects a reduced rate of electron donation to RC due to damages or inactivation of the oxygen evolving complex (OEC), and/or an increase of the functional PSII antenna size (STRASSER, 1997; STEFFEN et al., 2005; YUSULF et al., 2010). In the present study the concentrations of copper in its free form had no effect on OEC (by ratio  $F_{300\mu\text{s}}/F_J$ ) and fluorescence parameter  $F_{300\mu\text{s}}$  (Fig. 5AB), the results from  $\text{CuSO}_4$  and CuONPs treatments were similar to the control dose in OEC ratio (Fig. 5A). However, copper in its nanoparticulate form increase significantly the fluorescence intensity at  $F_{300\mu\text{s}}$ , despite did not differences on OEC ratio. The observed results (positive K-band) could be connected with a quenching of excited state of chlorophyll molecules; and it occurs whenever the balance of electron flow around PSII is causing electron deficit and formation of  $P_{680}^+$  that is an effective quencher (STRASSER, 1997; STEFFEN et al., 2005). On the other hand,  $V_I$  was not statistically different from control (Fig. 4EF and Fig. 5D). Despite the observed displacement trend, the variations in time on the KJIP steps did not differ upon treatments (Fig. S2).

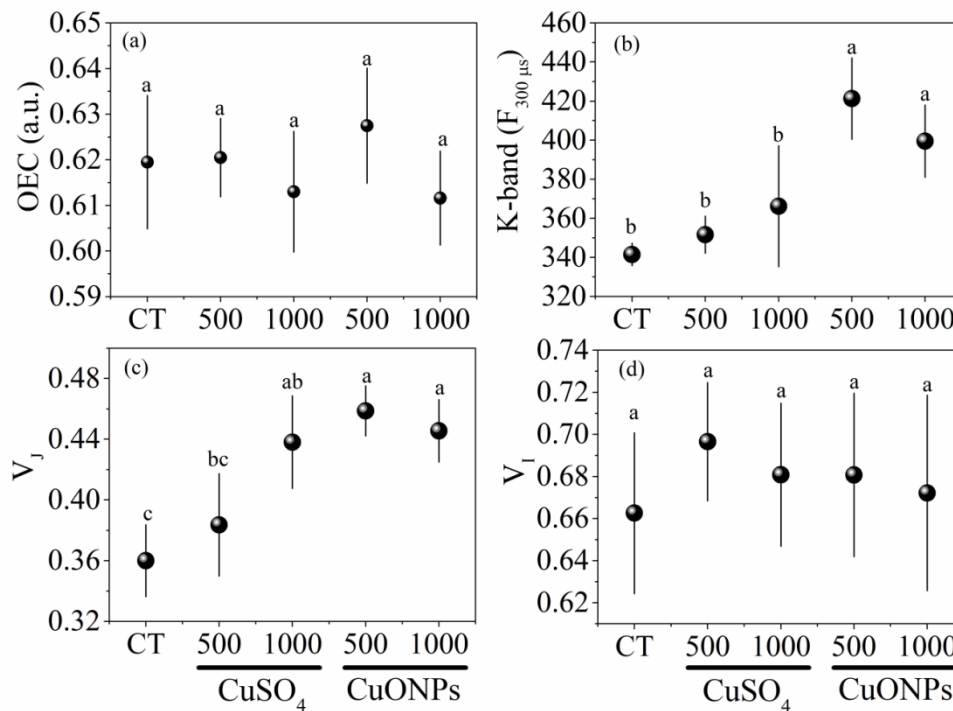


**Figure 5.** Chlorophyll a fluorescence parameters (a) ratio  $F_{300\mu s}/F_J$  related to oxygen-evolving complex; (b) intensities of K-band at  $300 \mu s$ ; (c) variable fluorescence at J-step ( $V_J$ ); and (d) variable fluorescence at I-step ( $V_I$ ) in *Lemna valdiviana* isolated chloroplast after *in vivo* exposure to ionic copper and copper oxide nanoparticles.

Table 2 shows the parameters extracted from the ChlF transient. Initial ( $F_o$ ), maximal ( $F_m$ ), variable ( $F_v$ ) and the potential photochemical quantum efficiency ( $F_v/F_m$ ) did not differ between treatments. However,  $F_v/F_o$  was significantly decreased and  $F_o/F_m$  was significantly increased at  $1000 \mu M$  for  $CuSO_4$  and in both cases for  $CuONPs$ , respectively. The  $F_v/F_o$  ratio is related to the maximum efficiency of the water diffusion reactions on the donor side of PSII, normal values are around 4.0-6.0, decrease in this ratio are common in plants under stress (KALAJI et al., 2017). Also, reflects the structural alterations on the PSII (HAVAUX AND LANNOYE, 1985) may be related to the efficiency of electron donation to PSII reaction center and the rate of photosynthetic quantum conversion at PSII reaction center level (BABANI AND LICHTENTHALER, 1996). The ratio  $F_o/F_m$  is linked to basal quantum yield of non-photochemical processes in PSII. Their normal values described in the literature are in the range of 0.14 to 0.20 (STRASSER et al., 2004). Our results suggest a possible inhibition at PSII acceptor side related to the increase in  $F_o/F_m$  values (DEWEZ et al., 2007).

**Table 2.** Chlorophyll a fluorescence parameter extracted from OJIP curves in isolated chloroplasts of *Lemna valdiviana* plants exposed to ionic copper and copper oxide nanoparticles. n=10. Mean  $\pm$  standard error.

Parameter	Copper bulk			Copper oxide nanoparticles	
	Control	500 $\mu$ M	1000 $\mu$ M	500 $\mu$ M	1000 $\mu$ M
Fo	218.4 $\pm$ 12.59 a	218.65 $\pm$ 16.91 a	227.2 $\pm$ 24.97 a	240.0 $\pm$ 20.13 a	241.3 $\pm$ 21.85 a
Fm	1164.12 $\pm$ 48.1 a	1202 $\pm$ 74.2 a	1074.2 $\pm$ 76.5 a	1126.1 $\pm$ 34.2 a	1077.1 $\pm$ 56.7 a
Fv	946.4 $\pm$ 37.73 a	977.79 $\pm$ 57.7 a	847 $\pm$ 56.42 a	882.4 $\pm$ 27.65 a	835.8 $\pm$ 63.12 a
Fv/Fm	0.81 $\pm$ 0.005 a	0.81 $\pm$ 0.004 a	0.79 $\pm$ 0.01 a	0.78 $\pm$ 0.01 a	0.76 $\pm$ 0.03 a
Fv/Fo	4.39 $\pm$ 0.15 a	4.42 $\pm$ 0.15 a	3.99 $\pm$ 0.30 b	3.905 $\pm$ 0.36 b	3.79 $\pm$ 0.43 b
Fo/Fm	0.18 $\pm$ 0.005 b	0.18 $\pm$ 0.004 b	0.20 $\pm$ 0.01 a	0.21 $\pm$ 0.01 a	0.23 $\pm$ 0.03 a

### 3.4. Biophysical parameters derived

Biophysical parameters, energy fluxes and yield ratios derived from the fluorescence transient curves and JIP-test are presented as radar plot in Fig. 6. All the data of fluorescence parameters were normalized to reference control and each variable at reference control was standardized by giving a numeric value of 1. The ABS/RC was slightly increased due to highest CuONPs dose but deviations within the sampling dates did not exhibit significant changes. On the other hand, the dissipated energy fluxes per reaction center (DIO/RC) was significantly high at 1000 and 1000  $\mu$ M CuONPs, and TRo/RC was significantly increased at 1000  $\mu$ M CuONPs. The quantum yield of electron transport ( $\phi_{Eo}$ ) was significant decreased at 1000  $\mu$ M for CuSO<sub>4</sub> and in both cases for CuONPs. This observed high rate of effective dissipation (as suggested by DIO/RC values) of trapped excitation (TRo/RC), may be associated with low level of quantum yield of electron transport ( $\phi_{Eo}$ ) as well as increased dissipation of excessive energy can be reported as a quick feedback to prevent photooxidative damage in the thylakoid membrane (STRASSER, 1997). Our data demonstrated changes for efficiency/probability with which an electron from the intersystem electron carriers moves to reduce end electron acceptors at the PSI acceptor side ( $\delta_{Ro}$ ) only at CuONPs treatment, and at highest CuONPs dose a significant decrease of the Q<sub>A</sub>-reducing RCs per PSII antenna Chl was observed (RC/ABS). The performance index and driving forces (per absorption basis) significant decreased at 1000  $\mu$ M for CuSO<sub>4</sub> and in both cases for CuONPs, respectively. Our results suggest that although the plants had expressed physiological responses, high level of CuSO<sub>4</sub> and two studied doses of CuONPs can affect the structure and function of photosynthetic apparatus in *L. valdiviana*.

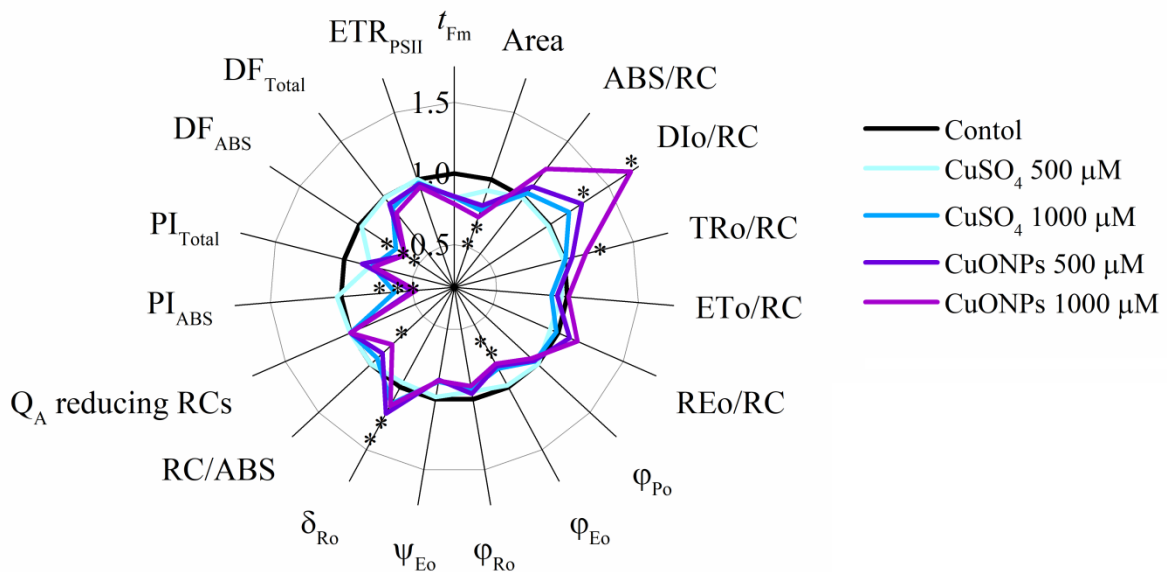


**Figure 6.** Radar plot of photosynthetic parameters deduced by the JIP-test analysis of fluorescence transient (see Supplementary Tab. S1). The data consists of 19 structural and functional photosynthetic parameters (average of 10 replicates), for each parameter the values were normalized, using as reference the control samples (all parameters equal to units). The parameters are related to energy fluxes, yields, driving forces and performance indexes, also, area, time to reach Fm and electron transport rate of PSII.

### 3.5. Photoenergetic system network

To assess changes in system network related to energy fluxes in the energy cascade, the related yields, and driving forces as paired variables of interest in the network, we evaluated the occurrence of differences in the network modulation via the measurement of global connectance (AMZALLAG, 2001). As a measure of the strength of the relationship or connection, we utilize the Pearson's correlation coefficients ( $r$ ) between each paired variables of interest in the network. The results of connection and global connectance ( $C_g$ ) are displayed in Fig. 7. To show a more intuitive, physiological understanding the data are presented as heat plot (Fig. 7a-e), there were remarkable differences in the strength of the relationship of paired variables. Also, suggest high changes induced at 1000 μM for CuSO<sub>4</sub> and in both cases for CuONPs in the stability of its system (TREWAVAS, 1986; EDELMAN AND GALLY, 2001).

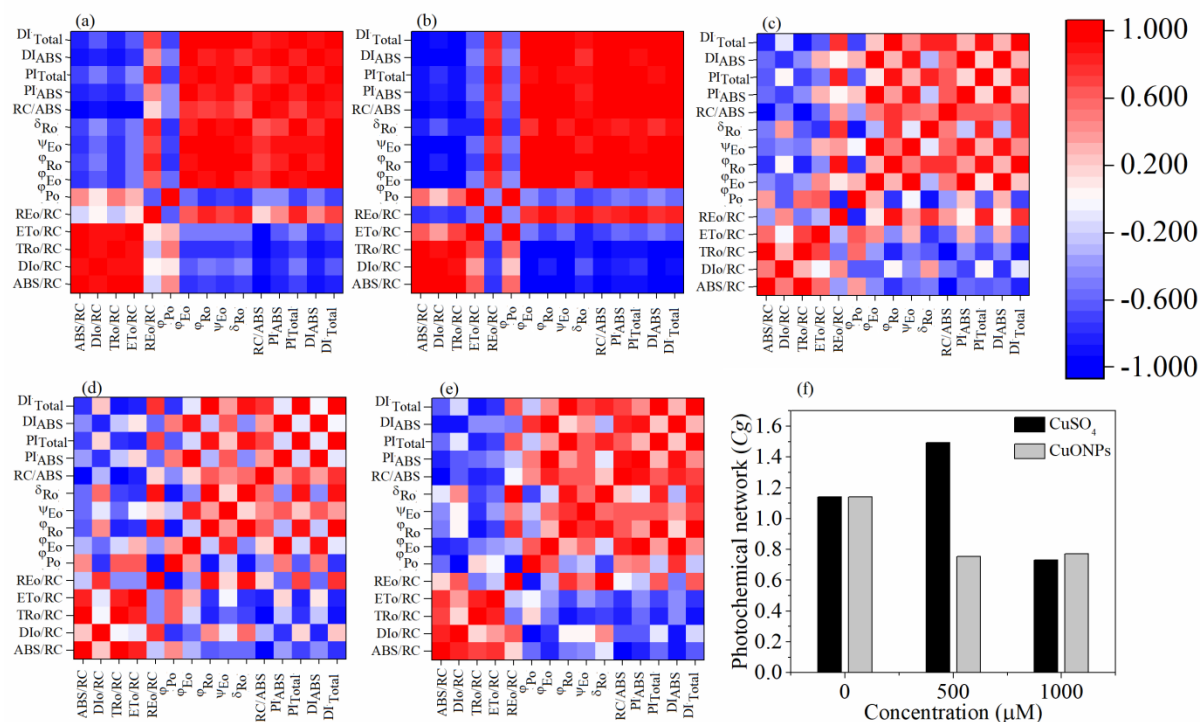


**Figure 7.** Heat plot of Pearson's correlation coefficient ( $r$ ) between photochemical (energy fluxes, yields, performances index and driving forces) parameters used to build and study connectance of photochemical network in *Lemna valdivina* (duckweed) exposed to copper bulk and copper oxide nanoparticles. (a) control, (b) CuSO<sub>4</sub> 500 mM, (c) CuSO<sub>4</sub> 1000 mM, (d) CuO NPs 500 mM, (e) CuO NPs 1000 mM, and (f) photochemical network ( $C_g$ ).

A great connectance was observed only at 500  $\mu$ M for CuSO<sub>4</sub> treatment and suggests higher system stability for this dose, although, at highest CuSO<sub>4</sub> treatment and all doses of CuONPs considerably modified the global connectance related to photochemical network of the system. Network connectance analysis is based on the general systems theory (systems biology), their aim is to better understand the dynamics of the interactions between the components of a complex system, in order to provide a holistic view of organisms or specific metabolic process responses to external stimuli (VON-BERTALANFFY, 1968; FRIBOULET AND THOMAS, 2005; SHETH AND THAKER, 2014; SOUZA et al., 2016). However, the application of such systems biology approaches has been surprisingly neglected in the field of chlorophyll *a* fluorescence studies, particularly, related to energy metabolism and electron transport chain data. Our results can be interpreted as being related to the disturbing effect of highest CuSO<sub>4</sub> treatment and all doses of CuONPs on the photochemical system in their network of relationships.

#### 4. Conclusion

In this study, our results indicate that CuONPs are potentially toxic to the functioning of photosynthetic apparatus and these toxic responses are higher than their ionic bulk. The photosynthetic parameters from chlorophyll *a* fluorescence induction curves demonstrated to be a reliable biomarker of CuONPs toxicity on the *L. valdiviana* plants. The Chl/Car ratio decrease at 1000  $\mu\text{M}$   $\text{CuSO}_4$ , and CuONPs at two concentrations, suggest the dissipation of excess energy in the form of heat. Our results to Chl/Car ratio corroborate with an increase in Fo/Fm and Df/RC, and may be associated to a prevention mechanism of photooxidative stress (ROS-induced) through the dissipation by non-photochemical way of the excess of absorption light. Also, our study showed that detailed quantitative analysis of photochemical network, and the results from *Cg* analysis indicate disturbances in the relationship among elements of the photosynthetic apparatus. In conclusion, under the perspective of complexity theory by using of network approach, we suggest that the CuONPs are able to induce changes in the behavior of network organization, related to alterations in system stability.

#### 5. References

- ALFAIFI, B.Y.; ULLAH, H.; ALFAIFI, S.; TAHIR, A.A.; MALLIC, T.K. Photoelectrochemical solar water splitting: from basic principles to advanced devices. **Veruscript Functional Nanomaterials**. v.2, n.3, 1-26, 2018.
- AMZALLAG, G.N. Data analysis in plant physiology: are we missing the reality? **Plant, Cell & Environment**. v.24, p.881–890, 2001.
- ARIF, N.; YADAV, V.; SING, S.; TRIPATHI, D.K.; DUBEY, N.K.; CHAUHAN, D.K.; GIORGETTI, L. Interaction of copper oxide nanoparticles with plants: uptake, accumulation and toxicity. In: TRIPATHI D.K.; et al. (ed) **Nanomaterials in Plants, Algae and Microorganisms: Concepts and Controversies**. Amsterdam, Netherlands. v. 1. 2018. p. 297-310.
- ARMBRUSTER, U.; CORREA-GALVIS, V.; KUNZM H.H.; STRAND, D.D. The regulation of the chloroplast proton motive force plays a key role for photosynthesis in fluctuating light. **Current Opinion in Plant Biology**. v.37, p. 56-62, 2017.



BABANI, F.; LICHTENTHALER, K.H. Light induced and age dependent development of chloroplasts in etiolated barley leaves as visualized by determination of photosynthetic pigments, CO<sub>2</sub> assimilation rates and different kinds of chlorophyll fluorescence ratios. **Journal of Plant Physiology**. v.148, p. 555-566, 1996.

BABU, T.S.; AKTHAR, T.A.; LAMPI, M.A.; TRIPURANTHAKAN, S.; DIXON, D.G.; GREENGERG, B.M. Similar stress responses are elicited by copper and ultraviolet radiation in the aquatic plant *Lemna gibba*: implication of reactive oxygen species as common signals. **Plant and Cell Physiology**. v.44, p.1320–1329, 2003.

BARAZZOUK, S.; KAMAT, P.V.; HOTCHANDANI, S. Photoinduced electron transfer between chlorophyll a and gold nanoparticles. **Journal of Physical Chemistry B**. v.109, p.716–723, 2005.

BARBER, J. Photosynthetic energy conversion: natural and artificial. **Chemical Society Reviews**. v.38, p.185–196, 2009.

BERTOLLI, S.C.; VITOLO, H.F.; SOUZA, GM. Network connectance analysis as a tool to understand homeostasis of plants under environmental changes. **Plants**. v.2, p.473-488, 2013.

BIMMIE, N.E.; HALEY, L.V.; MATTIOLI, T.A.; THIBODEU, D.L.; WANG, W.; KONINGSTEIN, J.A. Molecular emission and electronic structure of associated chlorophyll *a*. **Canadian Journal of Chemistry**. v.66, p.1728-1733, 1988.

BLANKENSHIP R.E.; et al. Comparing photosynthetic and photovoltaic efficiencies and recognizing the potential for improvement. **Science**. v.332, p.805–809, 2011.

CASPI, V.; DROPPA, M.; HORVATH, G.; MALKIN, S.; MARDER, J.B.; RASKIN, V.I. The effects of copper on chlorophyll organization during greening of barley leaves. **Photosynthesis Research**.v.62, n.2, p.165-174, 1999.

DEWEZ, D.; BOUCHER, N.; BELLEMARE, F.; POPOVIC, R. Use of different fluorometric systems in the determination of fluorescence parameters from spinach thylakoid membranes being exposed to atrazine and copper. **Toxicological and Environmental Chemistry**.v.89, n.4, p.655-664, 2007.

EDELMAN, G.M.; GALLY, J.A. Degeneracy and complexity in biological systems. **Proceedings of the National Academy of Sciences: PNAS**. v.98, p.13763–13768, 2001.



ELLIS, L.-J.A.; BAALOUSHA, M.; VALASAMI-JONES, E.; LEAD, J.R. Seasonal variability of natural water chemistry affects the fate and behaviour of silver nanoparticles. **Chemosphere**. v.191, p. 616-625, 2018.

FALCO, W.F.; BOTERO, E.R.; FALCÃO, E.A.; SANTIAGO, E.F.; BAGNATO, V.S.; CAIRES, A.R.L. In vivo observation of chlorophyll fluorescence quenching induced by gold nanoparticles. **Journal of Photochemistry and Photobiology A: Chemistry**. v.225, p.65–71, 2011.

FOY, D.C.; CHANEY, R.L.; WHITE, M.C. The physiology of metal toxicity in plants. **Annual Review in Plant Physiology**. v.29, p. 511-566, 1978.

FRIBOULET, A.; THOMAS, D. Systems biology an interdisciplinary approach. **Biosensors and Bioelectronics**. v.20, p.2404–2407, 2005.

GIESE, B.; KLAESSIG, F., PARK, B.; STEINFELDT, M.; WIGGER, H.; et al. Risks, release and concentrations of engineered nanomaterial in the environment. **Scientific Reports**. v.8, n.1565, 2018. DOI: 10.1038/s41598-018-19275-4

GRILLO, R.; JESUS, M.B.; FRACETO, L.F. Editorial: Environmental impact of nanotechnology: analyzing the present for building the future. **Frontiers in Environmental Science**. v.6, p.1-3, 2018.

HALDIMAN, P.; SATRASSER, R.J. Effects of anaerobiosis as probed by the polyphasic chlorophyll *a* fluorescence rise kinetic in pea (*Pisum sativum* L.). **Photosynthesis Research**. v.62, p.67–83, 1999.

HANSON, L.K. Chlorophylls. In: (SCHEER, H. Ed.) **Chlorophylls**. CRC Press, FL, 1991, p. 994

HAVAUX, M.; LANNOYE, R. Drought resistance of hard wheat cultivars measured by a rapid chlorophyll fluorescence test. **Journal of Agricultural Science**. v.104, p.501–504, 1985.

HOFF, A.J.; AMESZ, J. Chlorophylls, In: (SCHEER, H. Ed.) **Chlorophylls**. CRC Press, FL, 1991, p. 724.

JEFFREY, S.W.; MANTOURA, R.F.C.; WRIGHT, S.W. Phytoplankton pigments in oceanography: **Guidelines to Modern Methods**, UNESCO Publishing, Paris, 1996, p.1

- KALAJI, M.H.; GOLTSEV, V.N.; ZUK-GOLASZEWSKA, K.; ZIVCAV, M.; BRESTIC, M. **Chlorophyll Fluorescence: Understanding Crop Performance - Basics and Applications**. CRC Pres. Taylor & Francis Group, New York, USA, 2017. 222p.
- KATWAL, R.; KAURM, H.; SHARMA, G.; NAUSHAD, M.; PATHANIA, D. Electrochemical synthesized copper oxide nanoparticles for enhanced photocatalytic and antimicrobial activity, **Journal of Industrial and Engineering Chemistry**. v.31, p.173-184, 2015.
- KHASHAN, K.S.; SULAIMAN, G.M.; ABDULAMMER, F.A. Synthesis and antibacterial activity of CuO nanoparticles suspension induced by laser ablation in liquid. **Arabian Journal of Science Engineering**. v.41, p. 301-310, 2016.
- KHELLAF, N.; ZERDAOUI, M. Growth response of the duckweed *Lemna gibba* L. to copper and nickel phytoaccumulation. **Ecotoxicology**. v.19, p. 1363-1368, 2010.
- LAZÁR, D. Chlorophyll *a* fluorescence induction. **Biochimica et Biophysica Acta: Bioenergetics**. v.1412; p.1-28, 1999.
- LAZÁR, D. SCHANSKER, G. Models of chlorophyll *a* fluorescence transient. In: (LAISK, A.; NEDBAL, L.; GOVINDJEE (eds)). **Photosynthesis in silico: Understanding Complexity from Molecules to Ecosystems**, Springer, Dordrecht, pp. 85–123. 2009.
- LICHTENTHALER, H.K. Chlorophylls and carotenoids: pigments of photosynthetic biomembranes. **Methods In Enzimology**. v.148, p.350–382, 1987.
- LIOTENBERG, S.; STEUNOU, A.S.; DURAND, A.; BOURBON, M.L.; BOLIVAR, D.; HANSSON, M.; ASTIER, C.; OUCHANE, S. Oxygen-dependent copper toxicity: targets in the chlorophyll biosynthesis pathway identified in the copper efflux ATPase CopA deficient mutant. **Environmental Microbiology**. v.17, n.6, p. 1963-1976, 2015.
- LIU, J.; DHUNGANA, B.; COBB, G.P. Environmental behavior, potential phytotoxicity, and accumulation of copper oxide nanoparticles and arsenic in rice plants. **Environmental Toxicology and Chemistry**.v.37, p.11–20, 2018.
- LUCAS, M.; LAPLAZE, L.; BENNETT, M.J. Plant systems biology: network matters. **Plant, Cell & Environment**. v.34, p. 535-553, 2011.
- MAKSYMIEC, W.; BASZUNASKI, T. Chlorophyll fluorescence in primary leaves of excess Cu-treated runner bean plants depends on their growth stage and the duration of Cu-action. **Journal of Plant Physiology**. v.149, p.196-200, 1996

MALDONADO-RODRIGUEZ, R.; PAVLOV, S.; GONZALEZ, A.; OUKARROUM, A. STRASSER, R.J. Can machines recognize stress in plants? **Environmental Chemistry Letters**. v.1, n3, p.201-205, 2003.

MAXWEEL, K.; JOHNSON, G.N. Chlorophyll fluorescence – a practical guide. **Journal of Experimental Botany**. v.51, n.345, p.659-668, 2000.

MILENKOVIĆ, S.M.; ZVEZDANOVIĆ, J.B.; ANDELKOVIĆ, T.D.; MARKOVIĆ, D.Z. The identification of chlorophyll and its derivatives in the pigment mixtures: HPLC-Chromatography, visible and mass spectroscopy studies. **Advanced Technology**. v.1, n1, p.16-24, 2012.

OUZOUNIDOU, G. The use of photoacoustic spectroscopy in assessing leaf photosynthesis under copper stress: correlation of energy storage to photosystem II fluorescence parameters and redox change of P700. **Plant Science**. v.113, p. 229-237, 1996.

PERREAULT, F.; OUKARROUM, A.; MELEGARI, S.P.; MATIAS, W.G.; POPOVIC, R. Polymer coating of copper oxide nanoparticles increases nanoparticles uptake and toxicity in green alga *Chlamydomonas reinhardtii*. **Chemosphere**. v.87, p.1388-1394, 2012

PERREAULT, F.; POPOVIC, R.; DEWENZ, D. Different toxicity mechanisms between bare and polymer-coated copper oxide nanoparticles in *Lemna gibba*. **Environmental Pollution**. v.185, p.219-227, 2014.

POMPELLI, M.F.; MARTINS, S.C.; ANTUNES, W.C; CHAVES, A.M.R.; DaMATTA, F.M. Photosynthesis and photoprotection in coffee leaves is affected by nitrogen and light availabilities in winter conditions. **Journal of Plant Physiology**. v.167, n.13, p.1052–1060, 2010.

PONTES, M.S.; MALDONATO-RODRIGUEZ, R.; SANTIAGO, E.F. The energy flux theory celebrates 40 years: toward a systems biology concept? **Photosynthetica**. (in press), 2019.

RANA, S.V.S. Metals and apoptosis: recent developments. **Journal of Trace Elements in Medicine and Biology**. v.22, p.262–284, 2008.

REDILLAS, M.C.F.R.; STRASSER, R.J.; JEONG, J.S.; KIM, Y.S.; KIM, J.K. The use of JIP-test to evaluate drought-tolerance of transgenic rice overexpressing OsNAC10. **Plant Biotechnology Reports**. v.5, p.169–175, 2011.

- SANTIAGO, E.F.; LARENTIS, T.C.; BARBOSA, V.M.; CAIRES, A.R.L.; MORAIS, G.A.; SÚAREZ, Y.R. Can the chlorophyll-a fluorescence be useful in identifying acclimated young plants from two populations of *Cecropia pachystachya* Trec. (Urticaceae), under elevated CO<sub>2</sub> concentrations? **Journal of Fluorescence**. v.25, p.49-57, 2015.
- SCHROEDER, W.P.; ARELLANON, J.B.; BITTNER, T.; BARON, M.; ECKERT, H.J.; RENGER, G. Flash-induced absorption spectroscopy studies of copper interaction with photosystem II in higher plants. **Journal of Biological Chemistry**. v.30, p.32865–32870, 1994.
- SHELDON, J.S.; VERMA, S.S. Cu, CuO and Cu<sub>2</sub>O nanoparticles plasmons for enhanced scattering in solar cells. **Renewable Energy and the Environment, OSA Technical Digest (CD)** (Optical Society of America), paper JWE22, 2011.
- SHETH, B.P.; THAKER, V.S. Plant systems biology: insights, advances and challenges. **Planta**. v.240, p.33–54, 2014.
- SOUZA, G.M.; Prado, PRADO, C.H.B.A.; RIBEIRO, R.V.; BARBOSA, J.P.R.A.D.; GONÇALVES, A.N.; HABERMANN, G. Toward a systemic plant physiology. **Theoretical and Experimental Plant Physiology**. v.28, p.341–346, 2016.
- SOUZA, G.M.; RIBEIRO, R.V.; PRADO, C.H.B.S.; DAMINELI, D.S.C.; SATO, A.M.; OLIVEIRA, M.S. Using network connectance and autonomy analysis to uncover patterns of photosynthetic responses in tropical woody species. **Ecological Complexity**. v.6, p.15-26, 2009.
- SOUZA, P.V.L.; LIMA-MELO, Y.; CARVALHO, F.E.; REICHHELD, J.; FERNIE, A.; SILVEIRA, J.A.G.; DALOSO, D.M. Function and compensatory mechanisms among the components of the chloroplastic redox network. **Critical Reviews in Plant Science**. p.1-29, 2018. DOI:10.1080/07352689.2018.1528409
- STEFFEN, R.; ECKERT, H.J.; KELLY, A.A.; DORMANN, P.; RENGER, G. Investigations on the reaction pattern of photosystem II in leaves from *Arabidopsis thaliana* by time-resolved fluorometric analysis. **Biochemistry**. v.44, p.3123–3133, 2005.
- STIRBET, A.; LAZÁR, D.; KRONDIJK, J.; GOVINDJEE. Chlorophyll *a* fluorescence induction: Can just a one-second measurement be used to quantify abiotic stress responses? **Photosynthetica**. v.56, p.86-104, 2018.

- STRASSE, B. Donor side capacity of photosystem II probed by chlorophyll *a* fluorescence transient. **Photosynthesis Research**. v.52, p.147-155, 1997.
- STRASSER, R.J.; SRIVASTAVA, A.; GOVINDJEE. Polyphasic chlorophyll *a* fluorescence transient in plants and cyanobacteria. **Photochemistry and Photobiology**. v.61, p.32-42, 1995.
- STRASSER, R.J.; SRIVASTAVA, A.; TSIMILLI-MICHAEL, M. Analysis of the chlorophyll *a* fluorescence transient. In: PAPAGEORGIO, G.C.; GOVINDJEE (Eds.). **Chlorophyll *a* Fluorescence: A Signature of Photosynthesis. Advances in Photosynthesis and Respiration**. Springer, Dordrecht, 2004. pp. 321–362.
- STRASSER, R.J.; SRIVASTAVA, A.; TSIMILLI-MICHAEL, M. The fluorescence transient as a tool to characterize and screen photosynthetic samples. In (YUNUS, M.; PATHRE, U.; MOHANTY, P. (ed)): **Probing Photosynthesis: Mechanism, Regulation and Adaptation**. Taylor and Francis, UK, 2000. pp. 445–483.
- STRASSER, R.J.; TSIMILLI-MICHAEL, M. QIANG, S.; GOLSTEV, V. Simultaneous in vivo recording of prompt and delayed fluorescence and 820-nm reflection changes during drying and after re-hydration of the resurrection plant *Haberlea rhodopensis*. **Biochimica et Biophysica Acta: Bioenergetics**.v.1797, n.(6-7), p.1313-1326, 2010.
- TACHIBANA, Y.; VAYSSIERES, L.; DURRANT, J. Artificial photosynthesis for solar water-splitting. **Nature Photonics**. v.6, p.511-518, 2012.
- TREWAVAS, A. Understanding the control of plant development and the role of growth substances. **Australian Journal of Plant Physiology**. v.13, p.447-457, 1986.
- VON-BERTALANFFY, L. General System Theory. New York: 1968. George Braziller. 289p.
- XIONG, T.; DUMAT, C.; DAPPE, V.; VEZIN, H.; SCHRECK, E.; SHAHID, M.; PIERAL, A.; SOBANSKA, S. Copper oxide nanoparticle foliar uptake, phytotoxicity, and consequences for sustainable urban agriculture. **Environmental Science and Technology**. v.51,p. 5242-5251, 2017.
- YRUELA, I.; GATZEN, G.; PICOREL, R.; HOLZWART, A.R. Cu(II)-inhibitory effect on photosystem II from higher plants: a pico-second time-resolved fluorescence study. **Biochemistry**. v.35, p.9469–9474, 1996.

YUSUF, M.A.; KUMAR, D.; RAJWANSHI, R.; STRASSER, R.J.; TSIMILLI-MICHAEL, M.; GOVINDJEE, SARIN, N.B. Overexpression of  $\gamma$ -tocopherol methyl transferase gene in transgenic *Brassica juncea* plants alleviates abiotic stress: physiological and chlorophyll *a* fluorescence measurements. **Biochimica et Biophysica Acta: Bioenergetics**. v.1797, p. 1428-1438, 2010.

ZACRINAS, B.A.; CARTWRIGHT, B.; SPOUNCER, L.R. Nitric acid digestion and multi-element analysis of plant material by inductively coupled plasma spectrometry. **Communications in Soil Science and Plant Analysis**. v.18, n.1, p.131–146, 1987.



Supplementary materials

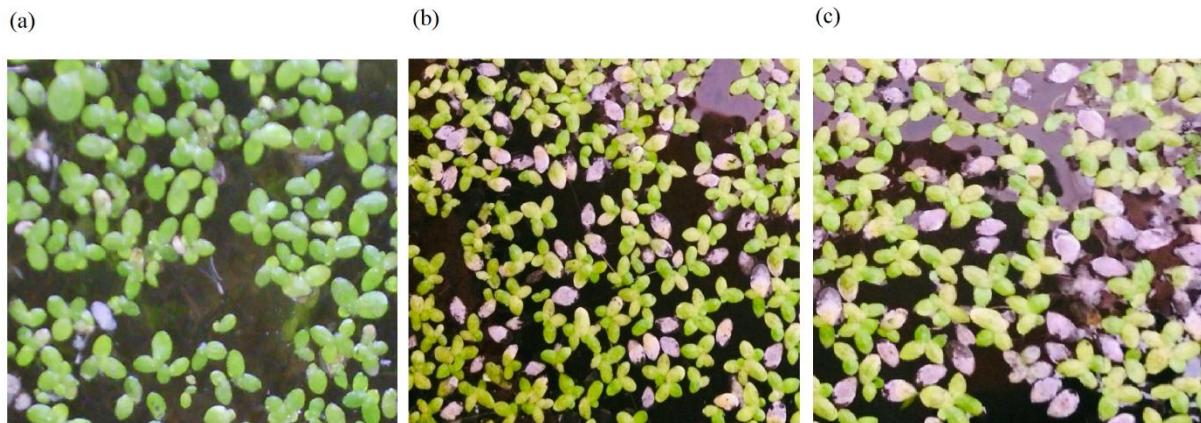


**Figure S1.** *Lemna valdiviana* plant treatments. (a) control. Higher doses (1000 mM) of (b)  $\text{CuSO}_4$  and (c)  $\text{CuONPs}$ . Visible necrosis was observed.

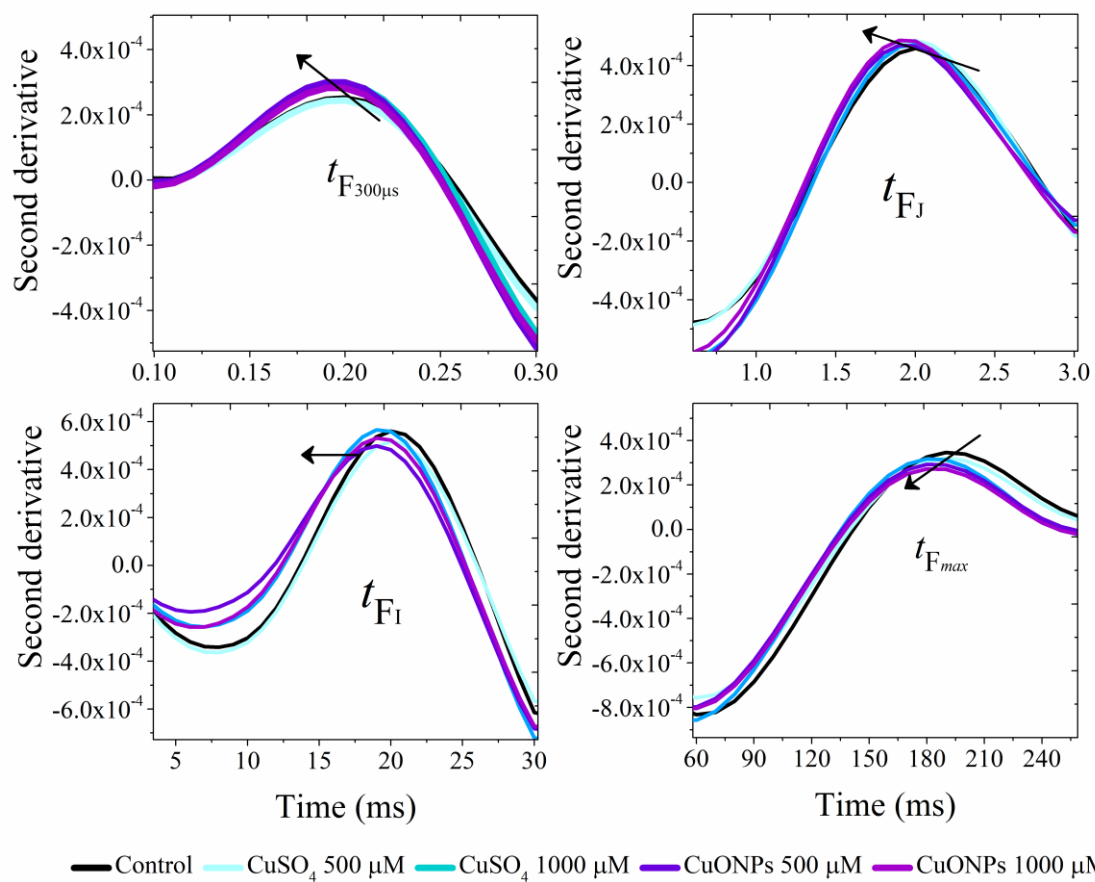


**Figure S2.** Second derivative of OJIP phases displaying the K-band, J-step, I-step and P-step, to providing quantitative information of time to reach KJIP events.

**Table S1.** Summary of fluorescence parameters, formulae and their description using data extracted from chlorophyll *a* fluorescence transient (OJIP-test)

<b>Fluorescence parameters Description</b>	
<b>Technical fluorescence parameters</b>	
$F_t$	Fluorescence intensity at time 't' after onset of actinic illumination
$F_o$	Minimum reliable recorded fluorescence at 50 $\mu$ s
$F_m$	Maximum recorded (= maximum possible) fluorescence at P-step
$F_v$	Maximum variable fluorescence ( $F_m - F_o$ )
Area	Total complementary area between fluorescence induction curve and $F = F_m$
$S_M = \text{Area}/F_V$	Normalized total complementary area above the OJIP transient (reflecting multiple turnover $Q_A$ reduction events)
$S_S = V_j/M_o$	Normalized total complementary area corresponding only to the O-J phase (reflecting single-turnover $Q_A$ reduction events)
$N = S_M/S_S = S_M M_o(1/V_j)$	Turnover number: number of $Q_A$ reduction events between time 0 and $t_{F_m}$
$V_j = (F_{2\text{ms}} - F_o)/(F_m - F_o)$	Relative variable fluorescence at the J-step (2 ms)
$V_i = (F_{30\text{ms}} - F_o)/(F_m - F_o)$	Relative variable fluorescence at the I-step (30 ms)
$M_o = 4(F_{300\mu\text{s}} - F_o)/(F_m - F_o)$	Approximated initial increment (in $\text{ms}^{-1}$ ) of the relative variable fluorescence
<b>Quantum efficiencies or flux ratios</b>	
$\phi_{P_o} = \text{TR}_o/\text{ABS} = 1 - (F_o/F_m) = F_v/F_m$	Maximum quantum yield of primary photochemistry at $t = 0$
$\phi_{E_o} = \text{ET}_o/\text{ABS} = (F_v/F_m) \times (1 - V_j)$	Quantum yield for electron transport at $t = 0$
$\psi_{E_o} = \text{ET}_o/\text{TR}_o = 1 - V_j$	Probability (at time 0) that a trapped exciton moves an electron into the electron transport chain beyond $Q_A^-$
<b>Specific energy fluxes (per <math>Q_A</math>-reducing PSII reaction center-RC)</b>	
$\text{ABS}/\text{RC} = M_o(1/V_j)(1/\phi_{P_o})$	Absorption flux (of antenna Chls) per RC (reflecting measure for an average antenna size)
$\text{TR}_o/\text{RC} = M_o(1/V_j)$	Trapped energy flux per RC (at $t = 0$ )
$\text{ET}_o/\text{RC} = M_o(1/V_j)\psi_o$	Electron transport flux per RC (at $t = 0$ )
$\text{DI}_o/\text{RC} = \text{ABS}/\text{RC} - \text{TR}_o/\text{RC}$	Dissipated energy flux per RC (at $t = 0$ )
$\text{PI}_{\text{ABS}} = (\text{RC}/\text{ABS})(\phi_{P_o}/(1-\phi_{P_o})) \times (\psi_o/(1-\psi_o))$	Performance index on absorption basis

\* For review see Strasser et al. (2004).



**CHAPTER IV – SYNERGISM AND INTERFERENCE OF  
BICARBONATE IONS ON NANCERIA EFFECTS IN *Salvinia auriculata*  
Aubl LEAF TISSUE: A CHLOROPHYLL FLUORESCENCE AND  
FOURIER TRANSFORM INFRARED PHOTOACOUSTIC  
SPECTROSCOPY STUDY**

Synergism and interference of bicarbonate ions on nanoceria effects in *Salvinia auriculata* Aubl leaf tissue: A chlorophyll *a* fluorescence and Fourier transform infrared photoacoustic spectroscopy study

M.S. Pontes<sup>a,b</sup>, R. Grillo<sup>c</sup>, D.E. Graciano<sup>d</sup>, W.F. Falco<sup>d</sup>, D.V. Lima<sup>b,e</sup>, S.M. Lima<sup>b,e</sup>, A.R.L. Caires<sup>d</sup>, L.H.C. Andrade<sup>b,e</sup>, E.F. Santiago<sup>a,b#</sup>

<sup>a</sup> Grupo de Estudos em Recursos Vegetais, Universidade Estadual de Mato Grosso do Sul, CP 350, 79804-970, Dourados, MS, Brazil.

<sup>b</sup> Programa de Pós-Graduação em Recursos Naturais, Centro de Estudos em Recursos Naturais, Universidade Estadual de Mato Grosso do Sul, CP 350, 79804-970, Dourados, MS, Brazil.

<sup>c</sup> Departamento de Física e Química, Faculdade de Engenharia de Ilha Solteira, Universidade Estadual Paulista (UNESP), Avenida Brasil, 56, Centro, 15385-000, Ilha Solteira, SP, Brazil.

<sup>d</sup> Grupo de Óptica Aplicada, Universidade Federal da Grande Dourados, CP 533, 79804-970, Dourados, MS, Brazil.

<sup>e</sup> Grupo de Espectroscopia Óptica e Fototérmica, Universidade Estadual de Mato Grosso do Sul, CP 350, 79804-970, Dourados, MS, Brazil.

<sup>f</sup> Grupo de Óptica e Fotônica, Instituto de Física, Universidade Federal de Mato Grosso do Sul, CP 549, 79070-900 Campo Grande, MS, Brazil

# Corresponding author: E-mail: felipe@uems.br

## ABSTRACT

With the continued increase of technological uses of cerium oxide nanoparticles (CeO<sub>2</sub> NPs or nanoceria) and their unregulated disposal, the accumulation of nanoceria in the environment is inevitable. Concomitantly, atmospheric carbon dioxide (CO<sub>2</sub>) levels continue to rise, increasing the concentrations of bicarbonate ions in aquatic ecosystems. This study investigates the influence of CeO<sub>2</sub> NPs (from 0 to 100 µgL<sup>-1</sup>) in the presence and absence of an elevated bicarbonate (HCO<sub>3</sub><sup>-</sup>) ion concentration (1 mM), on vibrational biochemical parameters and photosystem II (PSII) activity in leaf discs of *Salvinia auriculata*. Fourier transform-infrared photoacoustic spectroscopy (FTIR-PAS) was capable of diagnostic use to understand biochemical and metabolic changes in leaves submitted to the CeO<sub>2</sub> NPs and also detected interactive responses between CeO<sub>2</sub> NPs and HCO<sub>3</sub><sup>-</sup> exposure at the tissue level. The results showed that the higher CeO<sub>2</sub> NPs levels in the presence of HCO<sub>3</sub><sup>-</sup> decreased the non-photochemical quenching (NPQ) compared to the absence of HCO<sub>3</sub><sup>-</sup>. Moreover, the presence of HCO<sub>3</sub><sup>-</sup> significantly increased the NPQ at higher levels of CeO<sub>2</sub> NPs demonstrating that HCO<sub>3</sub><sup>-</sup> exposure may change the nonradiative process involved in the operation of the photosynthetic apparatus. Overall, the results of this study are useful for providing baseline information on the interactive effects of CeO<sub>2</sub> NPs and elevated HCO<sub>3</sub><sup>-</sup> ion concentration on photosynthetic systems.

**Keywords:** Bicarbonate; FTIR-PAS; Metabolite vibration modes; Nanoceria; Photosystem II

## RESUMO

Com a crescente utilização tecnológica de nanopartículas de óxido de cério ( $\text{CeO}_2$  NPs ou nanocério), associado ao seu descarte não regulamentado, o acúmulo ambiental de nanocério é inevitável. Concomitantemente, os níveis atmosféricos de dióxido de carbono ( $\text{CO}_2$ ) continuam crescentes ao longo dos anos, aumentando as concentrações de íons bicarbonato em ecossistemas aquáticos. Sendo assim, faz-se necessário uma avaliação do impacto ocasionado por estes materiais ao ambiente. Neste estudo avaliou-se a influência de  $\text{CeO}_2$  NPs (de 0 a  $100 \mu\text{gL}^{-1}$ ) na presença e ausência de uma concentração elevada de íons de bicarbonato ( $\text{HCO}_3^-$ ) (1 mM), sobre os parâmetros bioquímicos vibracionais e atividade do fotossistema II (PSII) em tecido foliar de *Salvinia auriculata*. A espectroscopia fotoacústica no infravermelho por transformada de Fourier (FTIR-PAS) foi capaz de diagnosticar às alterações bioquímicas e metabólicas em tecido foliar submetido às  $\text{CeO}_2$  NPs e também detectou respostas interativas entre as  $\text{CeO}_2$  NPs e a co-exposição à  $\text{HCO}_3^-$  em nível metabólico tecidual. Os resultados observados sugerem que os maiores níveis de  $\text{CeO}_2$  NPs na presença de íons de  $\text{HCO}_3^-$  diminuíram os valores do quenching-não-fotoquímico (NPQ), quando comparados à ausência de íons de  $\text{HCO}_3^-$  na solução. No entanto, a presença de íons de  $\text{HCO}_3^-$  diminuiu significativamente o NPQ nos maiores níveis de  $\text{CeO}_2$  NPs, demonstrando que a exposição ao  $\text{HCO}_3^-$  pode alterar o processo não-radioativo envolvido na operação do aparato fotossintético. No geral, os resultados deste estudo são úteis para fornecer informações básicas sobre os efeitos interativos das  $\text{CeO}_2$  NPs e íons  $\text{HCO}_3^-$  no aparato fotossintético.

**Palavras-chave:** Bicarbonato; FTIR-PAS; Modos vibracionais metabólicos; Nanocério; Fotossistema II

## 1. Introduction

Many properties of nanomaterials (NMs) have been studied due to their applicability in a variety of technological and industrial areas, such as solar cells, optics, catalysis, agriculture, medicine, and surface treatments (GRILLO et al., 2015; HANSEN et al., 2016). Currently, the estimated output of NMs produced is up to 270.000 metric ton/year (MEDINA-VELO et al., 2017; GRILLO et al., 2018). As a result, a great variety of NMs are released daily into the environment during the many steps of their manufacture, transport, use, and disposal (GRILLO et al., 2018). For example, cerium oxide nanoparticles (nanoceria) play an important role in cosmetic and consumer products, and due to their extensive use are released into the environment, with unpredictable consequences for natural systems and human health.

Cerium is the most abundant rare earth metal, and annual nanoceria production (around 10.000 metric tons/year) is one of the largest on the global metal oxide nanoparticles market (FEATURE MARKETS, 2012). It is estimated that by 2050 nanoceria will reach a maximum amount around  $62 \mu\text{g kg}^{-1}$  in agricultural soils and  $933 \mu\text{g kg}^{-1}$  in sludge treated soils (GIESE et al., 2018). Recent studies addressed the induction of plant stress by nanoceria exposure (RODEA-PALOMARES et al., 2012; MA et al., 2013), and also evaluated their effects on plants (ZHANG et al. 2015; ZHANG et al., 2017). However, our knowledge of the interactive effects of NMs and environmental factors remains incomplete (PÉREZ-DE-LUQUE, 2017; GIESE et al., 2018). Hence, there is a growing demand for studies that aim to understand the toxicity of NMs in combination with external environment influences (GRILLO et al., 2012; PIETROIUSTI et al., 2018; SIZOCHENKO et al., 2018).

In addition to the NMs released in the environment, other factors can accentuate the biotic responses, making it important to assess the synergism between NMs and other environmental conditioners and its effects on plant metabolism. Anthropogenic increases in atmospheric carbon dioxide ( $\text{CO}_2$ ) thought to be a factor in global climate change, also cause aquatic ecosystem acidification by reducing the concentration of carbonate ions ( $\text{CO}_3^{2-}$ ) and increasing the concentration of bicarbonate ions ( $\text{HCO}_3^-$ ) (ORR et al., 2005). In photosynthetic organisms, atmospheric  $\text{CO}_2$  diffuses through the cell wall into the cytosol and can dissolve in apoplast water to form  $\text{HCO}_3^-$  (RAMANAM et al., 2012). Under future climatic changes, elevated atmospheric  $\text{CO}_2$  concentrations ( $[\text{CO}_2]_e$ ) are expected to rise from the current 400 ppm to 550 ppm in 2050 (MISRA et al., 2015). Aquatic plants under elevated

$\text{HCO}_3^-$  concentration due to  $[\text{CO}_2]_e$  may employ a range of physiological and metabolic strategies in order to maintain growth and survival (RAMANAM et al., 2012). However, the mechanisms related to biochemical, metabolic, and photosynthetic responses in aquatic plants to elevated  $\text{HCO}_3^-$  concentration associated with NMs pollution are not known.

There is a need for fast analytical detection methods to evaluate the potential impact of these NMs on the environment and consequently on human health. To addressing this problem, diagnostic methods are needed to assess the NMs uptake, translocation, and bioaccumulation in trophic level (GONDIKAS et al., 2018). Methods based on chlorophyll *a* fluorescence (ChlF) are a powerful tool to understand the responses of photosynthetic organisms to several environmental stressors (RODRIGUEZ et al., 2003; CAIRES et al., 2011), and can be used to unravel the energy dissipation in photosystems (PSI and PSII) during the cyclic electron transport which occurs in both (SANTIAGO et al., 2015). On the other hand, metabolite changes modulate the plant survival under different environmental conditions.

Normally, to analyses these metabolite changes, an organism, tissue, or cell are exposed to various exogenous stimuli and the resulting metabolic variation are quantified. Vibrational spectroscopy has been established as a non-destructive method for qualitative and quantitative analysis of biomolecules and biochemical composition in biological samples (KWAK et al., 2007). Raman spectroscopy offers an alternative for photosynthetic pigment detection (VITEK et al., 2017). However, this powerful analytic technique has not yet been sufficiently exploited in photosynthetic organisms, especially upon environmental stressors or emergent pollutants contamination. Also, Fourier transform-infrared spectroscopy (FTIR) is an analytical device with enough high resolution, and a high-throughput to handle crucial information for understanding metabolic alterations based on vibrational modes of several functional groups (ANDRADE et al., 2008; KHAIRUDIN et al., 2014; SHARMA et al., 2018). FTIR spectroscopy provides a snapshot of metabolic and biochemical composition of biological samples, it can be compared with conventional techniques without the necessity of extraction procedures or sample preparation. Recently, this technique has been used to identify changes in plant biochemistry under stress condition (SHARMA AND UTTAM 2016; SHARMA et al., 2018).

The photosynthetic apparatus can be affected either directly or indirectly by the action of several NPs, including CuO, Ag and Au nanoparticles (PERREAUT et al., 2010; FALCO et al., 2011; FALCO et al., 2014; QUEIROZ et al., 2016) and has been probed by ChlF analysis. FTIR spectroscopy of plants exposed to NMs described potential variation in biochemical constituents of peanut leaves exposed to Fe<sub>2</sub>O<sub>3</sub> and CuO nanoparticles (SHURESH et al., 2016; SHURESH et al., 2016b; SHARMA AND UTTAM 2017) and wheat exposed to Au nanoparticles (SHARMA et al., 2018).

Although, the effects of elevated HCO<sub>3</sub><sup>-</sup> on plants have been widely studied, the short-term responses upon exposure to NMs are not reported. To determine how the presence of HCO<sub>3</sub><sup>-</sup> (1 mM) affected the effects of nanoceria at molecular and photosynthetic energy dissipation in leaf tissue of a floating aquatic macrophyte *Salvinia auriculata* Aubl., we performed metabolic characterization and photosynthetic physiological analysis based on FTIR-photoacoustic spectroscopy (PAS) and ChlF analysis to evaluate the interactive effects of nanoceria in an elevated bicarbonate ion concentration. Our basic hypothesis was that CeO<sub>2</sub> NPs and elevated HCO<sub>3</sub><sup>-</sup> would affect the photosystem complex in an isolated way or in a synergistic manner. It proposed that the FTIR-PAS would complement the ChlF in detecting physiological effects, primarily through the detection of alterations in protein structure and relative content of pigments.

## 2. Materials and methods

### 2.1 Cerium oxide nanoparticles

Nanoceria (99.99%, 130 nm) used in the present study were purchased from Ganzhou Wanfeng Advanced Materials Tech. Co., Ltd. (China). Different concentrations of CeO<sub>2</sub> NPs were twice dispersed by ultrasonic treatment (Ultrasonic Cleanser FS30, 100W, 42 kHz, Fisher Scientific, Atlanta, GA) in deionized H<sub>2</sub>O for 60 min and were maintained in the dark at room temperature overnight. The nanoparticles size and surface were estimated by scanning electron microscopy (SEM) and the mean size of the used CeO<sub>2</sub> NPs were 131.30 ± 2.4 nm. In addition, surface area and perimeter of cerium (II) oxide nanoparticles were estimated and present 1521 ± 50.7 nm<sup>2</sup> and 420 ± 7.62 nm, respectively. Additional information about the physicochemical characterization of the CeO<sub>2</sub> NPs is presented in the Supplementary Material (Figures S1, S2, and S3).

## 2.2 Plant materials and treatments

Shoots of *Salvinia auriculata* Aubl. (Salviniaceae) were manually collected from the Municipal Ecological Station Veredas of Taquarussu, Mato Grosso do Sul State, Brazil (22°37'50.4"S and 53°16'50.3"W) and washed in flowing water. The botanical identification was performed by Professor Dr. Etenaldo Felipe Santiago at the State University of Mato Grosso do Sul. These aquatic plants were separated according to size uniformity, rinsed with distilled water and maintained in polyethylene tanks (500 liters) due to their extremely fast growth. Young leaves were cut in small discs (diam. 10 mm) and surface sterilized by immersing for 15 min in 1.5% hypochlorite, leaf discs were rinsed with distilled water and transferred to Petri plates containing distilled water, and incubated at room temperature in the dark condition for 2 h. The leaf discs were immersed in nanoceria aqueous solution (0, 25, 50, 75, and 100  $\mu\text{gL}^{-1}$ ) in the absence and presence of  $\text{HCO}_3^-$ . The  $\text{HCO}_3^-$  was added to a final concentration of 1 mM. To replace air in the intracellular space with the media, we used infiltration medium. This was done to obtain information on the  $\text{HCO}_3^-$  effects in the presence of a minimum  $\text{CO}_2$  fixation as described by El-Shintinawy and Govindjee (1990). The duration of treatments was ~ 24 h, carried out in complete darkness.

## 2.3 Leaf uptake of cerium oxide nanoparticles

After the 24 h treatment, leaf tissues were cleaned with distilled water and dried in a 70°C incubator chamber for one week to remove water content. The dry leaf discs were milled into powder. To facilitate acid digestion, the tissues were baked at 550 °C in a Muffle furnace for 2 h before acid digestion. Leaf tissue digestion followed method described by Wang and co-authors (2012). The cerium ions measurements are carried out in the standard inductively coupled plasma-mass spectroscopy (ICP-MS) mode (PerkinElmer, USA). Calibration solutions (from 1  $\mu\text{gL}^{-1}$  to 100  $\mu\text{gL}^{-1}$ ) were prepared by serial dilution of the cerium standard solution ( $^{140}\text{Ce}$ , Sigma-Aldrich, Germany).

## 2.4 Fourier transform-infrared photoacoustic spectroscopy (FTIR-PAS)

Leaf discs were dried in a ventilated drying cabinet at 80 °C during 72 h before the measurements and then powdered using a mixer grinder. The FTIR-PAS absorption spectra



were performed with photoacoustic detection in the spectral region of 4000-400  $\text{cm}^{-1}$ , and sample spectra were obtained with an average of 128 samples scans and a resolution of 8  $\text{cm}^{-1}$  (Thermo Nicolet Nexus 670 spectrophotometer, Thermo Scientific, Waltham, MA, USA). Before each reading, the spectrometer was purged with dry compressed air to remove water vapor and  $\text{CO}_2$ , and the photoacoustic cell was purged with helium gas. A carbon black sample was used as reference of the infrared source, and new reference spectra were collected every 50 min. Leaf discs were dried in a ventilated drying cabinet at 80 °C during 72 h before the measurements and then powdered using a mixer grinder. From the obtained spectra, 13 absorption peaks were chosen, and the absorption intensities of the peaks were separated in a matrix, in which the frequency of each peak was used as variable with 100 permutations (Table 1). For carbohydrates peaks around 1200-900  $\text{cm}^{-1}$ , for proteins peaks around 1700-1500  $\text{cm}^{-1}$  and lipids the peaks around 3000-2800  $\text{cm}^{-1}$ .

### 2.5 Chlorophyll fluorescence imaging (ChlF)

Following the treatments, the leaf discs were removed from the solutions (in darkness) and dried in absorbent paper. Measurements were recorded after exposure at 1 and 24 h. All ChlF imaging inductions were measured using quenching analysis measuring protocols with actinic red light (617 nm: 600  $\mu\text{mol m}^{-2} \text{s}^{-1}$ ) and saturating pulse (cool white 2000  $\mu\text{mol m}^{-2} \text{s}^{-1}$ ) after ~ 1 h dark adaptation (FluorCam F-800, Photon Systems Instruments spol. sr.o.).

The ChlF parameters assessed were:

- maximum quantum yield of PSII photochemistry ( $F_v/F_m = [F_o - F_m]/F_m$ )
- effective quantum yield of PSII ( $\Phi_{\text{PSII}} = [qP_d[F_v/F_m]]/[1 + [1 - F_v/F_m]NPQ]$ )
- non-photochemical quenching ( $NPQ = [F_m - F_m']/F_m'$ )
- coefficient photochemical quenching in dark ( $qP_d = [F_m' - F_o'_{\text{act}}]/[F_m' - F_o'_{\text{calc}}]$ )

where  $F_o$  is the minimum ChlF yield in a dark-adapted state,  $F_o'$  is the minimum ChlF yield in a light adapted state,  $F_m$  is the maximum ChlF yield in a dark-adapted state,  $F_m'$  is the maximum ChlF yield in a light-adapted state,  $F_o'_{\text{act}}$  and  $F_o'_{\text{calc}}$  are the actual and calculated minimum levels of fluorescence in the dark after prior actinic light (AL) illumination.  $F_o'_{\text{calc}}$  is quantified as follows: ( $F_o'_{\text{calc}} = [1/[(1/F_o) - (1/F_m) + (1/F_m')]]$ ) (KITAJIMA AND BUTLER, 1975; GENTY et al., 1989; OXBOROUGH AND BAKER, 1997).

## 2.6 Statistical analysis

The experiments were carried out in randomized block design with three repetitions. Analysis were performed in R version 3.3.3. (R Developmental Core Team, R Foundation for Statistical Computing Platform), applying Student t test for comparison of means. For data analysis, the FTIR-PAS spectra were normalized and mean-centered. Normalized, transformed, imputed, outlier removed, and scaled peak area representative of relative metabolite amounts are presented in tables and figures. Values reported in all tables and text are presented as means, and differences were always considered significant when  $P < 0.05$ . The principal component analysis (PCA) was carried out to determine the factors that influence the variation in metabolite profile among the leaf samples treated with nanoceria in the absence and presence of  $\text{HCO}_3^-$ , where output consisted of score plot to visualize the contrast between different samples to explain the cluster separation. Hierarchical clustering analysis (HCA) using average linkage clustering was performed on Euclidean distances using Permut-Matrix, and for heat map, the data were normalized using z-scores of the intensity counts for each of the metabolites under the peak areas.

To assess changes in the homeostatic status of photosynthetic apparatus upon treatments, we evaluated differences in modulation of photochemical network connectance when individuals were submitted to stress conditions. Modulation was defined as the change in the mean strength of connections among network elements, which was measured through global connectance,  $C_g$ , following Amzallag (2001).

The Pearson's correlation coefficients ( $r$ ) between each paired variable were used to test the significance of the correlation and to measure the strength of the relationship, performing a z-transformation (AMZALLAG, 2001):  $z = 0.5 L_m [(1 + |r|)/(1 - |r|)]$ . The global network connectance ( $C_g$ ) was calculated as the average of z-values (2001). The photochemical network was formed by the relationships  $\Phi_{\text{PSII-qP}_d}$ ,  $\Phi_{\text{PSII-Fv/Fm}}$ ,  $\Phi_{\text{PSII-Fv'/Fm'}}$ ,  $\Phi_{\text{PSII-NPQ}}$ ,  $qP_d\text{-NPQ}$ ,  $Fv/Fm\text{-NPQ}$ ,  $Fv'/Fm'\text{-NPQ}$  and  $Fv/Fm\text{-qP}_d$ ,  $Fv'/Fm'\text{-qP}_d$  and their average strength yields the global connectance of the photochemical network ( $C_{g\text{pho}}$ ).

## 3. Results and discussion

### 3.1 Cerium uptake

The accumulation of Ce in leaf tissue was determined by ICP after 24 h of exposure. The concentrations of Ce in the CeO<sub>2</sub> NPs exposed tissue sample are shown in Fig. 1. The leaf tissue Ce ion concentrations increased gradually with increasing CeO<sub>2</sub> nanoparticles concentration treatments exposed upon leaf discs and more sharply in the presence of HCO<sub>3</sub><sup>-</sup> ions. This may be explained due to enhanced bioavailability Ce ions in low pH (TYLER AND OLSSON, 2002). Although, insights into the interactions of nanoceria and bicarbonate ions in plants are currently unavailable, different way of CeO<sub>2</sub> contamination and organ accumulate are described in the literature (ZHAO et al., 2012; HONG et al., 2014), For example, when exposed on soil, CeO<sub>2</sub> can affect tissues and the main accumulation is localized in roots (ZHAO et al., 2012). When applied directly on leaves, CeO<sub>2</sub> NPs can penetrate inner tissues and be relocated to the other plant parts (HONG et al., 2014). Besides that, physicochemical parameters of the nanoparticles, such as size, superficial charge, coating, and morphology may influence the interaction of nanoparticles with plants (PERALTA-VIDEA et al., 2014; BARRIOS et al., 2016; PEREZ-DE-LUQUE, 2017; BARRIOS et al., 2017). We hypothesized that CeO<sub>2</sub> nanoparticles will behave differently at leaf disc exposure, when compared to foliar injection, spray, or deposition is due to mechanical damage, and consequently may show different level of toxicity due to facilitated uptake.

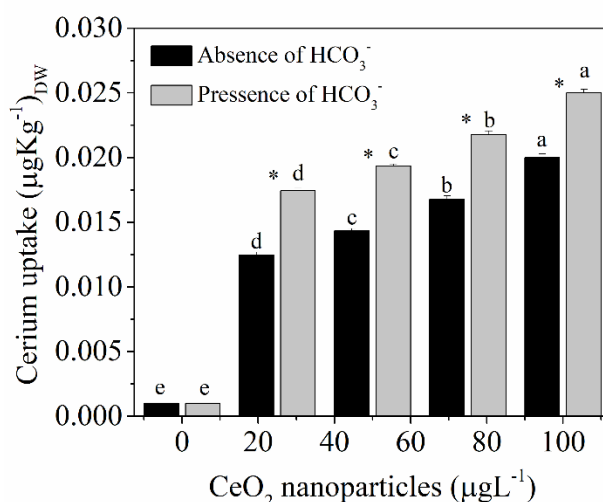


**Figure 1.** Accumulation of cerium ions in leaf tissues of *Salvinia auriculata* plants under different exposure concentrations of cerium oxide nanoparticles (CeO<sub>2</sub> NPs) in the absence and presence of HCO<sub>3</sub><sup>-</sup>. Data points are averages from triplicate samples, and error bars represent one standard error. Different letters indicate statistical difference ( $p < 0.05$ ) between

CeO<sub>2</sub> NPs doses; asterisks (\*0.05 and\*\*0.001) compare AB and PB treatments at the same dose.

### 3.2 Fourier transform-infrared photoacoustic spectroscopy

In leaf discs of *S. auriculata* exposed to CeO<sub>2</sub> NPs in presence and absence of HCO<sub>3</sub><sup>-</sup>, the thirteen peaks detected within FTIR-PAS analysis of *S. auriculata* leaf disc exposed to treatments are summarized in the Table 1 and represented in Fig. 2. FTIR-PAS absorption spectra of standard representing the biomolecular compounds analyzed in plant leaves tissue are depicted in Fig. 2 summarized as function of the presence and absence of HCO<sub>3</sub><sup>-</sup> in relationship to CeO<sub>2</sub> NPs concentrations (top-down). An enhancement of relative FTIR-PAS absorption intensity due to the NH stretching vibration mode of Amide A (~3356 cm<sup>-1</sup>) was clearly observed in case of treatment with HCO<sub>3</sub><sup>-</sup> in combination with increase of CeO<sub>2</sub> NPs level. This vibrational mode is exclusively localized on the proteins insensitive to the conformation of the polypeptide backbone (BARTH, 2007). Primary metabolites can be considered as essential plant constituents, directly involved in their growth, development, physiology, and reproduction. Thus, Figure S4 revealed the vibrational modes three functional groups of chemical compounds (lipids, proteins, and carbohydrates).

**Table 1.** Tentative frequency assignment of Fourier transform-infrared photoacoustic spectroscopy (FTIR-PAS) for the thirteen selected peaks.

Peak	Wavenumber (cm <sup>-1</sup> )	Functional group and vibration mode	Metabolic type
1	3356	vN-H	Amide A
2	2931	v <sub>as</sub> CH <sub>2</sub>	Lipids
3	2854	v <sub>s</sub> CH <sub>2</sub>	Lipids
4	1740	vC=O	α-amino acid side chain
5	~ 1650	vC=O	Amide I
6	~ 1550	δ <sub>s</sub> NH <sub>3</sub> <sup>-</sup>	Amide II
7	1420	δCOH or δCO <sub>2</sub> H	Amide II
8	1375	δ <sub>s</sub> CH <sub>3</sub>	Amide III
9	1315	δCH <sub>3</sub>	Amide III
10	1238	δN-H coupled with δC-H or vC-N	Amide III
11	1160	vC-O	Carbohydrate residues
12	1080	vC-O	Carbohydrate residues
13	1034	vC-O	Carbohydrate residues

v: stretching vibration, v<sub>s</sub>: symmetric stretching vibration, v<sub>as</sub>: asymmetric stretching vibration, δ: in plane bending vibration, δ<sub>s</sub>: asymmetric in plane bending vibration.

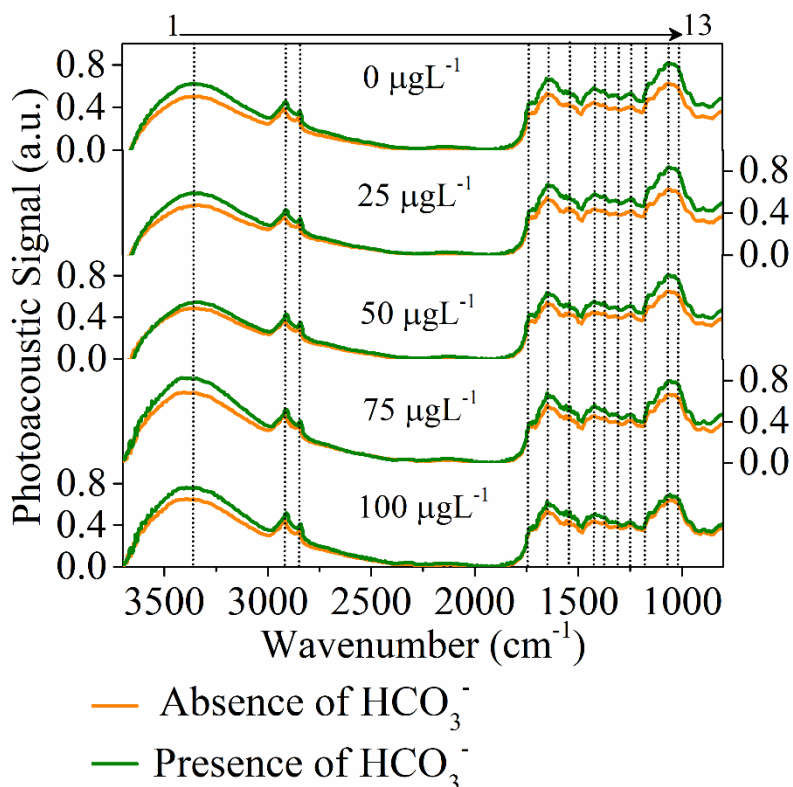


**Figure 2.** Average of Fourier transform-infrared photoacoustic absorption spectra of *Salvinia auriculata* leaf discs exposed to different concentrations of cerium oxide nanoparticles ( $\text{CeO}_2$  NPs) in the presence and absence of  $\text{HCO}_3^-$ . The lines indicate the thirteen most important peaks that were selected for statistical analysis

A list of thirteen metabolite peaks detected in both experiments can be seen in Figure 3. Hierarchical cluster analysis (HCA) rendered in heat maps were used for further understanding of how leaf metabolites changed in response to the  $\text{CeO}_2$  NPs in relation to bicarbonate presence or not. Compared with administration of  $\text{HCO}_3^-$ , the  $\text{CeO}_2$  NPs concentrations affect the metabolism; Euclidian distance reveals two major cluster shown clearly the absence and presence of  $\text{HCO}_3^-$ . However, the highest  $\text{CeO}_2$  NPs treatments are mostly linked in the absence and presence of  $\text{HCO}_3^-$ ; the lowest treatments in bicarbonate presence were separated. In the without  $\text{HCO}_3^-$ , three different subclusters were also separated.

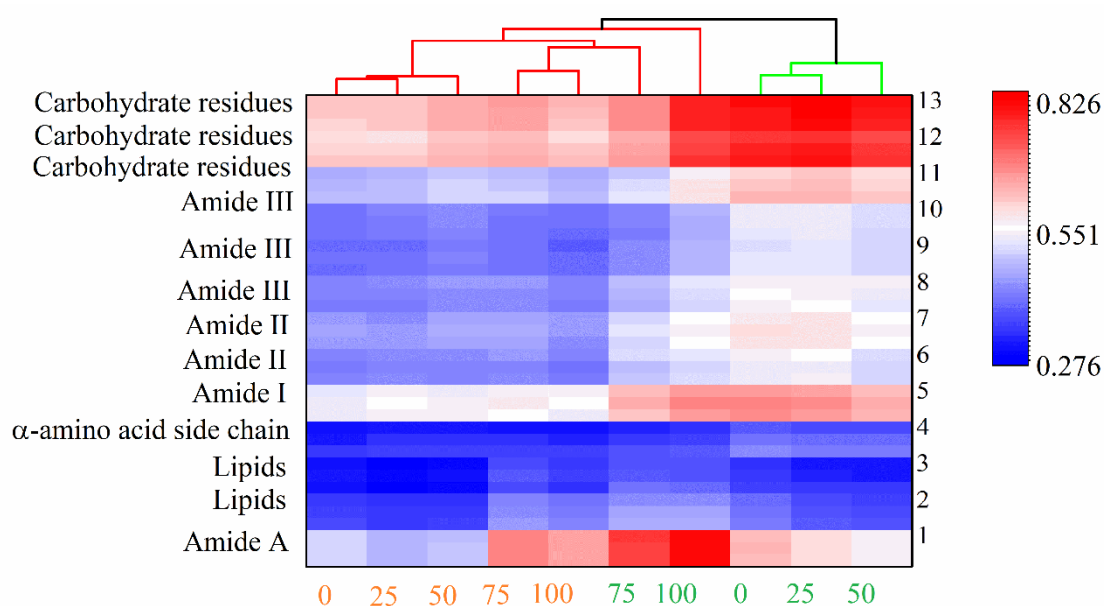


**Figure 3.** Unsupervised hierarchical clustering analysis (HCA) reveals distinct clusters of vibrational metabolic fingerprint based on the thirteen selected peaks of Fourier transform-infrared photoacoustic spectroscopy of *Salvinia auriculata* leaf discs obtained from distinct concentrations of cerium oxide nanoparticles ( $\text{CeO}_2$  NPs) in the presence and absence of  $\text{HCO}_3^-$ . Values were subjected to average linkage clustering (Euclidean distance) and heat maps showing metabolites vibrational modes in the absence (orange numbers) and presence (green numbers) of  $\text{HCO}_3^-$ .

PCA revealed grouped and differential responses of the metabolite vibrational modes to  $\text{CeO}_2$  NPs and the  $\text{HCO}_3^-$  with an interpretable visualization (Fig. 4). The resulting plots for FTIR photoacoustic absorption spectra explained 98% variations by two PCs (PC1 -75.70% and PC2 -22.43%) attributed to the variations from the presence of bicarbonate ions and  $\text{CeO}_2$  NPs treatment components. Additionally, nanoceria effects identification attributable to high concentrations was confirmed by PCA comparing against the HCA results shown in Fig. 3.

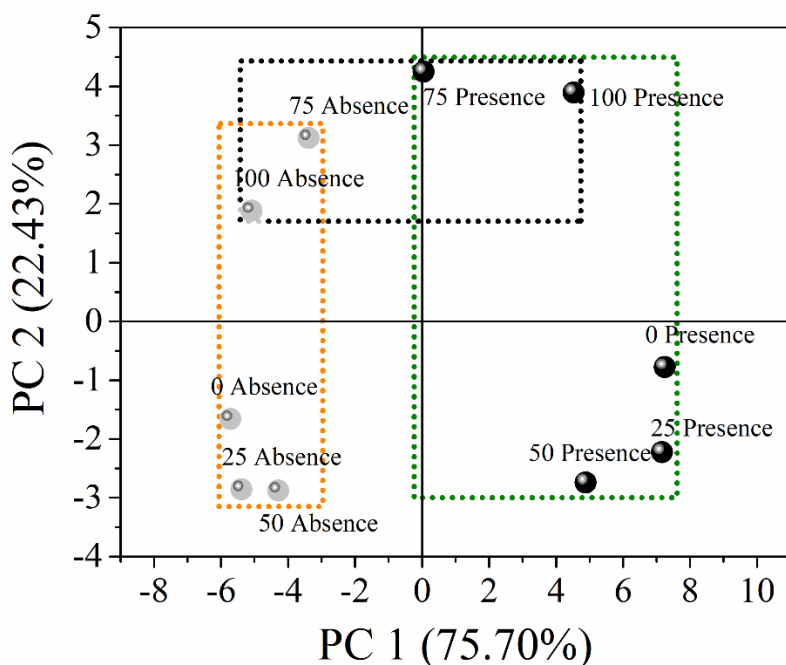


**Figure 4.** Principal component analysis (PCA) of metabolite changes in the thirteen selected peaks of Fourier transform-infrared photoacoustic spectroscopy of *Salvinia auriculata* leaf discs obtained from distinct concentrations of cerium oxide nanoparticles ( $\text{CeO}_2$  NPs) in the absence (grey symbols) and presence (black symbols) of  $\text{HCO}_3^-$ . PCA was performed using three replicate data of relative metabolite FTIR peak, and the generated PC1 and PC2 were plotted.

The band  $\sim 3356 \text{ cm}^{-1}$  represent the NH stretching vibrations (Amide A) and is exclusively localized on the proteins insensitive to the conformation of the polypeptide backbone (Fig. 2 and 5). Amide A originates from a Fermi's resonance between the first overtone of amide II and the N-H stretching vibration (KRIMM AND DWIVEDI, 1982; BANDEKAR, 1992; BARTH, 2007). The high concentrations of  $\text{CeO}_2$  NPs (75 and  $100 \mu\text{gL}^{-1}$ ) induces an enhancement of infrared absorption at the band between  $3310$  and  $3270 \text{ cm}^{-1}$  related to Amide A mode, suggest that the treatments can affect the protein structure caused by conformational disorders (Fig. 5). The Amide I vibration mode ( $\sim 1650 \text{ cm}^{-1}$ ) is primarily a C=O stretching vibration, with some contributions from the out-of-phase C-N stretching vibration and CNN deformation (KRIMM AND DWIVEDI, 1982). In the presence of  $\text{HCO}_3^-$  at the highest treatment of  $\text{CeO}_2$  NPs, an increasing helix length was observed due to decrease in intensity of Amide I band position, evidencing the synergistic effect between NPs and



$\text{HCO}_3^-$  at molecular level. The bicarbonate as well as nanoceria concentrations significantly influenced the Amides modes (II, IV, V, and V) absorption intensities. Except for Amide II band in without bicarbonate, Amide II mode is an out-of-phase combination of NH in-plane-bend and CN stretching vibration (BANDEKAR, 1992; BARTH, 2007). The Amides vibration provides a valuable structural information, the Amide IV band are clearly suppressed in the  $\text{HCO}_3^-$  presence or not in response to  $\text{CeO}_2$  NPs concentrations, this band is mainly CO in-plane-bend plus CC stretching vibration, with a small contribution from CNC deformation (BANDEKAR, 1992). The amide VI decrease may be attributed to changes in N and H atoms displaced during this normal mode of vibration (mainly CO out-plane-bend). Characteristic signals die to the fingerprint region of lipids (Fig. 2 and Fig. S4) were detected at 2854 and 2931  $\text{cm}^{-1}$  that were assigned to symmetric and asymmetric stretching vibration of lipids ( $\text{CH}_2$  group), respectively.

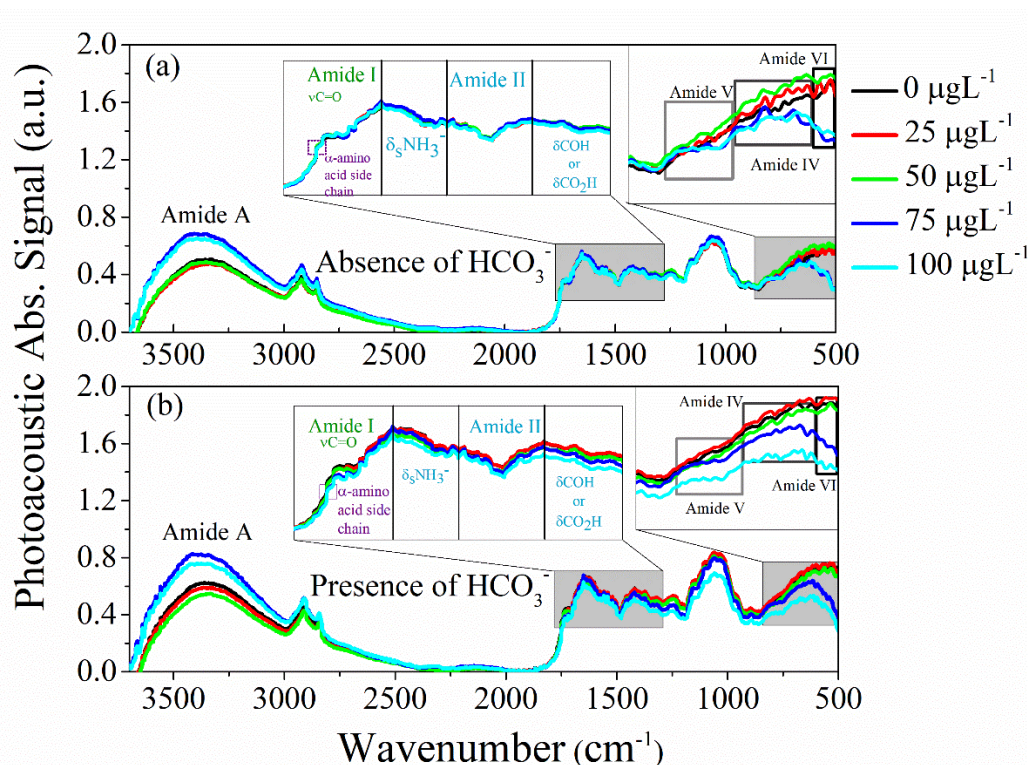


**Figure 5.** Average of Fourier transform photoacoustic infrared absorption spectra of *Salvinia auriculata* leaf discs obtained from distinct treatments of cerium oxide nanoparticles ( $\text{CeO}_2$  NPs) in the (a) absence and (b) presence of  $\text{HCO}_3^-$ . Inset graphs represent the vibrational modes of proteins (Amide I to Amide VI).



The relative biochemical changes induced by CeO<sub>2</sub> NPs as well as HCO<sub>3</sub><sup>-</sup> are assessed by calculating the average ratio of peak intensities corresponding to some selected wavenumber was shown in Fig. 6. The mean ratio related to protein relative concentration ( $I_{1540/3347} \text{ cm}^{-1}$ ) at higher concentrations ( $>75 \mu\text{gL}^{-1}$ ) decrease ( $\sim 34.5\%$ ) over the lowest ( $<25 \mu\text{gL}^{-1}$ ) samples ( $p < 0.001$ ). On the other hand, the relative protein found increased in 25 and 50  $\mu\text{gL}^{-1}$  ( $p < 0.05$ ). The glycoprotein ratio is more affected by the bicarbonate in relation to CeO<sub>2</sub> NPs exposure, first by an increased intensity followed by a decline at higher concentration used. Due to shift of photoacoustic absorbance intensity in the Amide I band is defined in terms to secondary structure elements, the intensity ratio at  $1550/1650 \text{ cm}^{-1}$  was used to estimate the deformation induced in FTIR-PAS spectra, and a semiquantitative estimation the content ratio of the  $\beta$ -sheet/ $\alpha$ -helix (Fig. 6c) (LITVINOV et al., 2012). Rico and co-authors demonstrated modifications in amino acid composition and fatty acid contents in *Oryza sativa* and *Triticum aestivum* after exposure to CeO<sub>2</sub> nanoparticles (RICO et al., 2013; RICO et al., 2014). A further confirmation of changes induced by CeO<sub>2</sub> nanoparticles in amylose, amino acids, and crude protein contents was provided by Pošćić et al. (2016) in *Hordeum vulgare*.

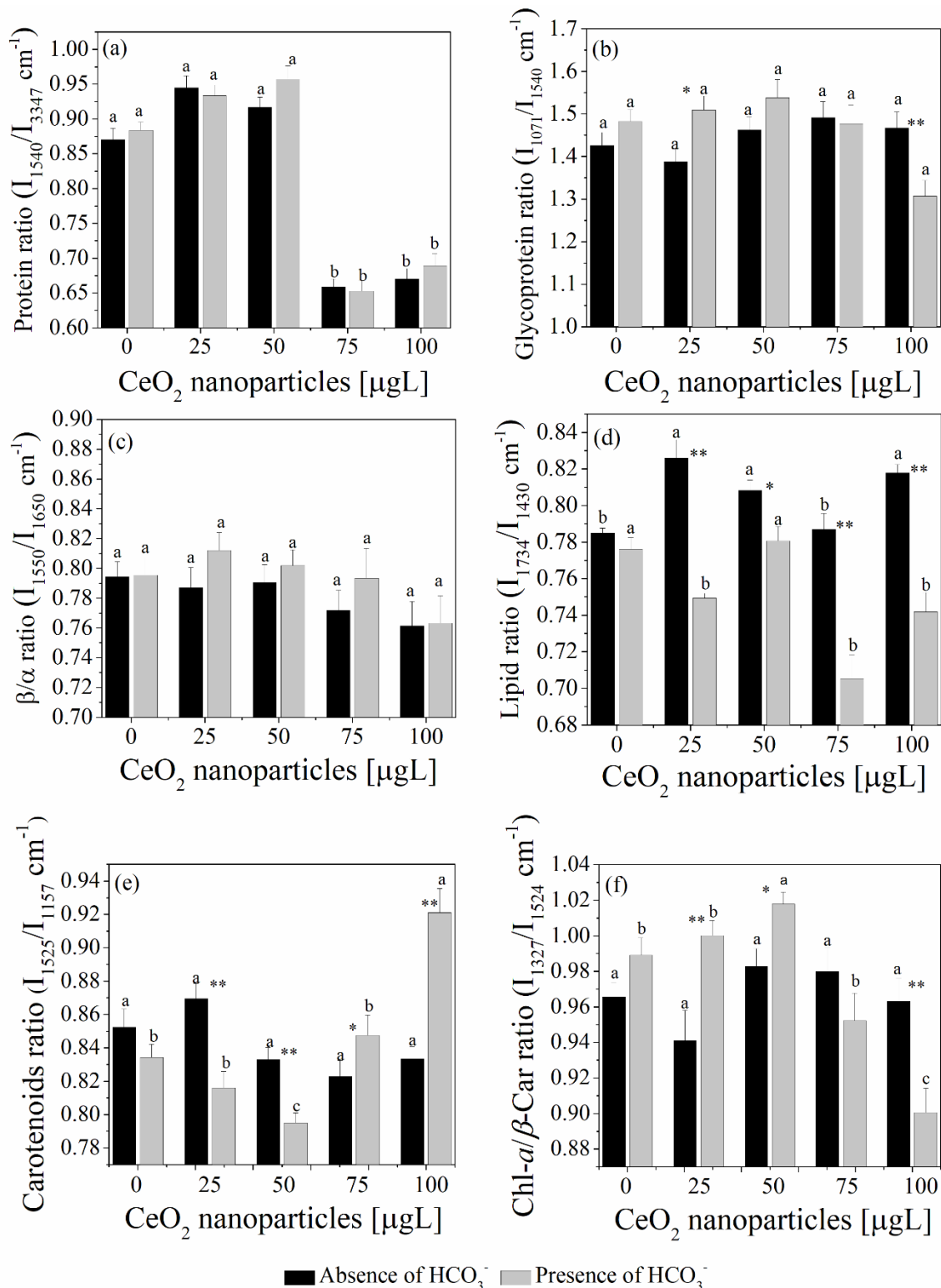


**Figure 6.** Average ratio of peak intensities of the Fourier transform photoacoustic infrared absorption spectra of *Salvinia auriculata* leaf discs obtained from distinct treatments of cerium oxide nanoparticles (CeO<sub>2</sub> NPs) in the (a) absence and (b) presence of HCO<sub>3</sub><sup>-</sup>. The infrared absorbance intensity ratios at (a) proteins; (b) glycoproteins; (c)  $\beta$ -sheet/ $\alpha$ -helix; (d)

lipids; (e) carotenoids; and (f) chlorophyll-*a*/  $\beta$ -carotene. Different letters indicate statistical difference ( $p < 0.05$ ) between CeO<sub>2</sub> NPs doses; asterisks (\*0.05 and\*\*0.001) compare AB and PB treatments at the same dose.

The average values to lipid ratio ( $I_{1734}/I_{1430} \text{ cm}^{-1}$ ) varied under different CeO<sub>2</sub> NPs doses with evident reduction to the HCO<sub>3</sub><sup>-</sup> treatment (Figure 6d). Modifications in lipid components under CeO<sub>2</sub> NPs exposure can be described as membrane damage, both of which lipid peroxidation and electrolyte leakage are good indicators (RICO et al., 2013b), these kinds of response are reactive oxygen species (ROS) related, the membrane structure can be rapidly attack by ROS. However, in some plants enzymes like catalase (CAT) and ascorbate peroxidase (APX) are useful to eliminate the excess of H<sub>2</sub>O<sub>2</sub>, avoiding the potential lipid damage caused by the CeO<sub>2</sub> NPs (SHARMA AND UTTAM, 2017).

For calculating relative carotenoids variation, and the relationship chlorophyll *a* (Chl-*a*) and  $\beta$ -carotene ( $\beta$ -car)  $I_{1327}/I_{1524} \text{ cm}^{-1}$ , the total carotenoids (Car) ratios at intensities  $I_{1525}/I_{1157} \text{ cm}^{-1}$  is calculated, respectively (Fig. 6e-f). Comparable results were obtained repeatedly from different CeO<sub>2</sub> NPs levels treated in the same way for HCO<sub>3</sub><sup>-</sup> and significantly, signs of changes in pigment content were observed. The higher level of CeO<sub>2</sub> NPs in the HCO<sub>3</sub><sup>-</sup> treatment resulted in an enhanced Car signal related to their relative concentration. Moreover, the Chl-*a*/ $\beta$ -car content decreases at relatively high doses of CeO<sub>2</sub> NPs, in the case of HCO<sub>3</sub><sup>-</sup> co-exposure. In fact, some experimental results showed that CeO<sub>2</sub> NPs induces the decrease in the chlorophyll concentrations in most crop plants (LIZZI et al., 2017); the Car enhancement at high CeO<sub>2</sub> doses can be related to their antioxidant effect or to prevent photooxidative damage. Under ROS stress Car includes the non-enzymatic antioxidants form to the antioxidant machinery, belonging to the lipophilic antioxidant family, localized in the plastids of photosynthetic and non-photosynthetic tissues (DAS AND ROYCHOUNDHURY, 2014). The carotenoids of the xanthophylls cycle (20-40% of the carotenoids pool) plays a vital role in photoprotective energy dissipation due to their peripherally association with light harvesting complex (DEMMIG-ADANS, 1990; RUBAN et al., 1999).

### 3.3 Chlorophyll *a* fluorescence (ChlF) imaging

We investigated the changes on the functioning of photosynthetic apparatus by using the pulse-amplitude modulated (PAM) approach. To further quantify the exogenous effects on overall leaf photosynthetic apparatus, the ChlF induction kinetics curves were determined. The ChlF emission kinetics induced by actinic illumination was not sensitive to different CeO<sub>2</sub> NPs concentrations used in this study (data are shown in Fig. S5), this may be partially attributed to the low concentrations of CeO<sub>2</sub> NPs used (at  $\mu\text{gL}^{-1}$  scales). In fact, CeO<sub>2</sub> NPs were shown to improve plant growth and yield under certain concentrations (WANG et al., 2012); moreover, changes on the ChlF emission kinetics are a non-mandatory response and it depending upon type, intensity and duration of stress as well as plant species, sensibility and its stage of development (RODRIGUEZ et al., 2003; CAIRES et al., 2011; SANTIAGO et al., 2015). However, the mechanisms related to positively or negatively impacts of CeO<sub>2</sub> NPs are not fully understood (PEREZ-DE-LUQUE, 2017).

Even though the ChlF kinetics curves have not been effective to express the CeO<sub>2</sub> NPs stress under experimental conditions, the differences in presence or absence of bicarbonate ions were clearly reflected by changes in non-photochemical quenching (NPQ). In the HCO<sub>3</sub><sup>-</sup> treated leaves, the significantly lower values of NPQ as compared to without HCO<sub>3</sub><sup>-</sup> were recorded (Fig. 7a-b). The NPQ reflects heat-dissipation of excitation energy in the light-harvesting antennae system. NPQ is a combination of photoprotective adjustment, photoinhibition and photodamage (KRAUSE AND WEISS, 1991). After 24 hours, leaf discs treated with 75 and 100  $\mu\text{gL}^{-1}$  of CeO<sub>2</sub> NPs and co-exposed with HCO<sub>3</sub><sup>-</sup> had significantly more heat-dissipation with respect to control. Our reported increase in NPQ indicate preferentially use this mechanism to manage excess energy generation in the presence of HCO<sub>3</sub><sup>-</sup>. NPQ was affected by the interaction of the CeO<sub>2</sub> NPs and HCO<sub>3</sub><sup>-</sup> treatments. The enhancement in NPQ in *S. auriculata* leaf tissue under elevated HCO<sub>3</sub><sup>-</sup> ion concentration suggest dissipative nonradiative losses of excitation energy absorbed by PSII and a probably protective role of HCO<sub>3</sub><sup>-</sup> on the functioning of photosynthetic apparatus related to preventing ROS mediated photodamage (KRAUSE AND WEISS, 1991). Fig. S6 shows NPQ images of leaf discs exposed to nanoceria. The HCO<sub>3</sub><sup>-</sup> effects in thylakoid membrane has been known to reversing the effects of inhibitory anions (EL-SHINTINAWY AND GOVINDJEE, 1900), particularly on the electron acceptor side of PSII between the first plastoquinone acceptor

( $Q_A$ ) and the plastoquinone pool (PQ-pool) (EL-SHINTINAWY AND GOVINDJEE, 1900; WYDRZYNSKI AND GOVINDJEE, 1975).

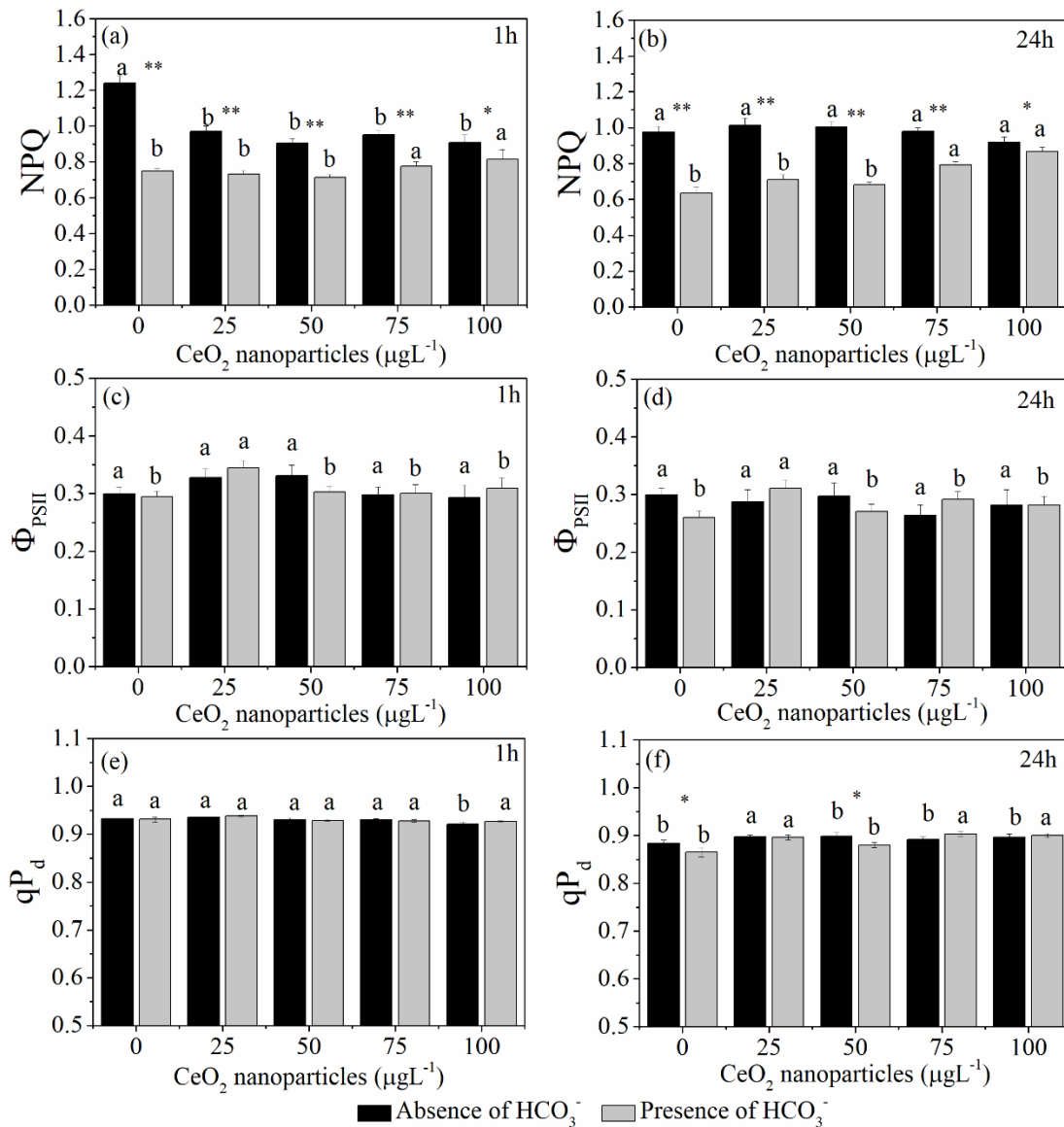


**Figure 7.** Chlorophyll *a* fluorescence parameters of *Salvinia auriculata* leaf discs obtained from distinct treatments of cerium oxide nanoparticles ( $CeO_2$  NPs) in the absence and presence of  $HCO_3^-$  after 1 and 24 hours exposure. Non-photochemical quenching (NPQ); Effective quantum yield of photosystem II or the proportion of the light absorbed by photosystem II that is used in photochemistry ( $\Phi_{PSII}$ ); Coefficient of photochemical quantum yield in dark ( $qP_d$ ). Different letters indicate statistical difference ( $p < 0.05$ ) between  $CeO_2$  NPs doses; asterisks (\*0.05 and\*\*0.001) compare AB and PB treatments at the same dose.

The proportion of the light absorbed by PSII that is used in photochemistry ( $\Phi_{\text{PSII}}$ ), significantly increased was observed only at the lowest level ( $25 \mu\text{gL}^{-1}$ ) of  $\text{CeO}_2$  NPs in the bicarbonate presence tested (Fig. 7c-d). Although in a nonlinear way, the quantum coefficient of photochemical quenching,  $qP_d$  was changed (especially after 24 hours after exposure) in response to  $\text{CeO}_2$  NPs levels in the  $\text{HCO}_3^-$  treatment (Fig. 7e-f). However,  $qP_d$  was stable at around  $\sim 0.9$  under all treatments. This parameter reflects the functionality of the RCs and the rate of oxygen evolution (GIOVAGNETTI AND RUBAN, 2015; TOWNSEND et al., 2017), our observed results suggest a linkage between the role of bicarbonate ions on the protective process of RC of PSII under  $\text{CeO}_2$  NPs exposure. The ChlF parameters  $qP_d$  and NPQ provide a rapid and non-invasive method to assessing PSII RCs functionality (TOWNSEND et al., 2017).

The maximal PSII fluorescence yield ( $F_v/F_m$ , in dark-adapted state) and maximum fluorescence yield of PSII at a steady-state of fluorescence ( $F_v'/F_m'$ , in light-adapted steady-state) (KRAUSE AND WEISS, 1991) exhibited the different patterns. After 1h of treatment exposure the highest levels of  $\text{CeO}_2$  NPs increase the  $F_v/F_m$  and  $F_v'/F_m'$ . After 24h of nanoceria exposure,  $F_v/F_m$  enhanced only at intermediary concentration ( $50 \mu\text{gL}^{-1}$ ) at the bicarbonate treatment (Fig. 8). Operational quantum yield ( $F_v'/F_m'$ ) appeared to be affected by a higher level of  $\text{CeO}_2$  NPs.

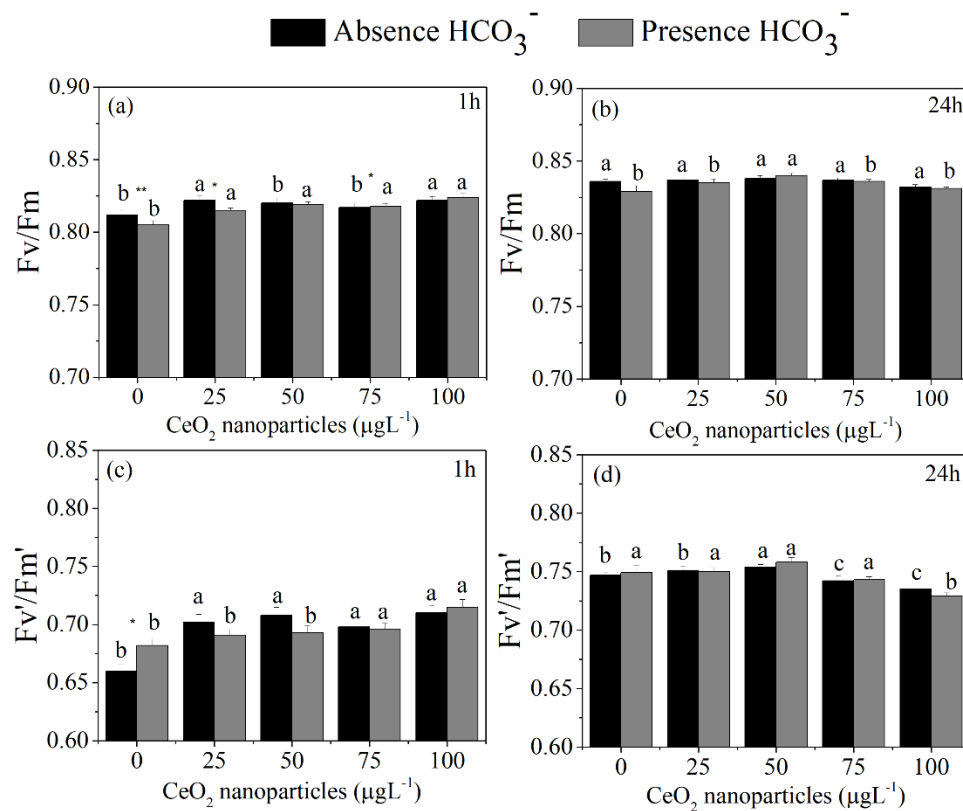


**Figure 8.** Chlorophyll *a* fluorescence parameters of *Salvinia auriculata* leaf discs obtained from distinct treatments of cerium oxide nanoparticles (CeO<sub>2</sub> NPs) in the absence and presence of HCO<sub>3</sub><sup>-</sup> after 1 and 24 hours exposure. Maximum photosystem II quantum yield in dark-adapted state (Fv/Fm) and; Maximum photosystem II quantum yield at steady-state (Fv'/Fm'). Different letters indicate statistical difference (p < 0.05) between CeO<sub>2</sub> NPs doses; asterisks (\*0.05 and \*\*0.001) compare AB and PB treatments at the same dose.

However, an inhibitory effect of CeO<sub>2</sub> NPs or HCO<sub>3</sub><sup>-</sup> on the functioning of PSII has not been observed. In this case, Fv/Fm is not a sensitive indicator to nanoceria toxicity in *Salvinia auriculata* at concentrations reported in this study. Additionally, similar results are also observed by Rodea-Palomares et al. (2012) in two aquatic organisms (cyanobacteria *Anabaena* CPB4337, and the green alga *Pseudokirchneriella subcapitata*) with a range of nanoceria concentrations from 0.01 to 100 mg/L. On the other hand, the experimental evidence obtained in our results using FTIR-PAS spectroscopy and ChlF can confirm the interactive effects of CeO<sub>2</sub> NPs and HCO<sub>3</sub><sup>-</sup>.

The results of network connectance analysis (Fig. 9) considering the variations in the modulation of photosystem II photochemical network, showed some differences among

treatments concerning how the PSII adjusts their function to imposed treatments. We observed in our results a general increasing trend in the connectance of photochemical network values on the exposure of CeO<sub>2</sub> NPs, related to homeostatic maintenance of photosynthetic apparatus upon NMs exposure. However, in the presence of HCO<sub>3</sub><sup>-</sup>, an inverses behavior was observed. These results may indicate a higher modulation (homeostatic adjustment) in the PSII photochemical network; enhanced connectance values can indicate great system stability, up to a critical threshold (BERTOLLI et al., 2013).

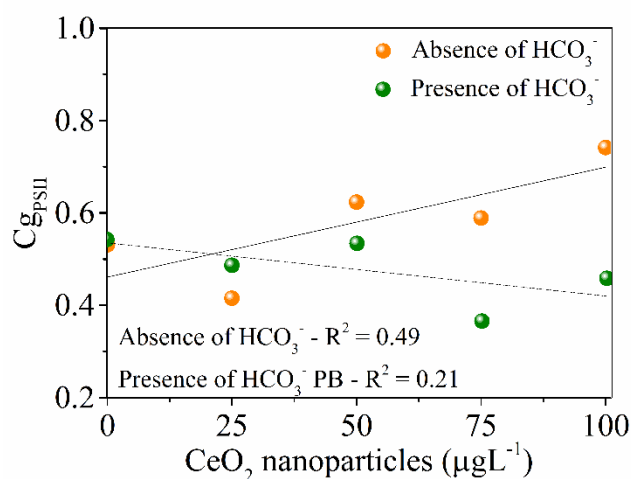


**Figure 9.** Global connectance of photosystem II photochemical network from leaf discs of *Salvinia auriculata* Aubl. submitted to distinct treatments of cerium oxide nanoparticles (CeO<sub>2</sub> NPs) in the absence and presence of HCO<sub>3</sub><sup>-</sup>. R<sup>2</sup> – coefficient of determination

#### 4. Conclusions

The uptake and accumulation of Ce in leaf samples were significantly higher compared to the non-exposed samples. Biochemical vibrational modes were strongly influenced after treatments with CeO<sub>2</sub> NPs upon presence or absence of HCO<sub>3</sub><sup>-</sup>. The effects of treatments have considerable influence on the proteins structure, photosynthetic pigments, lipids and carbohydrates constituents of leaf sample compared to control. The PCA and HCA analysis suggest that highest levels of CeO<sub>2</sub> NPs seriously impairing the metabolites level independent of the presence or absence of HCO<sub>3</sub><sup>-</sup>. This study showed that interactive responses of nanoceria and HCO<sub>3</sub><sup>-</sup> had a significant impact on the primary non-photochemical processes, and on the functionality of RCs of photosystem II. Network connectance analysis provides valuable information for further modeling of homeostatic adjustment of PSII



photochemistry. Elevated  $\text{HCO}_3^-$  ion concentration affects the ability of leaves uptake the  $\text{CeO}_2$  NPs.

## 5. References

HANSEN, S.F.; HEGGELUND, L.R.; BESORA, P.R.; MACKEVICA, A.; BOLDRIN, A.; BAUN, A. Nanoproducts - what is actually available to European consumers? **Environmental Science Nano**. v.3, p.169–180, 2016.

GRILLO, R.; ROSA, A.H.; FRACETO, L.F. Engineered nanoparticles and organic matter: a review of the state-of-the-art. **Chemosphere**. v.119, p.608–619, 2015.

MEDINA-VELO, I.A.; PERALTA-VIDEA, J.R.; GARDEA-TORRESDEY, J.L. Assessing plant uptake and transport mechanisms of engineered nanomaterials from soil. **MRS Bulletin**. v.42(5), p.379–383, 2017.

GRILLO, R.; JESUS, M.B.; FRACETO, L.F. Editorial: environmental impact of nanotechnology: analyzing the present for building the future. **Frontiers in Environmental Science**. 6:34, 2018. doi: 10.3389/fenvs.2018.00034

FUTURE MARKETS (2012), The global market for nanomaterials 2002–2016: production volumes, revenues and end use markets. Future Markets Inc., disponible in: [http://www.futuremarketsinc.com/index.php?option=com\\_content&view=article&id=176&Itemid=73](http://www.futuremarketsinc.com/index.php?option=com_content&view=article&id=176&Itemid=73). Accessed 25/08/2018.

RODEA-PALOMARES, I.; GONZALO, S.; SANTIAGO-MORALES, J.; LEGÁNES, F.; GARCÍA-CALVO, E.; ROSAL, R.; FERNÁNDEZ-PIÑAS, F. An insight into the mechanisms of nanoceria toxicity in aquatic photosynthetic organisms. **Aquatic Toxicology**. v.122-123, p.133-143, 2012.

MA, C.; CHHIKARA, S.; XING, B.; MUSTANTE, C.; WHITE, J.C.; DHANKHER, O.P. Physiological and molecular response of *Arabidopsis thaliana* (L.) to nanoparticles cerium and indium oxide exposure. **ASC Sustainable Chemistry and Engineering**. v.1, p.768-778, 2013.

ZHANG, W.; EBBS, S.D.; MUSANTE, C.; WHITE, J.C.; GAO, C.; MA, X. Uptake and accumulation of bulk and nanosized cerium oxide particles and ionic cerium by radish (*Raphanus sativus* L.). **Journal of Agriculture, Food and Chemistry**. v.63(2), p.382-390, 2015.

ZHANG, W.; DAN, Y.; SHI, H.; MA, X. Elucidating the mechanisms for plant uptake and in-plant speciation of cerium in radish (*Raphanus sativus* L.) treated with cerium oxide nanoparticles. **Journal of Environmental Chemistry and Engineering**. v.5, p.572-577, 2017.

PÉREZ-DE-LUQUE, A. Interaction of nanomaterials with plants: what do we need for real applications in agriculture? **Frontiers in Environmental Science**. v.5, p.1-7, 2017.

GIESE, B.; KLAESSING, F.; PARK, B.; KAEGI, R.; STEINFELDT, M.; WIGGER, H.; GLEICH, A.V.; GOTTSCHALK, F. Risks, release and concentrations of engineered nanomaterial in the environment. **Scientific Reports**. v.8, n.1565, 2018. doi: 10.1038/s41598-018-19275-4

PIETROIUSTI, A.; STOCKMANN-JUVALA, H.; LUCARONI, F.; SAVOLAINEN, K. Nanomaterial exposure, toxicity and impact on human health. **Wiley Interdisciplinary Reviews in Nanomedicine and Nanobiotechnology**. 2018;e1513. doi: 10.1002/wnan.1513

SIZOCHENKO, N.; MIKOLAJCZYK, A.; JAGIELLO, K.; PUZYN, T.; LESZCZYNSKI, J.; RASULEV, B. How toxicity of nanomaterials towards different species could be simultaneously evaluated: novel multi-nano-read-across approach. **Nanoscale**. v.10(2), p.582–591, 2018.

GRILLO, R.; SANTOS, N.Z.P.; MARUYAMA, C.R.; ROSA, A.H.; LIMA, R.; FRACETO, L.F. Poly( $\epsilon$ -caprolactone) nanocapsules as carrier systems for herbicides: Physico-chemical characterization and genotoxicity evaluation. **Journal of Hazardous Materials**. v.232, p.1-9, 2012.

ORR, J.C.; FABRY, V.J.; AUMONT, O.; BOPP, L.; DONEY, S.C.; FEELY, R.A.; GNANADESIKAN, A.; GRUBER, N.; ISHIDA, A.; JOOS, F.; KEY, R.M.; LINDSAY, K.; MAIER-REIMER, E.; MATEAR, R.; MONFRAY, P.; MOUCHET, A.; NAJJAR, R.G.; PLATTNER, G.-K.; RODGERS, K.B.; SABINE, C.L.; SARMIENTO, J.L.; SCHLITZER, R.; SLATER, R.D.; TOTTERDELL, I.J.; WEIRIG, M.-F.; YAMANAKA, Y.; YOOL, A. Anthropogenic ocean acidification over the twenty-first century and its impact on calcifying organisms. **Nature**. v.437, 681-686, 2005.

RAMANAM, R.; NADIMUTHU, V.; SARAVANA-DEVI, S.; KRISHNAMURTHI, K.; TAPAN, C. Influence of CO<sub>2</sub> concentration on carbon concentrating mechanisms in cyanobacteria and green algae: a proteomic approach. **Algae**. v.27, p.295–301, 2012.

- MISRA, B.B.; DE ARMAS, E.; TONG, Z.; CHEN, S. Metabolomic responses of guard cells and mesophyll cells to bicarbonate. **PLoS ONE**. v.10(12):e0144206, 2015.
- GONDIKAS, A.; VON DER KRAMMER, F.; KAEGI, R.; BOROVINSKAYA, O.; NEUBAUER, E.; NAVRATILOVA, V.; PRAETORIUS, A.; CORNELIS, G.; HOFMANN, T.T. Where is the nano? Analytical approaches for the detection and quantification of TiO<sub>2</sub> nanoparticles in surface waters. **Environmental Science Nano**. v.5, p.313-326, 2018.
- RODRIGUEZ, R.M.; PAVLOV, S.; GONZALEZ, A.; OUKARROUM, A.; STRASSER, R.J. Can machines recognize stress in plants? **Environmental Chemistry Letters**. v.1, p.201–205, 2003.
- CAIRES, A.R.L.; SCHERER, M.D.; SANTOS, T.S.B.; PONTIN, B.C.A.; GAVASSONI, W.L.; OLIVEIRA, S.L. Water stress response of conventional and transgenic soybean plants monitored by chlorophyll *a* fluorescence. **Journal of Fluorescence**. v.20, p.645-649, 2011.
- SANTIAGO, E.F.; LARENTIS, T.C.; BARBOSA, V.M.; CAIRES, A.R.L.; MORAIS, G.A.; SÚAREZ, Y.R. Can the chlorophyll *a* fluorescence be useful in identifying acclimated young plants from two populations of *Cecropia Pachystachya* Trec. (Urticaceae), under elevated CO<sub>2</sub> concentrations? **Journal of Fluorescence**. v.25, p.49-57, 2015.
- KWAK, C.W.; CHOUNG, D.; MIN, S.R.; KIM, S.W.; LIU, J.R.; CHUNG, H. Fast determination of the ripeness stage of Strawberries using infrared spectroscopy combined with principal component analysis. **Analytical Science**. v.23, p.895-899, 2007.
- VÍTEK, P.; NOVOTNÁ, K.; HODŇOVÁ, P.; RAPANTOVÁ, B.; KLEN, K. Detection of herbicide effects on pigment composition and PSII photochemistry in *Helianthus annuus* by Raman spectroscopy and chlorophyll *a* fluorescence. **Spectrochimica Acta Part A. Molecular and Biomolecular Spectroscopy**. v.170, p.234-241, 2017.
- ANDRADE, L.H.C.; FREITAS, P.G.; MANTOVANI, B.G.; FIGUEIREDO, M.S.; LIMA, R.A.; LIMA, S.M.; RANGEL, M.A.S.; MUSSURY, R.M. Detection of soybean rust contamination in soy leaves by FTIR photoacoustic spectroscopy. **European Physics Journal: Special Topics**. v.153, p.539-541, 2008.
- SHARMA, S.; UTTAM, R.; SINGH, P.; UTTAM, K.N. Detection of vibrational spectroscopy biomarkers of the effect of gold nanoparticles on wheat seedlings using attenuated total reflectance Fourier transform infrared spectroscopy. **Analytical Letters**. v.51(14), p.2271-2294, 2018.

KHAIRUDIN, K.; SUKIRAN, N.A.; GOH, H.; BAHARUM, S.N.; NOOR, N.M. Direct discrimination of different plant populations and study on temperature effects by Fourier transform infrared spectroscopy. **Metabolomics**. v.10(2), p.203-211, 2014.

SHARMA, S.; UTTAM, K.N. Investigation of the manganese stress on wheat plant by attenuated total reflectance Fourier transform infrared spectroscopy. **Spectroscopic Letters**. v.49, p.520-28, 2016.

PERREAULT, F.; OUKARROUM, A.; PIRASTRU, L.; SIROIS, L.; MATIAS, W.G.; POPOVIC, R. Evaluation of copper oxide nanoparticles toxicity using chlorophyll *a* fluorescence imaging in *Lemna gibba*. **Journal of Botany**. ID 763142, 9 pages, 2010.

FALCO, W.F.; QUEIROZ, A.M.; FERNANDES, J.; BOTERO, E.R.; FALCÃO, E.A.; GUIMARÃES, F.E.G.; MPEKO, J.-C.; OLIVEIRA, S.L.; COLBECK, I.; CAIRES, A.R.L. Interaction between chlorophyll and silver nanoparticles: A close analysis of chlorophyll fluorescence quenching. **Journal of Photochemistry and Photobiology A: Chemistry**. v.299, p.203-209, 2015.

QUEIROZ, A.M.; MEZACASA, A.V.; GRACIANO, D.E.; FALCO, W.F.; MPEKO, J.-C.; GUIMARÃES, F.E.G.; LAWSON, T.; COLBECK, I.; OLIVEIRA, S.L.; CAIRES, A.R.L. Quenching of chlorophyll fluorescence induced by silver nanoparticles. **Spectrochimica Acta Part A. Molecular and Biomolecular Spectroscopy**. v.168, p.73-77, 2016.

FALCO, W.F.; BOTERO, E.R.; FALCÃO, E.A.; SANTIAGO, E.F.; BAGNATO, V.S.; CAIRES, A.R.L. In vivo observation of chlorophyll fluorescence quenching induced by gold nanoparticles. **Journal of Photochemistry and Photobiology A: Chemistry**. v.225, p.65-71, 2011.

SURESH, S.; KARTHIKEYAN, S.; JAYAMOORTHY, K. FTIR and multivariate analysis to study the effect of bulk and nano copper oxide on peanut plant leaves. **Journal of Science: Advanced Materials Devices**. v.1, p.343-350, 2016.

SHARMA, S.; UTTAM, K.N. Rapid analyses of stress of copper oxide nanoparticles on wheat plants at an early stage by laser induced fluorescence and attenuated total reflectance Fourier transform infrared spectroscopy. **Vibrational Spectroscopy**. v.92, p.135-150, 2017.

SURESH, S.; KARTHIKEYAN, S.; JAYAMOORTHY, K. Effect of bulk and nano-Fe<sub>2</sub>O<sub>3</sub> particles on peanut plant leaves studied by Fourier transform infrared spectral studies. **Journal of Advanced Research**. v.7(5), p.739-747, 2016.

EL-SHINTINAWY, F.; GOVINDJEE. Bicarbonate effects in leaf discs from spinach. **Photosynthesis Research**. v.24, p.189-200, 1990.

WANG, Q.; MA, X.; ZHANG, W.; PEI, H.; CHEN, Y. The impact of cerium oxide nanoparticles on tomato (*Solanum lycopersicum* L.) and its implications for food safety. **Metallomics**. v.4, p.1105-1112, 2012.

KITAJIMA, M.; BUTLER, W.L. Quenching of chlorophyll fluorescence and primary photochemistry in chloroplasts by dibromothymoquinone. **Biochimica et Biophysica Acta**. v.376, p.105-115, 1975.

GENTY, B.; BRIANTAIS, J.M.; BAKER, N.R. The relationship between the quantum yield of photosynthetic electron and quenching of chlorophyll fluorescence. **Biochimica et Biophysica Acta**. v.990, p.87-92, 1989.

Oxborough, K.; Baker, N.R. Resolving chlorophyll a fluorescence of photosynthetic efficiency into photochemical components – calculation of qP and Fv' /Fm' without measuring Fo'. **Photosynthesis Research**. v.54, p.135–142, 1997.

R CORE TEAM (2013). R: A language and environment for statistical computing. R Foundation for Statistical Computing, Vienna, Austria. Austria. URL <http://www.R-project.org/>.

AMZALLAG, G.N. Data analysis in plant physiology: are we missing the reality? **Plant Cell and Environment**. v.24, p.881–890, 2001.

TYLER, G.; OLSSON, T. Conditions related to solubility of rare and minor elements in forest soils. **Journal of Plant Nutrition and Soil Science**. v.165, p.594-601, 2002.

ZHAO, L.; PENG, B.; HERNANDEZ-VIEZCAS, J.Á.; RICO, C.; SUN, Y.; PERALTA-VIDEA, J.R.; TANG, X.; NIU, G.; JIN, L.; VARELA-RAMIREZ, A.; ZHANG, J.Y.; GARDEA-TORRESDEY, J.L. Stress response and tolerance of *Zea mays* to CeO<sub>2</sub> nanoparticles: cross talk among H<sub>2</sub>O<sub>2</sub>, heat shock protein and lipid peroxidation. **ACS Nano**. v.6(11), p.9615-9622, 2012.

HONG, J.; PERALTA-VIDEA, J.R.; RICO, C.; SAHI, S.; VIVEROS, M.N.; BARTONJO, J.; ZHAO, L.; GARDEA-TORRESDEY, J.L. Evidence of translocation and physiological impacts of foliar applied CeO<sub>2</sub> nanoparticles on Cucumber (*Cucumis sativus*) plants. **Environmental Science and Technology**. v.48, p.4376-4385, 2014.

- BARTH, A. Infrared spectroscopy of proteins. **Biophysica et Biochimica Acta**. v.1767, p.1073-1101, 2007.
- KRIMM, S.; DWIVEDI, A.M. Vibrational analysis of peptides, polypeptides and proteins. XII-Fermi resonance analysis of the unperturbed ND stretching fundamental in polypeptides. **Journal of Raman Spectroscopy**. v.12, p.133-137, 1982.
- BANDEKAR, J. Amide modes and protein conformation. **Biophysica et Biochimica Acta**. v.1120, p.123-146, 1992.
- LITVINOV, R.I.; FAIZULLIN, D.A.; ZUEV, Y.F.; WEISEL, J.W. The  $\alpha$ -helix to  $\beta$ -sheet transition in stretched and compressed hydrated fibrin clots. **Biophysical Journal**. v.103, p.1020-1027, 2012.
- RICO, C.M.; MORALES, M.I.; BARRIOS, A.C.; MCCREARY, R.; HONG, J.; LEE, W.Y.; NUNEZ, J.; PERALTA-VIDEA, J.R.; GARDEA-TORRESDEY, J.L. Effect of cerium oxide nanoparticles on the quality of rice (*Oryza sativa* L.) grains. **Journal of Agriculture, Food and Chemistry**. v.61, p.11278–11285, 2013.
- RICO, C.R.; LEE, S.C.; RUBENECIA, R.; MUKHERJEE, A.; HONG, J.; PERALTA-VIDEA, J.R.; GARDEA-TORRESDEY, J.L. Cerium oxide nanoparticles impact yield and modify nutritional parameters in wheat (*Triticum aestivum* L.). **Journal of Agriculture, Food and Chemistry**. v.62, p.9669–9675, 2014.
- POŠĆIĆ, F.; MATTIELLO, A.; FELLET, G.; MICELI, F.; MARCHIOL, L. Effects of cerium and titanium oxide nanoparticles in soil on the nutrient composition of barley (*Hordeum vulgare* L.) kernels. **International Journal of Environmental Research Public Health**. v.13, p.577-592, 2016.
- RICO, C.M.; MORALES, M.I.; MCCREARY, R.; CASTILHO-MELHO, H.; BARRIOS, A.C.; HONG, J.; TAFOYA, A.; LEE, W.Y.; VARELA-RAMIREZ, A.; PERALTA-VIDEA, J.R.; GARDEA-TORRESDEY, J.L. Cerium oxide nanoparticles modify the antioxidative stress enzyme activities and macromolecule composition in Rice seedlings. **Environmental Science and Technology**. v.47(24), p.14110-14118, 2013.
- LIZZI, D.; MATTIELLO, A.; MARCHIOL, L. (2017). Impacts of cerium oxide nanoparticles ( $n\text{CeO}_2$ ) on crop plants: a concentric overview. In: (Ed.) TRIPATHI, D.K.; AHMAD, P.; SHARMA, S.; CHAUHAN, D. **Nanomaterials in Plants, Algae, and Microorganisms**. 1st Ed. Concepts and Controversies: Vol. 1, Elsevier. 2017. 550p.



- DAS, K.; ROYCHOUDHURY, A. Reactive oxygen species (ROS) and response of antioxidants as ROS-scavengers during environmental stress in plants. **Frontiers in Environmental Science**. v.2(53), p.1-13, 2014.
- DEMMIG-ADAMS, B. Carotenoids and photoprotection: a role for the xanthophyll zeaxanthin. **Biochimica et Biophysica Acta**. v.1020, 1–24, 1990.
- RUBAN, A.V.; LEE, P.J.; WENTWORTH, M.; YOUNG, A.J.; HORTON, P. Determination of the stoichiometry and strength of binding of xanthophylls to the photosystem II light-harvesting complexes. **Journal of Biological Chemistry**. v.274, p.10458–10465, 1999.
- KRAUSE, G.H.; WEIS, E. Chlorophyll fluorescence and photosynthesis: the basics. **Annual Review in Plant Physiology Plant Molecular Biology**. v.42, p.313–349, 1991.
- WYDRZYNSKI, T.; GOVINDJEE A new site of bicarbonate effect in Photosystem II of photosynthesis: evidence from chlorophyll fluorescence transients in spinach chloroplasts. **Biochimica et Biophysica Acta**. v.387, p.403-408, 1975.
- TOWNSEND, A.J.; WARE, M.A.; RUBAN, A.V. Dynamic interplay between photodamage and photoprotection in photosystem II. **Plant, Cell and Environment**. v.41, p.1098-1112, 2017.
- GIOVAGNETTI, V.; RUBAN, A.V. (2015). Discerning the effects of photoinhibition and photoprotection on the rate of oxygen evolution in *Arabidopsis* leaves. **Journal of Photochemistry and Photobiology B: Biology**. v.152, p.272-278, 2015.
- BERTOLLI, S.C.; VITOLO, H.F.; SOUZA, G.M. Network connectance analysis as a tool to understand homeostasis of plants under environmental changes. **Plants**. 2(3), 473-488, 2013.



Supplementary materials

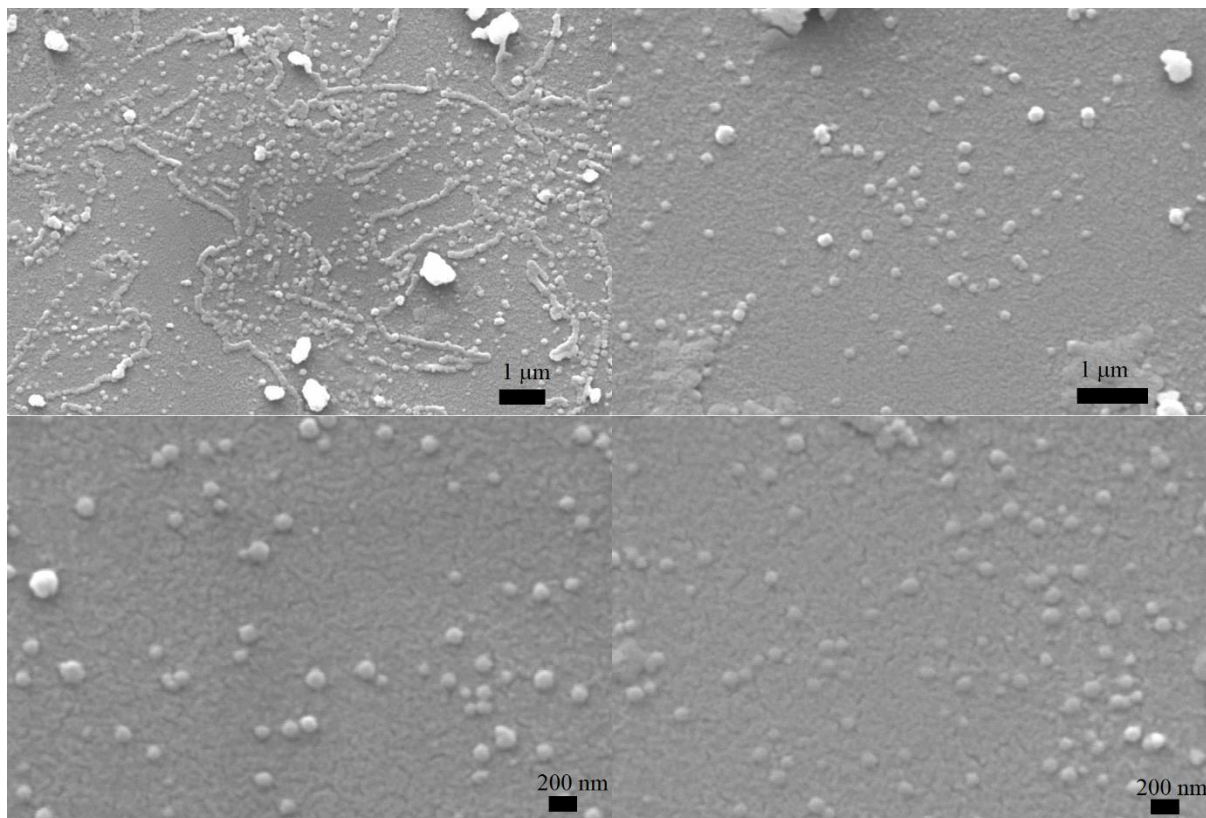


**Figure S1.** (a-d) Analysis of the nanocereria using scanning electron microscopy (SEM) of cerium (II) oxide nanoparticles.

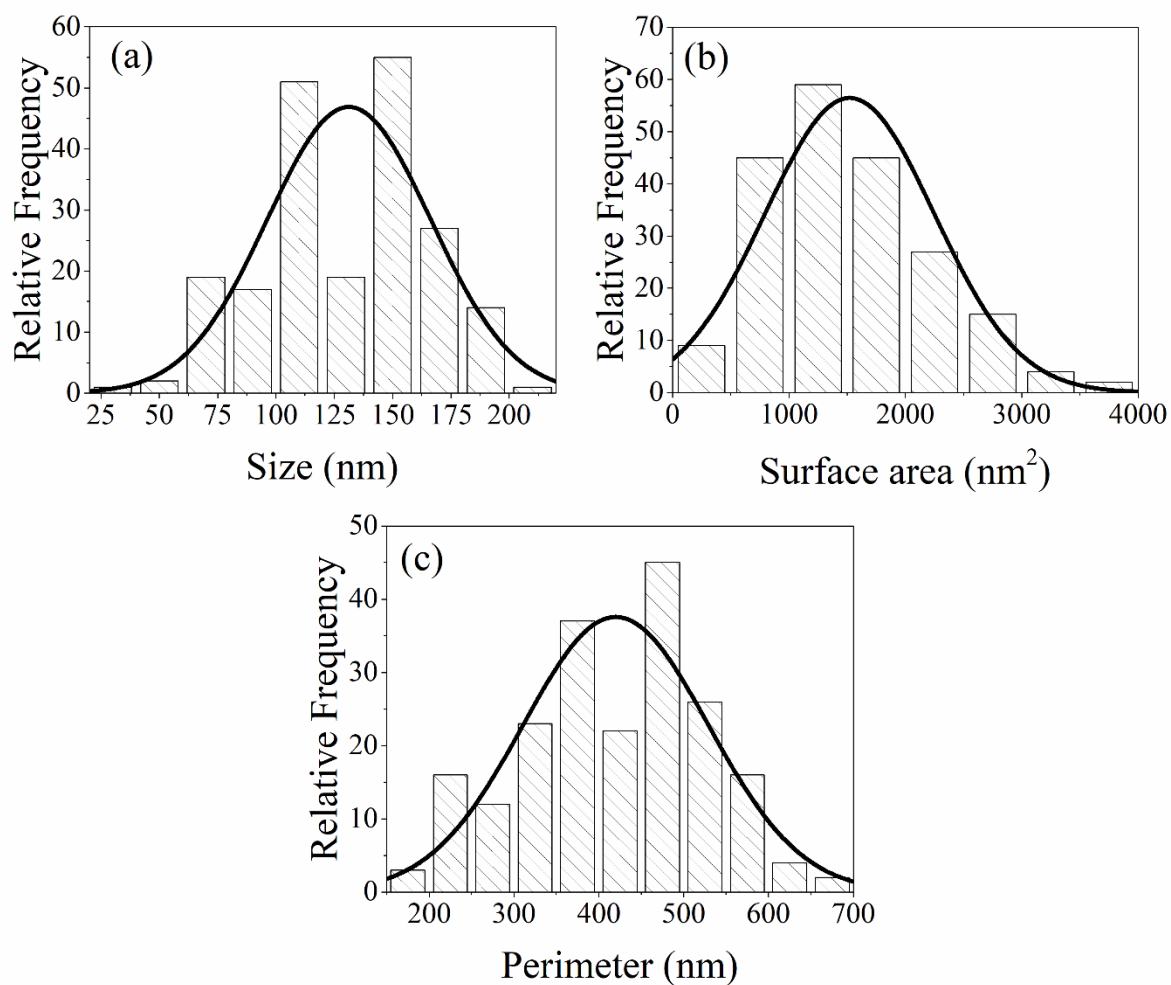


**Figure S2.** Frequency distribution of (a) size, (b) surface area, and (c) perimeter of cerium (II) oxide nanoparticles.

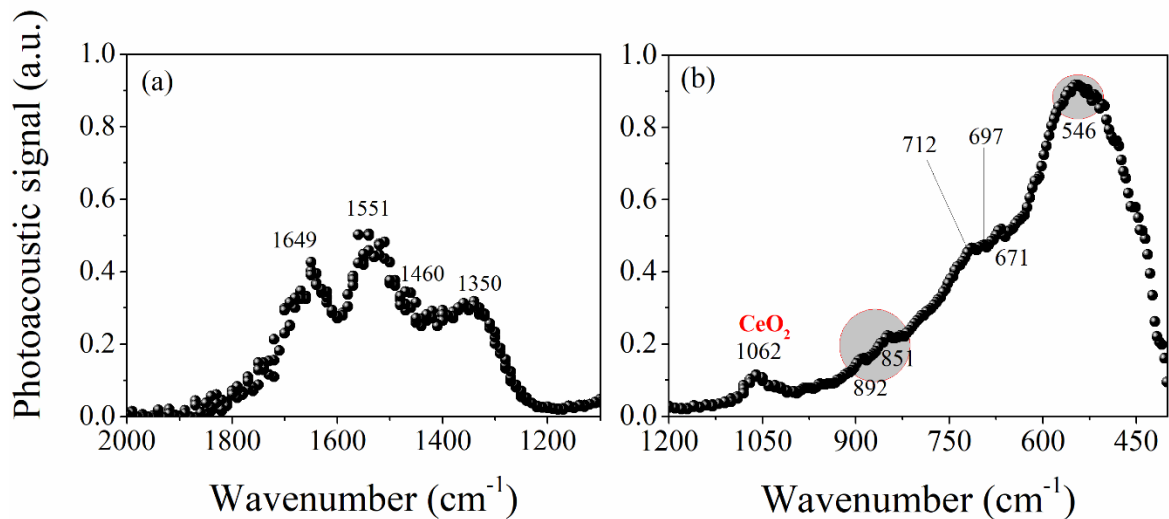


**Figure S3.** Analysis of the nanoceria using Fourier transform infrared spectroscopy (FTIR) coupled with photoacoustic cell.

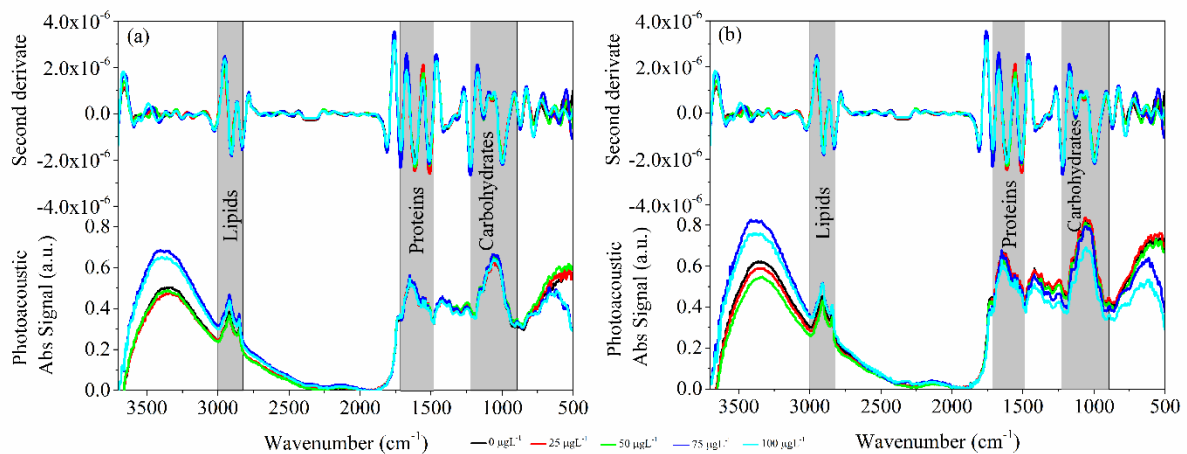


**Figure S4.** Second derivative and zero-order Fourier transform infrared spectroscopy (FTIR) photoacoustic absorption of leaf discs exposed to nanoceria in the (a) absence and (b) presence of bicarbonate ions.

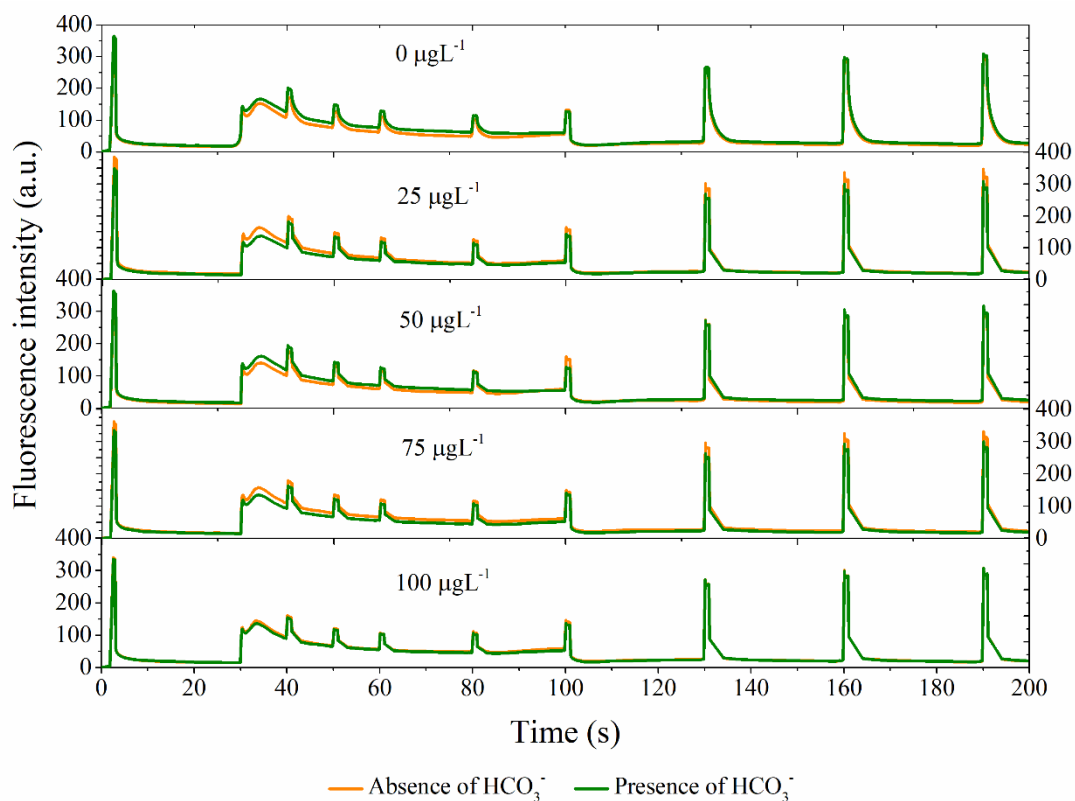


**Figure S5.** Typical pulse amplitude-modulated (PAM) chlorophyll *a* fluorescence kinetics for individual cerium oxide nanoparticles (CeO<sub>2</sub> NPs) treatments in the presence or absence of HCO<sub>3</sub><sup>-</sup> used to determine chlorophyll fluorescence parameters.

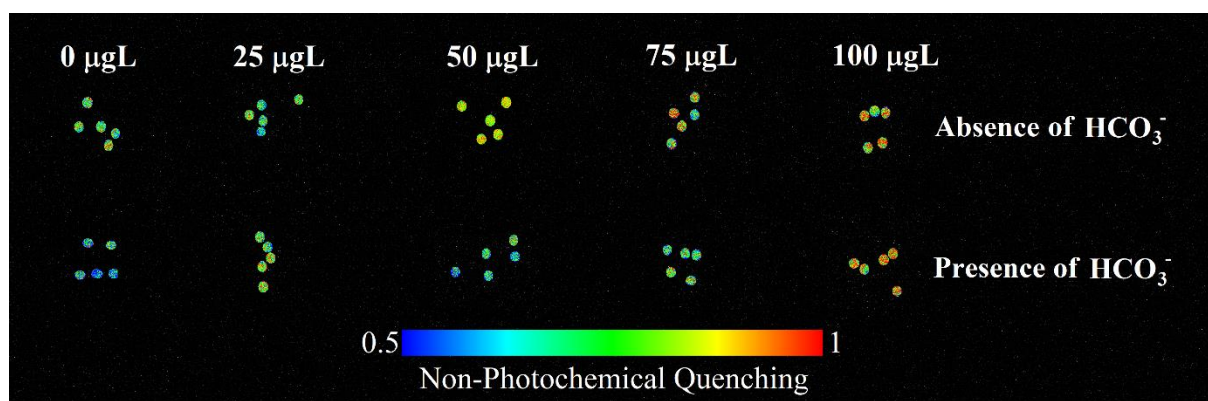


**Figure S6.** Non-photochemical quenching (NPQ) of leaf discs of *Salvinia auriculata* plants exposed to individual cerium oxide nanoparticles (CeO<sub>2</sub> NPs) treatments in the presence or absence of HCO<sub>3</sub><sup>-</sup>.

### **General conclusion and future work**

Nanotechnology has grown rapidly in the last years, with a range of different nanomaterials (applications and products). Despite this, nanomaterials shown a risk to the environmental and may impact human health. The importance of this study comes from several points. This studies to consider the impact of engineered nanomaterials on the photosynthetic apparatus of aquatic plant species from the Neotropical region, using non-destructive techniques. Also, the network approach may be a promising tool for physiological studies related to nanotoxicity. Therefore, further experiments have to be performed to clarify this phenomena.

*In vivo* and *in vitro* studies are essential to asses the potential impact of metal oxide nanoparticles on the ecosystems. We demonstrate that chlorophyll *a* fluorescence induction and optical spectroscopy are sensitive tools for diagnostic the impact of nanomaterials in plant tissues. In conclusion, we suggest caution in the use and production of these nanoparticles in industrial sector, particularly, related to their final disposal.

## List of publications

### Related to dissertation

1. Pontes, M.S.; Rodriguez, R.M.; Santiago, E.F. The energy flux theory celebrates 40 years: toward a systems biology concept? **Photosynthetica**. 2019. *Accepted paper*.
2. Pontes, M.S.; Grillo, R.; Graciano, D.E.; Falco, W.F.; Lima, D.V.; Lima, S.M.; Caires, A.R.L.; Andrade, L.H.C.; Santiago, E.F. Synergism and interference of bicarbonate ions on nanoceria effects in *Salvinia auriculata* Aubl leaf tissue: A chlorophyll a fluorescence and Fourier transform infrared photoacoustic spectroscopy study. **Ecotoxicology and Environmental Safety** (Submitted)
3. Pontes, M.S. et al. Using network connectance for estimating bulk and nanosized copper effects on the photosystem II activity in a floating macrophyte *Lemna valdiviana* Phil. (Lemnaceae). (Under preparation).
4. Pontes, M.S. et al. Environmentally friendly synthesis of colloidal copper oxide nanoparticles: antioxidant, antimicrobial activity and in vitro toxicity. (Under preparation).

### Non-related to dissertation and/or collaboration during master of science degree

1. Pontes, M.S.; Santiago, E.F.; Nobrega, M.A.S.; Freitas, V.M.B. Caracterização morfológica usando dimensões lineares sobre os atributos biométricos em sementes de *Annona reticulata* (L.) Vell. (Annonaceae). **Ciência Florestal**, v.28(2), p.696-707, 2018.
2. Pontes, M.S.; Montefusco-Pereira, C.V.; Misra, B.B.; Ribeiro-Junior, H.L.; Graciano, D.E.; Santos, J.S.; Nobrega, M.A.S.; Fernandes, S.S.L.; Caires, A.R.L.; Santiago, E.F. High-throughput phenotyping by applying digital morphometrics and fluorescence induction curves in seeds to identifying variations: a case study of *Annona* (Annonaceae) species. **Information Processing in Agriculture**, v.5(4), p. 443-455, 2018.
3. Nobrega, M.A.S.; Pontes, M.S.; Santiago, E.F. Aplicação exógena de GA<sub>3</sub> e Tiametoxan sobre a dinâmica da germinação de sementes de *Psidium guineense* Swartz. (Myrtaceae). **Acta Biomedica Brasiliensia**. v.9(2), p.58-66, 2018.
4. Mezacasa, A.V.; Queiroz, A.M.; Graciano, D.E.; Pontes, M.S.; Santiago, E.F.; Oliveira, I.P.; Lopez, A.J.; Casagrande, G.A.; Scherer, M.D.; dos Reis, D.D.; Oliveira, S.L., Caires, A.R.L. Chlorophyll and pheophytin interaction with gold nanoparticles: an optical and computational study. **Spectrochimica Acta Part A: Molecular and Biomolecular Spectroscopy**. (Submitted)
5. Nobrega, M.A.S.; Pontes, M.S.; Santiago, E.F. Incorporação de lodo de esgoto na composição de substrato para produção de mudas nativas. **Acta Biomedica Brasiliensia**. v.8(1), p.43-55, 2017.
6. Souza, E.F.; Nobrega, M.A.S.; Pontes, M.S. Musgos como biondicadores de metais pesados no ambiente. **Acta Biomedica Brasiliensia**. v.8(2), p.13-22, 2017.

### List of conferences

#### Poster presentation

1. Pontes, M.S.; Grillo, R.; Nobrega, M.A.S.; Santos, J.S.; Fernandes, S.S.L.; Graciano, D.E.; Falco, W.F.; Ribeiro, C.A.L.; Andrade, L.H.C.; Caires, A.R.L.; Santiago, E.F. Chlorophyll fluorescence imaging in leaf discs of *Salvinia auriculata* exposed to cerium oxide nanoparticles. In: **2º Simpósio Científico Sobre Recursos Naturais - SCRN, 2018**, Dourados-MS. Anais do 2º Simpósio Científico Sobre Recursos Naturais, 2018.
2. Pontes, M.S.; Grillo, R.; Nobrega, M.A.S.; Santos, J.S.; Fernandes, S.S.L.; Graciano, D.E.; Falco, W.F.; Andrade, L.H.C.; Lima, S.M.; Caires, A.R.L.; Santiago, E.F. Cyanobacterial light-harvesting protein phycocyanin as a biosensor for detection of copper oxide nanoparticles. In: **2º Simpósio Científico sobre Recursos Naturais - SCRN, 2018**, Dourados. Anais do 2º Simpósio Científico Sobre Recursos Naturais, 2018.
3. Pontes, M.S.; Antunes, D.R.; Santiago, E.F.; Fraceto, L.F.; Grillo, R. Effect of chitosan/tripolyphosphate nanoparticles loaded with paraquat herbicide on photosystem I of spinach leaves. In: **III Workshop on Environmental Nanotechnology, 2018**, Sorocaba, São Paulo, Brazil. Annals III Workshop on Environmental Nanotechnology, 2018. p. 63-63.

#### Oral presentation

1. Pontes, M.S.; Santiago, E.F.; Andrade, L.H.C.; Caires, A.R.L.; Grillo, R.; Falco, W.F.; Graciano, D.E. Fluorescence quenching induced by nanosized copper around cyanobacterial light-harvesting protein phycocyanin. In: **IV Encontro de Pesquisadores em Ciência e Engenharia dos Materiais, EPCEM - 2018**, Ilha Solteira-SP. Anais do IV Encontro de Pesquisadores em Ciência e Engenharia dos Materiais. Ilha Solteira: Editora UNESP, 2018.



Cadastro no Sistema Nacional de Gestão do Patrimônio Genético e do Conhecimento Tradicional Associado – SISGEN.

Cadastro Número: A754D47



Ministério do Meio Ambiente  
CONSELHO DE GESTÃO DO PATRIMÔNIO GENÉTICO

SISTEMA NACIONAL DE GESTÃO DO PATRIMÔNIO GENÉTICO E DO CONHECIMENTO TRADICIONAL ASSOCIADO

Comprovante de Cadastro de Acesso

Cadastro nº A754D47

A atividade de acesso ao Patrimônio Genético, nos termos abaixo resumida, foi cadastrada no SisGen, em atendimento ao previsto na Lei nº 13.123/2015 e seus regulamentos.

Número do cadastro:	A754D47
Usuário:	Etenaldo Felipe Santiago
CPF/CNPJ:	436.268.741-68
Objeto do Acesso:	Patrimônio Genético
Finalidade do Acesso:	Pesquisa

**Espécie**

Lemna valdiviana

Salvinia auriculata

Arthrospira platensis

Título da Atividade:	Monitoramento das alterações induzidas em organismos fotossintéticos por nanopartículas via técnicas de fluorescência da clorofila-a e espectroscopia óptica
----------------------	--------------------------------------------------------------------------------------------------------------------------------------------------------------



Universidade Estadual de Mato Grosso do Sul

Unidade Universitária de Dourados

Programa de Pós-Graduação em Recursos Naturais

---